Computational Study of Conformational Behavior and Analyses of Vibrational Spectra of Some Ketenes

by

Abdulaziz Abdulrahman Al-Saadi

A Thesis Presented to the

FACULTY OF THE COLLEGE OF GRADUATE STUDIES

KING FAHD UNIVERSITY OF PETROLEUM & MINERALS

DHAHRAN, SAUDI ARABIA

In Partial Fulfillment of the
Requirements for the Degree of

MASTER OF SCIENCE

In

CHEMISTRY

May, 2000

INFORMATION TO USERS

This manuscript has been reproduced from the microfilm master. UMI films the text directly from the original or copy submitted. Thus, some thesis and dissertation copies are in typewriter face, while others may be from any type of computer printer.

The quality of this reproduction is dependent upon the quality of the copy submitted. Broken or indistinct print, colored or poor quality illustrations and photographs, print bleedthrough, substandard margins, and improper alignment can adversely affect reproduction.

In the unlikely event that the author did not send UMI a complete manuscript and there are missing pages, these will be noted. Also, if unauthorized copyright material had to be removed, a note will indicate the deletion.

Oversize materials (e.g., maps, drawings, charts) are reproduced by sectioning the original, beginning at the upper left-hand corner and continuing from left to right in equal sections with small overlaps.

Photographs included in the original manuscript have been reproduced xerographically in this copy. Higher quality 6" x 9" black and white photographic prints are available for any photographs or illustrations appearing in this copy for an additional charge. Contact UMI directly to order.

Bell & Howell Information and Learning
300 North Zeeb Road, Ann Arbor, MI 48106-1346 USA
800-521-0600

COMPUTATIONAL STUDY OF CONFORMATIONAL BEHAVIOR AND ANALYSES OF VIBRATIONAL SPECTRA OF SOME KETENES

BY

Abdulaziz Abdulrahman Al-Saadi

A Thesis Presented to the
DEANSHIP OF GRADUATE STUDIES

KING FAHD UNIVERSITY OF PETROLEUM & MINERALS
DHAHRAN, SAUDI ARABIA

In Partial Fulfillment of the
Requirements for the Degree of

MASTER OF SCIENCE
In
CHEMISTRY

May 2000

KING FAHD UNIVERSITY OF PEROLEUM AND MINERALS

DHAHRAN 31261, SUADI ARABIA

DEANSHIP OF GRADUATE STUDIES

This thesis, written by **Abdulaziz Abdulrahman Al-Saadi**,
under the direction of his Thesis Advisor and approved by his Thesis Committee, has been presented to and accepted by the Dean of the Graduate Studies, in partial fulfillment of the requirements for the degree of

MASTER OF SCIENCE IN CHEMISTRY

Thesis Committee

Prof. Hassan M. Badawi
Thesis Advisor

Dr. Wolfgang Forner
Member

Sk. Asraf Ali

Prof. Shaikh A. Ali
Member

Dr. Asaad A. Al-Thukair
Department Chairman

Dr. Abdullah M. Al-Shehri
Dean, Graduate Studies

Date: 2/5/2003

To My Parents

and My Wife

ACKNOWLEDGMENT

All praise be to Allah for the help and guidance. The please of Allah be upon the profit Mohammad. Acknowledgment is directed to King Fahd University of Petroleum and Minerals, Dhahran, Saudi Arabia, for its support for my thesis work. I would like to express my gratitude and appreciation to my thesis advisor, Prof. Hassan Mohammad Badawi, Professor of physical chemistry for his unforgotten directions and patience throughout my work. I learned from him a lot, and the participation with his research group was very useful. I am also debited to Dr. Wolfgang Förner, Associate Professor of physical chemistry for his cooperation and respectable interaction. I also would like to thank Prof. Shiakh Asrof Ali, Professor of organic chemistry for his consistent support and valuable comments and suggestions. All faculty members, staff, graduate assistants and lecturer B's deserved my thanks. Special appreciations are forwarded to the current chairman, Dr. Asaad A. Al-Thukair, the previous chairman, Prof. Abdulrahman A. Al-Arfaj, Prof. Mohammad Z. Al-Faer and Prof. Mohammad F. Ali for their continuous encouragements and helpful cooperation. Finally, I must give my thank to my parents and my family for their moral support and remembered effort.

TABLE OF CONTENTS

LIST OF TABLES

LIST OF FIGURES

THESIS ABSTRACT

NAME: Abdulaziz Abdulrahman Al-Saadi.

TITLE: Computational Study of Conformational Behavior and Analyses of Vibrational Spectra of Some Ketenes.

FIELD: Physical Chemistry.

DATE: May 2000.

The structural stability of a chosen set of important ketenes was investigated using ab initio calculations. The 6-311++G** extended basis set at the DFT-B3LYP level was employed in most of the work. Full energy optimization was performed at the ground states as well as the transition states for the systems under the study. It was found that when the conjugation effect in formyl ketene, fluorocarbonyl ketene, chlorocarbonyl ketene and vinyl ketene is dominant, theses systems exist as a mixture of *cis* and *trans* conformations. Moreover, they were of a relatively high-calculated rotational barrier as compared to the corresponding isocyanates. In the case of non-conjugated ketenic systems, such as trifluoromethyl ketene and chloromethyl ketene, the barrier to interconversion was calculated to be considerably lower and the *gauche* form was expected to appear as a stable form. In such systems, the steric effect, the intramolecular electrostatic attraction and the molecular orbital destabilization may play competitive roles in controlling the conformational behavior. The *cis* form was calculated to be the most stable conformation in tri- and difluoromethyl ketene with the *gauche* conformation being the less stable form in only the difluoro derivative. While in halomethyl ketene only the *gauche* form was the stable form. Additionally, complete normal coordinate analyses were performed to derive the potential energy distributions (PED) for each stable conformation in the molecular systems. The calculated vibrational spectra for each system were plotted and reliable assignments of the vibrational wavenumbers were made based on the vibrational frequencies, calculated PED values, Raman activities, IR intensities, depolarization ratios as well as the observed frequencies of similar molecules.

MASTER OF SCIENCE DEGREE

KING FAHD UNIVERSITY OF PETROLEUM AND MINERALS

Dhahran, Saudi Arabia

May 2000

خلاصة الرسالة

الاسم : **عبد العزيز بن عبد الرحمن حمد السعدي.**

عنوان الرسالة : **دراسة الثبات البنائي وتحليل الأطياف الاهتزازية لبعض الكيتينات بواسطة الطرق الحاسوبية.**

التخصص : **كيمياء فيزيائية.**

التاريخ : **صفر ١٤٢١ ــ مايو ٢٠٠٠.**

تم دراسة الثبات البنائي وحساب حاجز الطاقة لبعض الكيتينات بواسطة حسابات ab initio النظرية، واستخدمت المجموعة الأساسية المطورة 6-311++G** عند مستوى DFT-B3LYP من الحسابات. وأُجريت كذلك الحسابات المثالية للطاقة لتحديد طول الروابط وقيمة الزوايا الجزيئية في الأشكال البنائية عند الحالة الأرضية المستقرة وعند الحالة الانتقالية، لقد وُجد في المركبات الكيتينية التي تتضمن خصيصة التناوب في روابطها الجزيئية أن الشكل البنائي المستوي s-*cis* و s-*trans* هو الأفضل حرارياً مع حاجز عالٍ للطاقة اللازمة للانتقال من أحد الشكلين المستويين إلى الآخر، وحينما تُقارن حواجز الدوران لتلك المركبات الكيتينية المسطّحة بنظائرها الأيسوسيانائية تبيّن أن هناك اختلافاً كبيراً يتمثل في انحدار ملموس في حاجز الدوران للمركبات الأيسوسيانائية، و أظهرت الحسابات النظرية كذلك أن الشكل البنائي *cis* هو الأكثر احتمالاً للمركبين ثلاثي فلورو ميثيل كيتين وثنائي فلورو ميثيل كيتين مع وجود الشكل البنائي الأقل احتمالاً *gauche* في مشتقة ثنائي الفلورو فقط، أما في حالة وجود ذرة فلور أو كلور واحدة في الهالوميثيل كيتين فقد وجد أن الشكل البنائي *gauche* فقط هو السائد، وفي هذه المجموعة من المركبات يُرجّح أنه يوجد أكثر من شكل من القوى تؤثر على ثباتها؛ كقوة التجاذب الكهروستاتيكية و الإعاقة الفراغية بين ذرات الجزيء الواحد، بالإضافة إلى ما سبق فقد تم حساب الأطياف الاهتزازية لكل المركبات التي تحت الدراسة وتم تحديد جميع الصيغ الاهتزازية بناءً على القيم المحسوبة لتوزيع الطاقة الكامنة عبر إحداثيات التناظر في هذه المركبات ؛ والمقارنة مع النتائج العملية لمركبات مماثلة أو شبيهة، ومما يجدر ذكره أن النتائج النظرية عند مستوى DFT-B3LYP من الحسابات أعطت توافقاً جيداً مع النتائج التجريبية.

درجة الماجستير في العلوم

جامعة الملك فهد للبترول والمعادن

الظهران–المملكة العربية السعودية

مايو ٢٠٠٠

CHAPTER 1

INTRODUCTION

Structure of chemical compounds is always of a fundamental importance to chemists. By the knowledge of the molecular structure of any compound, chemical and physical properties could be predicted [1-3]. For this reason there have been many investigations of the structural features of a great number of molecules, that were carried out during the last decades.

The intramolecular rotation in a particular compound is a very important factor that greatly influences the conformational behavior of that molecule [4]. Such rotation (or inversion) determines the physical and chemical nature of the molecule. In addition, the conformational study of a molecule under investigation gives a reasonable prediction of the chemical reactivity of the substance and the possible pathway followed in a given reaction mechanism. Furthermore, a very essential parameter that is surly changed while the rotation takes place is the energy. The energy of a particular conformer could be calculated, and hence both the most stable conformer (at the ground state) and the unstable one (at the excited state) could be determined.

For instance, it was found that both the *cis* and the *trans* conformations in fluoroacetaldehyde and chloroacetaldehyde [5,6] are the stable forms, whereas the *gauche* conformation was determined to be the transition state in the two molecules. Moreover, the *trans* conformer, in which the halogen atom eclipses the carbonyl group, has been found to be the high energy conformer. In the case of fluoroacetaldehyde [6] the *trans* form was predicted from ab initio calculations to be 1.70 kcal/mol higher in energy than the *cis* form. However, the relative energy of the chloro derivative [5] was calculated to be 1.46 kcal/mol, which is lower than the corresponding value of the fluoro derivative. The steric effect of the bulkier chlorine atom was believed to play an important role in decreasing the energy difference between the stable conformations of the chloro derivative.

Conformational behavior of molecules can be characterized by both experimental and theoretical techniques. Electron diffraction, vibrational far infrared, Raman and rotational microwave spectroscopic techniques are generally the most applicable methods to study the conformational equilibrium of small molecules [4]. However, systems of multiple substituents usually exist in a mixture of stable conformers at room temperature. This leads to extremely complex molecular spectra.

The recently advanced computer technology made theoretical *ab initio* methods a reliable tool to provide important information to spectroscopists and structural chemists. This information helps so much in the interpretation of such molecular spectra [7-11]. Ab initio calculation methods using very high basis sets, such as 6-311++G**, have showed very good agreements with the experimental results for many small molecular systems.

Ab initio methods have been used to study the conformational preferences of a large number of important chemical systems during last decades. The structures of series of halo [12-16] and cyano [17] derivatives of acetaldehyde and acetyl halides have been studied over the past few years. The objective was to determine the nature of the interaction between the carbonyl group and the substituent of the alkyl group. The replacement of the aldehydic hydrogen with the halogen atom greatly influences the conformational behavior in the corresponding halides. For example, the *trans* conformer of the fluoroacetyl chloride (the halogen atoms are *trans* with respect to each other) was found to be more stable than the *cis* conformer [14]. The *trans*-to-*cis* and the *cis*-to-*trans* energy barriers were calculated to be 4.16 and 2.61 kcal/mol, respectively. Additionally, the vibrational frequencies and the potential energy distributions were derived for the two stable conformations of fluoroacetyl chloride [14].

In the case of cyanoacetaldehyde [17], the *cis* form, in which the cyano group and the aldehydic hydrogen eclipse each other, was predicted to be slightly more stable than the *trans* conformer. When the investigation was extended to cyanoacetyl fluoride and chloride, the *trans* form was calculated to be the thermodynamically preferred conformation. The barriers of the internal rotation in these three molecules were predicted to follow the order: cyanoacetaldehyde > cyanoacetyl fluoride > cyanoacetyl chloride.

The reactivity of vinyl and linear butadienes in synthetic and polymer chemistry has attracted the attention. The role of these compounds as models for understanding conjugation and polarization effects have prompted several studies to investigate the conformational equilibrium in some vinyl and 1,2-butadiene compounds with CXO group,

where X is the hydrogen atom, fluorine atom, and chlorine atom [18-21]. In such unsaturated compounds, the conjugation largely influences the internal rotation of the CXO rotor. This leads to a highly energetic barrier between the two planar conformers as compared to the saturated analogues. Additionally, the intramolecular rotation of the CXO group about the C-C bond alters the partial double bond character in these molecules. This suggests the need to include electron correlation in the calculations to account for the changes in the π-system upon the internal rotation.

These studies were extended to small ring compounds [22-32], such as cyclopropylcarboxyaldehyde and its fluoride and chloride derivatives [28,29]. Furthermore, the 3-cyclopropenecarboxyaldehyde and the corresponding 3-methyl-3-cyclopropenecarboxyaldehyde and their fluoride derivatives have been investigated [30,31]. The compounds were found to exist as the *cis* and the *trans* conformers. The *trans* conformer (the carbonyl group is *trans* to the three-membered ring) was determined to be slightly more stable than the *cis* conformer. The repulsive interaction occurring between the carbonyl group and π-electrons of the double bond of the ring destabilizes the *cis* conformer in the molecule. The vibrational assignments for the normal modes of the two stable conformations of the 3-cyclopropenecarboxylic acid fluoride were made based on the derived potential energy distributions at the density functional level of calculations [32]. The assignments were of a reasonable agreement with the experimentally obtained ones for similar molecules.

Recently, the structure of conducting polymers has attracted considerable attention as a new emerging class of electronic materials [33-35]. The polymerization of acetylenic

hydrocarbons was in particular of a great interest [35]. The stability of the oligomers formed at early stages of polymerization of these systems was not known and ab intio method was shown to be a reliable tool for such studies. The relative thermodynamic energies of the poly(1-propyne) dimers and trimers show that both the conjugation and steric forces play an important role on the structural stability of these systems. By utilizing ab initio calculations, the most likely polymer formation of such systems is based on the *cis-trans* and the *trans-trans* trimers with the tail-head-tail-head addition [35].

In addition to studies concerning the conformational stabilities and structural behavior, calculated vibrational infrared and Raman spectra of some compounds have been carried out. For example, the vibrational frequencies, IR intensities, Raman activities and depolarization ratios of the two stable conformers (the *cis* and the *trans*) of 2,3-butadienal were calculated [36]. Then, the computed vibrational frequencies were scaled and verified by direct comparison to those made experimentally for similar molecules.

Many important chemical features of some ketenic molecules have been studied using computational methods over the last few years [37-39]. Some theoretical calculations were used to investigate the mechanistic behavior of the (2+2) cycloaddition reactions of ketenes with other unsaturated systems [40-42]. Furthermore, some studies have concerned the ketenic radicals using the density functional calculation [43]. In addition, the behavior of some polymerization reaction of ketenes with phosphaketenes, acetylene, and ethylene were investigated using ab initio calculation of the transition structures [44,45]. The great attention paid to the ketenic molecular systems is a result of the particular importance of this organic functional group in synthetic chemistry [46,47]. Ketenes are capable to undergo the

(2+2) cycloaddition reaction with different unsaturated compounds to produce a vast array of four-membered ring compounds. Moreover, ketenes can undergo nucleophilic addition reactions with different nucleophiles [46].

As a continuation of these studies, the structural stability of some ketenes will be investigated by utilizing ab initio calculations. The molecular systems included in this work could be classified into three different sets. The first set is of the general formula R-CXO, where R is the ketenic functional group –C=C=O and X could be the hydrogen, fluorine or chlorine atom. The second investigated set is vinyl ketene and vinyl isocyanate of the formula R-CH=CH_2, where R is the ketenic functional group in the case of vinyl ketene and the isocyanato –N=C=O group in the case of vinyl isocyanate. Finally, the third set that will be studied includes trifluoromethyl ketene (CF_3–CH=C=O), difluoromethyl ketene (CHF_2–CH=C=O) and fluoro- and chloromethyl ketene (CH_2X–CH=C=O), where X is the fluorine or chlorine atom.

The structure of the compounds under investigation in their stable conformers will be optimized by minimizing the energy with respect to all the geometrical parameters at DFT B3LYP level of calculations. Additionally, the energies, rotational constants, and dipole moments will also be predicted. The conformational stability will be determined by comparing the calculated total energies. Full geometry optimizations will be carried out at the transition states and the barrier to internal rotation in the molecules with the CXO, the CH=CH_2 or the CX_3 rotor will be then calculated. Moreover, the normal coordinate modes of the stable conformers will be analyzed, and the symmetry coordinate of each molecule will be constructed. The wavenumbers, IR intensities, Raman activities, depolarization

ratios, and PED values will be calculated for each mode of vibration. Based on these data, the infrared and Raman spectra will be plotted. The assignment of the vibrational wavenumbers will be made for each stable conformer of the aforementioned systems. The assignment will be performed based on the PED values as well as the experimental frequencies of the same molecules or other similar molecules. The results of our work will be presented in this thesis.

CHAPTER 2

AB INITIO CALCULATIONS

2.1 INTRODUCTION

The investigation for accurate electronic wave functions of polyatomic molecules uses mainly the molecular orbital methods "MO". The presence of several nuclei causes greater computational difficulties than for diatomic molecules. Moreover, the electronic wave function of a diatomic molecule is a function of only one parameter: the bond distance. The electronic wave function of a polyatomic molecule, however, depends simultaneously on several parameters: the bond distances, bond angles, and dihedral angles of rotation about single bonds (these angles define the molecular conformation).

A full theoretical treatment of a polyatomic molecule involves calculation of the electronic wave function for a range of each of these parameters; the equilibrium bond distances and angles are then found as those values that minimize the electronic energy. In general, semiempirical or ab initio molecular quantum-mechanical methods are used to study geometrical structures of polyatomic molecular systems.

2.1.1 Semiempirical Methods

Semiempirical methods apply a simpler Hamiltonian than the correct molecular Hamiltonian and use parameters whose values are adjusted to fit experimental data or the results of ab initio calculations [48]. They are classified into two general categories: one-electron methods and two-electron methods. Free-Electron Molecular Orbital method 'FEMO', Hückel Molecular Orbital method 'HMO' and Extended Hückel Molecular Orbital 'EH' method are examples of the one electron methods, while Pariser-Parr-Pople 'PPP' method is an example of the two electron methods.

The simplest semiempirical treatment of conjugated molecules is the Free-Electron Molecular Orbital method. The FEMO method deals only with the π electrons. It assumes that each π electron is free to move along the perimeter of the molecule (potential energy $V = 0$), but cannot move beyond the ends of the molecule (potential energy $V = \infty$). This is the potential energy of a particle in a box, and the FEMO method feeds electrons into the MOs of a one-dimensional box.

The Hückel Molecular Orbital method can provide better results for polyene systems. The HMO deals only with the π electrons. It considers each π MO as a linear combination of the $2p_z$ atomic orbitals (AOs) of the conjugated carbon atoms. These linear combinations are used in the variational integral which is expressed as a sum of integrals involving the various AOs. The Hückel method approximates many of these

integrals as zero and leaves other parameters whose values are picked to give the best fit to experimental data.

An improved version of the Hückel method applicable to both conjugated and non-conjugated molecules is the Extended Hückel method (EH). The EH method treats all the valence electrons of a molecule and neglects fewer integrals than the Hückel method. Calculations with the EH methods are relatively easy to perform because of the many simplifying approximations made [49]. These three methods give correct representations of the shapes and trends in the charge distributions of the various molecular orbitals. However, they are roughly reliable for the description of molecular geometry. Moreover, these methods tend to include large errors in the calculation of total energies of molecules and can be used only to compare energies in closely related structures where errors can be assumed to cancel.

The Pariser-Parr-Pople 'PPP' method is a semiempirical π-electron theory that takes electronic repulsion into account and thereby improves on the Hückel method. In this method, the π-electron Hamiltonian including electron repulsion is used, and the π-electron wave function is written as an antisymmetrized product of π-electron spin orbitals. The PPP method is not usually used to determine equilibrium geometries, but is used to calculate ionization energies for π-electrons and the part of electronic spectrum due to π-electron transitions.

2.1.2 Ab Initio Calculations

Ab initio is Latin for "from the beginning" and indicates a calculation based on fundamental principles. Ab initio calculations, which are less frequently referred to as "nonempirical" calculations, apply the correct Hamiltonian and do not use experimental data other than the values of the fundamental physical constants. The term ab initio, however, should not be interpreted to mean 100 % accurate. An ab initio SCF calculation uses the approximation of taking ψ as antisymmetrized product of one electron spin orbitals and a finite (and hence incomplete) basis set. The next four sections summarize the development of some quantum theories that are commonly used to study many-electron molecular systems by utilizing ab initio calculations.

2.2 THE HARTREE-FOCK SELF CONSISTENT FIELD (SCF) METHOD

For an isolated molecular system, the complete Hamiltonian includes nuclear and electronic kinetic energy operators, electrostatic interactions between all charged particles, and interactions between all magnetic moments due to spin and orbital motions of nuclei and electrons. Since the *Schrödinger* Equation ($\hat{H}\psi = E\psi$) can not be solved exactly for systems with more than one electron, approximate solutions are needed. Usually, the total wave function is built from molecular orbitals (MOs) wave functions. In

general for symmetric molecules, if we consider one particular electron (i) in an averaged potential field created by the nucleus and the remaining electrons, the indicated averaged potential field should be symmetrical. Thus, the Schrödinger equation can be separated into spatial coordinates ($\underline{\mathbf{r}}_i$) with the spin variable σ_i of the electron i. Such a molecular orbital is also called a *spin orbital* since it depends on the spin of the electron. The simplest wave function built from molecular orbitals is a Hartree product:

$$\Psi(1,2,\ldots,n) = \Phi_1(1)\Phi_2(2)\ldots\Phi_n(n) \qquad (2\text{-}1)$$

$\Psi(1,2,\ldots,n)$ is now an approximate wave function and stands for $\Psi(\underline{\mathbf{r}}_1,\sigma_1,\ldots,\underline{\mathbf{r}}_n,\sigma_n)$. The subscript in $\Phi_1(1)$ refers to the molecular orbital and the number in parentheses refers to the electron [4].

However, the Hartree product does not meet the requirement of Pauli exclusion principle stating that no two electrons can have all quantum numbers to be the same. This requirement is satisfied if the wave function is an antisymmetrized product of spin orbitals or a Slater determinant. Therefore, we take the trial function Ψ to be made up of a Slater determinant containing spin orbitals Φ_i. If we are dealing with an atom, then the Φ_i's are atomic spin orbitals.

In 1928, Douglas Hartree introduced a procedure to calculate the molecular orbital wave functions Φ_n's shown in Equation (2-1). The total wave function Ψ can be assumed to be a product of hydrogen-like molecular orbitals [50]. The instantaneous interactions between the electron (1) and the other electrons in a specific system can be

averaged out, and then the potential energy of the interaction between point charges Q_1 and Q_2 is given by:

$$V_{12} = \frac{Q_1 Q_2}{4\pi\varepsilon_o r_{12}} \tag{2-2}$$

The point charge Q_2 could be replaced by the charge density per unit volume ($\int \rho_2 dV_2$). The term ρ_2 is equal to $-e|\Phi_2|^2$ (hypothetical charge cloud). Then, the potential energy of the interaction of electron (1) with electron (2) could be rewritten as:

$$V_{12} = e'^2 \int \frac{|\Phi_2|^2}{r_{12}} dV_2 \tag{2-3}$$

where $|\Phi_2|^2$ is the probability density of electron (2), $e'^2 = e^2/4\pi\varepsilon_o$ and Q_1 is simply $-e$.

To calculate the total potential energy of the interactions of electron (1) with all other n electrons, we have:

$$\sum_{j=2}^{n} V_{1j} = \sum_{j=2}^{n} e'^2 \int \frac{|\Phi_j|^2}{r_{1j}} dV_j \tag{2-4}$$

Furthermore, the total potential energy of the interactions between electron (1) and all other electrons as well as the nucleus is given by:

$$V_1(\underline{\mathbf{r}}_1) = \sum_{j=2}^{n} e'^2 \int \frac{|\Phi_j|^2}{r_{1j}} dV_j - \frac{Ze'^2}{r_1} \qquad (2\text{-}5)$$

On this basis, a new potential energy field (of an improved orbital) could be calculated for the electron (1) and will be closer to the truth than the one originally assumed. The improved-orbital potential energy is calculated for each electron in the system to create a set of improved orbitals for n-electrons. This iterative procedure is repeated until there is no further change in the individual electronic distributions or their potential energy fields, which are then said to be *self-consistent* [50].

If many-electron systems are considered, certain atoms in their ground states are fairly well described by assigning two electrons, one of each spin, to each atomic orbital starting with the lowest energy atomic orbital and working up until all the electrons are assigned. If the last electron is to complete the filling of all the AO's at a given energy level with two electrons each, then we have a *closed subshell* atomic system. Such systems are well approximated by a single determinantal wave function if the highest filled level is not close in energy to the lowest empty level. A similar situation holds for molecules; that is, the wave functions of many molecules in their ground states are well represented by single determinantal wave functions with electrons of paired spins occupying identical MO's. Such molecules are said to be *closed shell* systems. The trial wave function for a 2n-electron closed shell system can be represented as

$$\Psi_{closed\ shell} = |\Phi_1(1)\overline{\Phi}_1(2)\Phi_2(3)\overline{\Phi}_2(4)...\Phi_n(2n-1)\overline{\Phi}_n(2n)| \qquad (2\text{-}6)$$

where the shorthand form is used for a Slater determinant, the bar (-) over spatial orbitals denotes the β spin and the absence of the bar denotes the α spin.

For a closed shell of 2n electrons with paired spins, the best one-electron spatial orbitals are the solutions of the Hartree-Fock self consistent field (SCF) equation:

$$F\Phi_i = \varepsilon_i \Phi_i \tag{2-7}$$

The F is called the Fock operator and ε_i is the orbital energy or the one electron energy. In 1951, Roothaan treated the molecular systems by expanding the unknown molecular orbitals in terms of a fixed basis set χ_r to get:

$$\Phi_i = \sum_r C_{ri} \chi_r \tag{2-8}$$

This is a linear combination of atomic orbitals (LCAO-MO) method. The corresponding LCAO-MO-SCF equation for the closed-shell case was also proposed by Roothaan [51, 52] as:

$$FC = SC\varepsilon \tag{2-9}$$

where F is the Fock matrix, C is the matrix of expansion coefficients and S is the overlap matrix. Since the Fock matrix (F) is dependent on the coefficients C, an iterative procedure is needed to solve the Roothaan equation. Many calculations of barrier heights have been done with the LCAO-MO-SCF method.

For open shell systems, in which electrons are not completely assigned to orbitals in pairs, the Roothaan equation needs further modifications. Simple molecular orbital theory can be extended to open shell systems in two possible ways. The first is described as spin-restricted open-shell Hartree-Fock (ROHF) theory. In this approach, a single set of molecular orbitals is used, some being doubly occupied and some being singly occupied with an electron of α spin. The second type of molecular orbital theory in common use for open shell systems is spin-unrestricted Hartree-Fock (UHF) theory. In this approach, different spatial orbitals are assigned to α and β electrons. Thus, there are two distinct sets of molecular orbitals Ψ_i^{α} and Ψ_i^{β} ($i = 1,2,\ldots,n$). It is noticeable that the previously doubly occupied orbital is now replaced by two distinct orbitals: Ψ_i^{α} and Ψ_i^{β} [53].

In the Hartree-Fock method, the wave function of a closed-shell system of electrons is represented as one Slater determinant. The molecular orbitals are the solutions of one-electron equations with each electron moving in the 'average field' of all the other electrons. This is an independent particle model which neglects the correlation between the motions of electrons [54]. The incomplete description of the electron correlation is in fact the main deficiency of the Hartree-Fock theory. Even with large and nearly complete basis sets, the full solution of the Schrödinger equation cannot be expressed in terms of a single electron configuration. This limitation leads to calculated Hartree-Fock energies that are above the exact values.

To correct for that deficiency, it is necessary to use wave functions that are more powerful than the Hartree-Fock model functions. Such wave functions should represent

more than a single electron configuration. If Ψ_o is the full Hartree-Fock many-electron wave function, a more accurate wave function Ψ can be written in an approximated form as following:

$$\Psi = a_n\Psi_n + a_1\Psi_1 + a_2\Psi_2 + ... + a_n\Psi_n \qquad (2\text{-}10)$$

where Ψ_1, Ψ_2,..... Ψ_n are wave functions for other configurations and the linear coefficients a_o, a_1,....,a_n are to be determined. Inclusion of wave functions for all possible alternative electron configurations are referred as full configuration interaction.

2.3 MϕLLER-PLESSET PERTURBATION THEORY

A Hartree-Fock SCF wave function takes into account the interactions between electrons only in an average way [50]. However, we must consider the instantaneous interactions between electrons. Because electrons repel each other, they tend to keep away from each other. When the relative motion of electrons is correlated with each other, we speak of electron correlation in which the instantaneous electron correlation is introduced into the wave function.

Since the Hartree-Fock wave function satisfies the antisymmetry requirement of the Pauli principle, it, therefore, vanishes when two electrons with the same spin have the same spatial coordinates. For the Hartree-Fock function, there is a small probability of

finding electrons of the same spin in the same region of space, hence the Hartree-Fock function includes some correlation of the motion of electrons of the same spin.

By convention, the energy difference between the Hartree-Fock energy and the exact (nonrelativistic) energy is the correlation energy:

$$E_{(exact)} = E_{(Hartree-Fock)} - E_{(correlation)} \tag{2-11}$$

The neglect of correlation between electrons of opposite spin leads to a number of qualitative deficiencies in the description of electronic structures. There are different theoretical methods that were developed to overcome the correlation problem. The most economical general correlation methods are based on the perturbation theory of Møller-Plesset [55], which are formulated by first introducing a generalized Hamiltonian, $\hat{H}_\lambda$, according to:

$$\hat{H}_\lambda = \hat{H}_o + \lambda\hat{V} \tag{2-12}$$

Here, $\hat{H}_o$ is an operator such that the matrix with elements

$$\int\cdots\int \Psi_s \hat{H}_o \Psi_t d\tau_1 d\tau_2 \ldots d\tau\tau_n \tag{2-13}$$

is diagonal. The perturbation, $\lambda\hat{V}$, is defined by

$$\lambda\hat{V} = \lambda(\hat{H} - \hat{H}_o) \tag{2-14}$$

where $\hat{H}$ is the correct Hamiltonian and λ is a dimensionless parameter. Clearly, $\hat{H}_\lambda$ coincides with $\hat{H}_o$ if $\lambda = 0$, and with $\hat{H}$ if $\lambda = 1$. In the Møller-Plesset theory, the zero-order Hamiltonian, $\hat{H}_o$, is taken to be the sum of the one-electron Fock operators. The eigenvalue, E_s, corresponding to a particular determinant, Ψ_s, is the sum of the one-electron energies, ε_i, for the spin orbitals which are occupied in Ψ_s.

The exact or full configuration interaction ground-state wave function, Ψ_λ, and energy, E_λ, for a system described by the Hamiltonian, $\hat{H}_\lambda$, may now be expanded in powers of λ according to Rayleigh- Schrödinger perturbation theory,

$$\Psi_\lambda = \Psi^{(0)} + \lambda\Psi^{(1)} + \lambda^2\Psi^{(2)} + \ldots \qquad (2\text{-}15)$$

$$E_\lambda = E^{(0)} + \lambda E^{(1)} + \lambda^2 E^{(2)} + \ldots \qquad (2\text{-}16)$$

Practical correlation methods may now be formulated by setting the parameter $\lambda = 1$, and by truncation of the series in equation (2-16) to various orders. The energy $E^{(0)} + E^{(1)}$, correct to first order in the Møller-Plesset (MP) expansion, is identical to the Hartree-Fock energy. This is the unrestricted (UHF) result for the open-shell systems. The simplest approximation to the energy correction due to correlation is the second order quantity $E^{(2)}$. If the expansion is terminated here, the model may be described as MP2. The third- and the fourth-order methods may be denoted by MP3 and MP4, respectively.

Additionally, MP calculations truncated at any order can be shown to be size consistent. A size-consistent quantum mechanical method is one for which the energy and

hence the energy error in the calculation is proportional to the size of the molecule. Generally, the perturbation expressions are more satisfactory in determining correlation energies as compared to other methods, such as CID and CISD. On the other hand, perturbation theory results, terminated at any order, are no longer variational, since they are not derived as expectation values of the Hamiltonian.

2.4 DENSITY-FUNCTIONAL THEORY

Density-functional theory (DFT), in its various forms, has become an important research tool for chemists, physicists, as well as material scientists. The DFT model has undergone a great growth over the last decade and is successfully challenging traditional wave function-based methods as the technique of choice in large-scale quantum chemistry calculations [56,57]. As it has been discussed above, the conventional calculations of the properties of molecules is based on a description of the motion of individual electrons. For this reason, such methods are mathematically extremely complicated. However, in the case of the DFT method, it is not necessary to consider the motion of each electron; it is sufficient to know the average number of electrons located at any one point in space. In fact, this leads to a computationally simpler method that is the *density-functional theory*.

2.4.1 The DFT Fundamental Principles

Modern DFT has its fundamental roots in the theorem of Hohenberg and Kohn [58]. For an N-particles system interacting with a given interparticle interaction, the Hamiltonian and thus the ground-state wave function and energy are completely determined by specification of the external field $\phi(\mathbf{r})$. In other words, the ground state energy is a functional of $\phi(\mathbf{r})$. In a simple proof, Hohenberg and Kohn showed in 1964 that there is a one-to-one correspondence between the external field $\phi(\mathbf{r})$ and the single-particle density $\rho(\mathbf{r})$ and that as consequence it is possible to write the total ground-state energy as a functional of $\rho(\mathbf{r})$,

$$E[\rho] = E_a[\rho] + \int \phi(\mathbf{r})\rho(\mathbf{r})d\mathbf{r} \tag{2-17}$$

Here $E[\rho]$ is a function that is independent of the external potential, $\phi(\mathbf{r})$, i.e., it is a universal functional for a given interparticle interaction. Hohenberg and Kohn also proved a second theorem which provides an energy variational principle. They showed that for any trial density $\overline{\rho}(\mathbf{r})$ that satisfies $\int \rho(\mathbf{r})d\mathbf{r} = N$,

$$E[\overline{\rho}] \geq E_g \tag{2-18}$$

where E_g is the true ground-state energy.

The Hohenberg-Kohn theorems apply specifically to the ground-state energy and therefore apply strictly only at zero absolute temperature. Many applications require the extension of these theorems to non-zero temperatures. This was accomplished by Mermin [59] who showed that for a system at a fixed temperature, T, the chemical potential, μ, and external single-particle potential, $\upsilon(\mathbf{r})$, there exists a functional $\Theta[\rho(\mathbf{r})]$, independent of $\upsilon(\mathbf{r})$ and μ, such that the functional

$$\Omega[\rho(\mathbf{r})] = \Theta[\rho(\mathbf{r})] + \int d\mathbf{r}[\upsilon(\mathbf{r}) - \mu] \tag{2-19}$$

is a minimum for the correct equilibrium density $\rho(\mathbf{r})$ subject to the external potential. The value of Ω at this minimum is the grand potential.

2.4.2 DFT for Many Electron Systems

The basic notion in density-functional theory of many electron systems is that the energy of an electronic system can be expressed in terms of its density [56]. Kohn and Sham derived a set of one-electron equations from which one in principle could obtain the exact electron density and thus the total energy. The Kohn-Sham equation served as a starting point for new approximate DF methods. The total energy of an n-electron system can be written without approximations as

$$E_{el} = -\frac{1}{2}\sum_{i}\int \phi_i(\mathbf{r}_1)d\mathbf{r}_1 + \sum_{A}\frac{Z_A}{|\mathbf{R}_A - \mathbf{r}_1|}\rho(\mathbf{r}_1)d\mathbf{r}_1 + \frac{1}{2}\int\frac{\rho(\mathbf{r}_1)\rho(\mathbf{r}_2)}{|\mathbf{r}_1 - \mathbf{r}_2|}d\mathbf{r}_1 d\mathbf{r}_2 + E_{XC} \quad (2\text{-}20)$$

The first term in equation (2-20) represents the kinetic energy of n non-interacting electrons with the same density $\rho(\mathbf{r}_1)$. The second term accounts for the electron-nucleus attraction and the third term for the Coulomb interaction between the two charge distributions $\rho(\mathbf{r}_1)$ and $\rho(\mathbf{r}_2)$. The last term contains the exchange-correlation energy, E_{XC}.

The various SCF-schemes based on DFT are attractive alternatives to some common conventional methods in studies on large size molecules since the computational effort increases as n^3 with the number of electrons, n, as opposed to between n^4 and n^7 for post-HF methods of similar accuracy. The scope of density-functional based methods has further been enhanced to include pseudo-potentials, relativistic effects, as well as energy gradients of use in geometry optimization and analytical second derivatives with respect to nuclear displacements.

2.5 SELECTION OF BASIS SETS AND CORRECTION FUNCTIONS

An appropriate model has to be selected in order to link the molecular quantum-mechanical methods, like SCF, MP perturbation theory and DFT, with the computational

task to calculate specific molecular properties. The use of an adequate basis set to run the calculation procedure is an essential requirement for the work to succeed [53].

2.5.1 Gaussian-Type Functions

For diatomic molecules, the basis functions are usually taken as atomic orbitals; some centered on one atom, the remainder centered on the other atom; each atomic orbital can be represented as a linear combination of one or more Slater-Type Orbitals (STOs). For polyatomic molecules, the Linear Combination of Slater Type Orbitals (LC-STO) method uses STOs centered on each of the atoms. The presence of more than two atoms causes difficulties in evaluating the integrals needed. To simplify molecular integral evaluation, Boys proposed in 1950 the use of Gaussian-Type Functions (GTFs) instead of STOs for the atomic orbitals in an LCAO wave function [60]. The Cartesian Gaussian functions suggested by Boys was in the following form:

$$g(a, A, i, j, k) = N_{a,i,j,k}(x - x_A)^i (y - y_A)^j (z - z_A)^k e^{-a(r - R_A)^2} \qquad (2\text{-}21)$$

Here a is a positive parameter (orbital exponent), i, j and k are integers ≥ 0. Functions with $i = j = k = 0$ are referred to as s-type functions, functions with $i = 1, j = k = 0$ as p_x-type functions, etc. The parameter $N_{a,i,j,k}$ is a normalizing factor [61].

To get an accurate representation of an AO, a linear combination of several Gaussians must be used. Therefore, an LC-GTF SCF MO calculation involves the evaluation of much more integrals than the corresponding LC-STO SCF MO calculations,

since the number of two electron integrals is roughly proportional to the fourth power of the number of basis functions. However, Gaussian integral evaluation takes much less computer time than Slater integral evaluation. The Gaussian product theorem states only that the product of two Gaussians is equal to a linear combination of single Gaussians centered elsewhere and with different exponents. Thus all three and four-center two electron repulsion integrals are reduced to a linear combination of two center integrals each.

The development of the GTFs has gone through various levels of calculations. Some examples of the commonly used basis sets are the 3-21G, 6-21G, 6-31G* and the extended one employed in this work; the 6-311++G** basis set. The 3-21G and the 6-21G basis sets which are also termed as split-valence basis sets, describe the inner-shell atomic orbitals by a single contracted GTF centered at the nucleus. In the 6-21G basis set, each inner-shell AO is represented by a single function that is written in terms of six Gaussian primitives.

2.5.2 Polarization and Diffuse Functions

One feature common to the STO-3G (a minimal basis set), 3-21G and the 6-21G basis sets is that they comprise functions constrains to be centered at the nuclear positions. However, highly polar molecules and small strained rings require some allowance be made for the possibility of a nonuniform displacement of the charge away from the atomic centers. Without such allowance, comparison of properties between, for

example, small ring compounds and their acyclic isomers are likely to lead to unreliable results. A possible strategy to allow for small displacements of the center of the electronic charge away from the nuclear center is simply to include correction functions of higher angular quantum number (*d*-type functions on heavy atoms and *p*-type functions on hydrogen atoms) in the basis set. The *polarization basis set* provides for such displacement, that is, charge polarization [53].

For instance, the 6-31G* polarization basis set (defined for the atoms H through Ar) is constructed by the addition of a set of six-second order (*d*-type) gaussian primitives to the split-valence 6-31G basis set description of each heavy atom. Other examples are the 6-31G** and 6-311G** basis sets. In the former, a single set of gaussian *p*-type functions is added to the 6-31G* basis set. While the latter which is called the larger polarization basis sets is used with correlated wave functions.

Polarization function basis sets are more suitable for molecules in which the electrons are tightly held to the nuclear centers than they are for species with a significant electron density far removed from those centers. Thus, calculations involving anionic molecules or electrons allocated to antibonding orbitals are so deficient. This problem has been overcame by introducing highly *diffuse functions* that are capable to properly describe the long-range behavior of molecular orbitals with energies close to the ionization limit. It has been shown that the addition of diffuse functions has dramatic effects on calculated electron affinities, proton affinities and inversion barriers [53].

The 3-21+G and 6-31+G* basis sets are examples of basis sets having a single set of diffuse gaussains *s*-and *p*-type functions as compared to the corresponding 3-21G and

6-31G* sets. The highly extended basis set, 6-311++G**, was used throughout our investigation in this thesis in order to get more reliable results for describing the tested molecular systems.

2.6 NORMAL COORDINATE ANALYSES

A molecule possesses three types of internal energy. These are, in decreasing order, electronic, vibrational and rotational energies. Our scope in this section is forwarded to molecular vibrations that have their own interesting symmetry arguments. Every molecule at all temperatures, including even the absolute zero, is continuously executing vibrational motions, that is, motions in which its distances and internal angles keep changing without producing any net translation of the center of the mass of the molecule or imparting any net angular momentum (rotatory motion) to the molecule [62].

An important aspect of studying vibrational spectroscopy is to understand the forces that hold atoms together in a molecule [63,64]. The sum of these forces in a molecule is usually referred to as the molecular force field, and is mathematically described by the potential energy function. For simple molecules, the procedure can be reasonably applied without extreme difficulties. In the cases of molecules containing four or more atoms, however, the more powerful method that E. B. Wilson developed using techniques of the group theory allows a considerable simplification of the secular equation.

The secular determinantal equation derived by Wilson that is used is

$$|\mathbf{FG} - \mathbf{E}\lambda| = 0 \qquad (2\text{-}22)$$

The symbol **F** represents a symmetrical matrix whose elements are linear combinations of elementary force constants derived from the potential-energy expression. The symbol **G** represents a symmetrical matrix whose elements are linear combinations of geometrical parameters (bond distances and angles) derived from the kinetic-energy expression. The symbol **E** is a unit matrix and λ is a diagonal matrix having elements $\lambda_i = 4\pi^2 c^2 \omega_i^2$. In most of the cases, the observed vibrational frequencies, ω_i's, are used to generate, for a particular molecule, a set of f_{ii}'s contained in the **F** matrix.

2.6.1 Internal and Symmetry Coordinates

Symmetry coordinates can be constructed from the linear combinations of *internal coordinates*. Internal coordinates ($\mathbf{s}_i$'s) are displacements from equilibrium bond lengths (Δr_i's) and bond angles ($\Delta\theta_i$'s), as well as torsions and wags. Both the internal and the symmetry coordinates are chosen in such a way that they also provide a basis of for the various vibrational symmetry species or irreducible representations (Γ_{vib}'s). That is, the symmetry coordinates constructed ($\mathbf{S}_1, \mathbf{S}_2, \ldots$) must transform like the vibrational symmetry species ($\Gamma_1, \Gamma_2, \ldots$) under the group operations.

The symmetry coordinates for nondegenerate vibrations can be generated using the following expressions:

$$\mathbf{S}_j^{(\Gamma_i)} = N\sum_k \chi_k^{(\Gamma_i)} R\mathbf{s}_1 \qquad (2\text{-}23)$$

where $\mathbf{S}_j^{(\Gamma_i)}$ is the jth symmetry coordinate, Γ_i is the ith vibrational irreducible representation (symmetry species), N is a normalization constant, $\chi_k^{(\Gamma_i)}$ is the character of the kth operation belonging to the Γ_ith irreducible representation, and $R\mathbf{s}_1$ is the equivalent transformed coordinate resulting from the symmetry operation R. This sum needs to be applied to only as many of the group operations as are necessary to generate the different equivalent internal coordinates in each summation at least once.

The number of vibrational modes ($3N-6$ or $3N-5$) must be equal to the number of the symmetry coordinates.

2.6.2 The F and G Matrix

The potential energy in terms of symmetry coordinates is given by

$$2U = \sum_{ij} \mathbf{F}_{ij}\mathbf{S}_i\mathbf{S}_j \qquad (2\text{-}24)$$

where the $\mathbf{F}_{ij}$'s are the elements of the **F** matrix consisting of linear combinations of the f_{ij}'s. These elementary bond, angle and interaction force constants one wants to obtain. An equivalent way of expressing the potential energy above in matrix notation is:

$$2U = \mathbf{S'FS} \tag{2-25}$$

where **S** is a column matrix and **S'** is a row matrix, in terms of the internal coordinates; **S'** is the transpose of **S**. We need U in terms of **S** for maximum symmetry factoring and in terms of the f_{ij}'s for chemical and physical interpretation. The relation between the f_{ij}'s and **F** is:

$$\mathbf{F} = \mathbf{UfU'} \tag{2-26}$$

In the equation above the **U** and its transpose **U'** are used to symmetry-factor, the **f** matrix, which consists of the elements f_{ij}. The **f** matrix is generated by constructing a multiplication table of the internal coordinates.

In addition, the **G** matrix is constructed like the **F** matrix since

$$\mathbf{G} = \mathbf{UgU'} \tag{2-27}$$

where **g** is the matrix that contains elements in terms of the atomic masses and the geometrical parameters. Carrying out the same procedure as done above for the **F** matrix, the **G** matrix could be constructed from the symmetry factorization of the matrix **g**. The

elements of the **G** matrix are directly obtainable from the expression for the kinetic energy:

$$2T = \dot{\mathbf{S}}'\mathbf{G}^{-1}\dot{\mathbf{S}} \qquad (2\text{-}28)$$

The $\mathbf{G}^{-1}$ matrix is the inverse of the **G** matrix, $\dot{\mathbf{S}}$ is the time derivative of the symmetry coordinate matrix, and $\dot{\mathbf{S}}'$ is of the transpose.

2.7 METHODOLOGY AND COMPUTATIONS

2.7.1 Energy and Structural Parameter Optimizations

In most of our work, the GAUSSIAN 98 program [65] running on an IBM RS/6000 43P model 260 workstation, was used to carry out the LCAO-MO-SCF DFT-B3LYP calculations using the extended 6-311++G** basis set. Under the denotation B3LYP, Gaussian uses the B3 exchange function of Becke [66], while as correlation functional a combination of the Lee-Yang-Parr (LYP) [67] and the Vosko-Wilk-Nusair (VWN) [68] functionals is used. Only the calculations related to the first system of this study (formyl ketene) were performed using the GAUSSIAN 94 program [69] running on an IBM RS/6000 model 7015-R24 workstation, based on three different methods; the Restricted Hartree-Fock (RHF-SCF), the Second-Order Møller-Plesset (MP2) and the DFT-B3LYP, at the same basis set for the purpose of comparison.

The extended 6-311++G** basis set was employed to optimize the structures of the molecules under investigation and calculate their important chemical parameters, such as energies, rotational constants and dipole moments. The structural parameters of the molecules in their stable conformers were optimized by minimizing the energy with respect to all the geometrical parameters. The conformational stabilities were determined by comparing the calculated total energies. The calculated structural parameters are compared to those obtained from microwave or electron diffraction data for similar molecules.

2.7.2 Potential Surface Scan

A potential surface scan for the internal rotation about the C-C (in the case of ketenes) or the C-N (in the case of isocyanates) single bonds was obtained by allowing the CCCO or the CNCO dihedral angle (ϕ) to vary from 0° (*cis* position) to 180° (*trans* position) by 15° increments. Full geometry optimizations at each of the fixed dihedral angle (ϕ) of angles, 15°, 30°, 45°, 60°, 75° 90°, 105°, 120°, 135°, 150° and 165° were carried out at DFT-B3LYP/6-311++G** level of calculations. The barriers to interconversion in all the molecules were calculated. The torsional potential was represented as a Fourier cosine series in the dihedral angle (ϕ):

$$V(\phi) = V_o + \sum_{n=1}^{6} \frac{V_n}{2}(1 - \cos(n\phi)) \qquad (2\text{-}29)$$

where V_n is the potential coefficient of the *cis* conformation, and the potential coefficients from V_1 to V_6 are considered adequate to describe the potential function [70]. The results of the energy optimizations were used to calculate the six coefficients by least-squares fitting.

2.7.3 Vibrational Frequencies and Normal Coordinate Analyses

Normal coordinate analyses were carried out for the stable conformers of the molecules in order to provide a complete assignment of the fundamental vibrational frequencies. A computer program was written for this purpose by following Wilson's method [71]. The cartesian coordinates for the stable conformers together with the normal modes (in cartesian coordinates) and the frequencies from the GAUSSIAN 98 output were used as an input in the program. A complete set of internal coordinates was used to form symmetry coordinates for each molecular system.

The normal modes were next transformed to mass-weighted cartesian coordinates, which were then used to calculate the force constant matrix. This was diagonalized and its eigenvectors and eigenvalues were used in the further calculations. Following this step the force constant matrix was transformed to internal coordinates. To ensure correctness, this transformation was checked numerically in both directions. At this point the force constant matrix in internal coordinates could be scaled if desired, back-transformed to mass weighted cartesians and diagonalized again to get scaled frequencies and normal modes. The matrix was finally transformed to symmetry coordinates where again all

possible numerical checks were performed. In the next step the normal modes were also transformed to symmetry coordinates.

2.7.4 Potential Energy Distributions

The potential energy distribution (PED) for each normal mode among the symmetry coordinates was calculated and shown for each symmetry coordinate. The potential energy distribution (E_υ) was determined from the following equation

$$E_\upsilon = \frac{1}{2}\sum_{i,j} f_{ij}\mathbf{S}_i\mathbf{S}_j \qquad (2\text{-}30)$$

where f_{ij} is an **F**-matrix element.

The proposed vibrational assignments of the fundamental frequencies were made based on the calculated PED values, as well as the infrared band intensities, Raman line activities and depolarization ratios.

2.7.5 Calculation of the Vibrational Spectra

The vibrational infrared and Raman wavenumbers (ν_i's) were taken from the Gaussian 98 outputs. To calculate the Raman spectra we used the frequencies ν_i, the scattering activities S_i and the depolarization ratios ρ_i as calculated at the DFT-B3LYP level (6-311++G** basis set for all) in most of our work as mentioned earlier. Then, the

Raman cross-sections ($\partial\sigma_i/\partial\Omega$), which are proportional to the intensities [72,73], are given as:

$$\frac{\partial\sigma_i}{\partial\Omega} = \frac{2^4\pi^4}{45}(\nu_o - \nu)^4\left(\frac{h}{8\pi^2 c\nu_i}\right)S_i\left\{\frac{(1-\rho_i)/(1+\rho_i)}{1-e^{(-hc\nu_i/k_BT)}}\right\} \qquad (2\text{-}31)$$

Since we use only relative intensities, we calculated them as:

$$I_i = \frac{(\partial\sigma_i/\partial\Omega)}{(\partial\sigma_{jm}/\partial\Omega)} \qquad (2\text{-}32)$$

where *jm* denotes the normal mode having the largest Raman cross-section. The laser wavelength we took $\lambda_o = 514.5$ nm ($\nu_o = 1/\lambda_o$) which corresponds to an argon ion laser. If more than one stable conformer was predicted, the temperature was assumed to be $T =$ 300 K.

Then the line shapes are calculated as Lorentzians (L) with a width of $\Delta\nu = 12$ cm^{-1}. Thus, the final spectrum is calculated as:

$$I(\nu) = \sum_i I_i L(\nu - \nu_i) \qquad (2\text{-}33)$$

$$L(\nu - \nu_i) = \left(\frac{1}{\pi}\right)\left(\frac{\Delta\nu}{2}\right)\Big/\left[(\nu - \nu_i)^2 + \left(\frac{\Delta\nu}{2}\right)^2\right] \qquad (2\text{-}34)$$

$$\int_{-\infty}^{+\infty} L(\nu)d\nu = 1 \qquad (2\text{-}35)$$

where j runs over all normal modes. For the plots we used a grid of a step size of 10 cm^{-1}, but not when a spectral line appears between two consecutive grid points. In this case we inserted 12 points with step size of 0.5 cm^{-1} into this interval which include the exact location of the center of the line. For the infrared spectrum we used the intensities as given by the DFT-B3LYP/6-311++G** calculations and converted them to relative transmittance.

In the case that we have two or more stable conformations, the Boltzmann Distribution was used to superimpose the spectra of the stable conformers of the molecule. Accordingly, the total line intensity was calculated as a function of frequency. For $N + 1$ different energy minima we have:

$$I(\nu) = \frac{\sum_{l=0}^{N} g_l I_l(\nu) e^{-\Delta E_l / k_B T}}{\sum_{l=0}^{N} g_l e^{-\Delta E_l / k_B T}} \qquad (2\text{-}36)$$

where $I_l(\nu)$ are the line intensities for the respective minima, $\Delta E_l = E_l - E_0$, and g_l is a degeneracy factor, which is unity for the planar *cis* and *trans* conformers while is two for the non-planar *gauche* conformers. Additionally, E_l represents the total energy of conformer l corrected with the corresponding zero-point energy. The label $l = 0$ is given to the lowest energy conformer.

CHAPTER 3

AN INVESTIGATION OF STRUCTURAL STABILITY AND ANALYSIS OF VIBRATIONAL SPECTRA OF FORMYL KETENE BASED ON AB INITIO CALCULATIONS

3.1 INTRODUCTION

In the past few years the structural stability of some unsaturated aldehydes [17,30,36,74-84] have been investigated. The reactivity of these compounds in synthetic organic and in polymer chemistry has attracted the attention to study their conformational behavior.

When conjugation was the predominant force, the molecules were determined to exist as a mixture of the planar s-*cis* and s-*trans* conformations with a relatively high rotational barrier. For example, propenal [74,75], 2-methylpropenal [76], 2,3-dimethyl-propenal [78,79], and 2,3-butadienal [36,77], all were found to exist as s-*cis* $\Leftrightarrow$ s-*trans* conformational equilibrium. In these compounds, the π-π interaction between the C=O bond

of the carbonyl group and the substituent of the vinyl or 1,2-butadiene groups greatly stabilizes the planar forms.

For cyanoacetaldehyde [17], 3-butynal [81,82], and isocyanatoacetaldehyde [83], in which there is no longer π-π interaction between the substituents, the nonplanar *gauche* form was determined to be one of the thermodynamically preferred conformation.

Additionally, some theoretical investigations were performed on 3-cyclopropenecarboxaldehyde [83] and 4-cyclopentenecarboxaldehyde [84] as examples of unsaturated cyclic aldehydes. In the case of the 3-cyclopropenecarboxaldehyde, the repulsive interaction between the charge distributions of the double bond in the ring and a lone pair orbital at oxygen stabilized the *trans* form relative to the *cis* conformer [83]. The case of the corresponding five-membered ring was different, in which 4-cyclopentenecarboxaldehyde was predicted to exist in a complex mixture of both axial and equatorial conformations at ambient temperature [84].

We investigated the structure of formyl ketene and carried out normal coordinate calculations by utilizing ab initio calculations. The rotational barrier for the internal rotation in the molecule was calculated and the potential energy distributions among symmetry coordinates were derived. The vibrational assignments of the normal modes were made for the *cis* and *trans* conformations of the molecule. The results of the work are presented in the rest of this chapter.

3.2 AB INITIO CALCULATIONS

The GAUSSIAN 94 program [69] running on an IBM RS/6000 model 7015-R24 workstation, was used to carry out the LCAO-MO-SCF Restricted Hartree-Fock calculations. The extended 6-311++G** basis set was employed to optimize the structures and predict the energies and dipole moments of formyl ketene in its stable conformations. The calculations were extended to the Density Functional B3LYP level. From full energy optimization the *cis* and the *trans* conformations (Figure III-1) were found to be the energy minima for the molecule. The optimized structural parameters that are shown in Table III-1 were used to compute their vibrational frequencies at the HF/6-311++G** and DFT-B3LYP/6-311++G** levels of calculation. Normal coordinate calculations were then used to derive the potential energy distributions for the molecule.

3.2.1 Asymmetric Torsional Potential Function

The potential scan for the internal rotation about the C-C single bond was obtained by allowing the OCCC dihedral angle (ϕ) to vary from 0° (*cis* position) to 180° (*trans* position). Full geometry optimizations at each of the fixed dihedral angle (ϕ) of, 15°, 30°, 45°, 60°, 75°, 90°, 105°, 120°, 135°, 150°, and 165° were carried out at the three levels of calculations. The barrier to interconversion in the molecule was calculated and listed in

Table III-2. The torsional potential was represented as a Fourier cosine series in the dihedral angle (ϕ): $V(\phi) = V_0 + \sum(V_n/2)[1-\cos(n\phi)]$, where the potential coefficients from V_1 to V_6 are considered adequate to describe the potential function. The results of the energy optimizations were used to calculate the six coefficients by least-squares fitting (Table III-3). The potential function is shown in Figure III-2.

3.2.2 Vibrational Frequencies and Normal Coordinate Analyses

Formyl ketene in the *cis* and *trans* conformations has C_s symmetry. The 15 vibrational modes span the irreducible representations: 11 A' and 4 A". The A' modes should be polarized while the A" modes be depolarized in the Raman spectra of the liquid.

Normal coordinate analyses were carried out for the stable *cis* and *trans* conformers of the molecule in order to provide a complete assignment of the fundamental vibrational frequencies. A computer program was written for this purpose by following Wilson's method [71]. The cartesian coordinates for the stable conformers together with the normal modes (in cartesian coordinates) and the frequencies from the Gaussian 94 output were used as input in the program. A complete set of internal coordinates (Table III-4 and Figure III-1) was used to form symmetry coordinates (Table III-5).

The potential energy distribution (PED) for each normal mode among the symmetry coordinates was calculated and is given in Tables III-6 and III-7. A complete vibrational assignment of the fundamentals was proposed. The assignments were made based on

calculated PED, infrared band intensities, Raman line activities and depolarization ratios. The data of the vibrational assignments are listed in Tables III-6 and III-7.

3.2.3 Calculation of Vibrational Spectra

To calculate the Raman spectrum we used the frequencies ν_j as calculated on DFT-B3LYP level (6-311++G** basis set for all), while the scattering activities S_j, and the depolarization ratios ρ_j are only available on RHF level. Then we followed the procedure shown in the methodology section of chapter two in this thesis. For the infrared spectrum we used the intensities as given by the DFT-B3LYP/6-311++G** calculations and converted them to relative transmittance.

The Boltzmann Distribution was then used to superimpose the spectra of the *cis* and the *trans* conformers of the molecule. Accordingly, the total line intensity was calculated by following equation (2-36). For formyl ketene, the values of the degeneracy factor (g_i) are unity. For the temperature, $T = 300\ K$ was used. The calculated vibrational Raman and infrared spectra of the mixture of the two conformers are shown in Figures III-3 and III-4. The mixture at 300 K was calculated to contain 66% *trans* and 34% *cis* conformer.

3.3 DISSCUSION

The conformational equilibrium and structure of propenal, 2,3 butadienal, and their halo derivatives and also of polynes were of a great interest to many researchers for many years [36,77-79,82,85]. The chemical reactivity of ketenes particularly in organic chemistry [47,86] initiated the present work to investigate the structure and vibrational spectra of formyl ketene. As mentioned earlier, the conjugation effect in such conjugated systems stabilizes the planar s-*cis* and s-*trans* forms and considerably hinders the internal rotation of the CHO rotor in this compound [36]. This leads to a high rotational barrier as compared to those in the saturated analogues. In the case of propanal the *gauche* form was determined to be the second stable conformer [87]. The 2,3-butadienal was indeed determined to have the s-*trans* for the lower energy conformer with relatively high *trans* to *cis* barriers.

In a similar way formyl ketene was predicted by all levels to exist only in the planar form as shown in Figure III-2. From the energy optimization at HF level and MP2, the *cis* conformer was calculated to be slightly more stable than the *trans* conformer. However, at the DFT-B3LYP level the conformational behavior was reversed, and the *trans* became the thermodynamically more preferred conformation for formyl ketene. This behavior is more consistent with the idea that eclipsing the two hydrogens in the *cis* form should destabilize the molecule in this conformation. For the molecule, the carbonyl oxygen and not the aldehydic hydrogen should eclipse the ketenic hydrogen in the *trans* conformation of the molecule.

From the calculations, a difference of about 1.0 Debye was noticed between the dipole moments of the two stable conformers of formyl ketene. This difference indicates a significant charge density variation with the rotation of the carbonyl group about the C-C bond. Therefore, the dipolar effects are expected to play an important role in the determination of the conformational and structural stability of such type of molecules. Hence, the rotation of the CHO group should influence the π character of the double bond, especially, when it is close to planarity. This is consistent with the change in the calculated structural parameters of the -CHO group as going from the *cis* to the *trans* conformer as shown in Table III-1.

The vibrational wavenumbers of formyl ketene in the *trans* and the *cis* conformers were calculated and vibrational infrared and Raman spectra were plotted in Figures III-3 and III-4. The vibrational assignments of most of the fundamental vibrations of the two conformers were straightforward based on the calculated PED as shown in Tables III-6 and III-7. Some of the calculated modes were predicted to be mixed with other modes.

There are two stretches that are associated with C-H modes (S_1 and S_2). These stretches were calculated to have the highest Raman activities in the Raman spectra of the molecule (Tables III-6 and III-7). The C=O stretching mode (S_3) was calculated to have a small degree of mixing for the *cis* (PED of 89%) and the *trans* (PED of 90%) conformers. The assignment of this fundamental vibration was straightforward to the line with the second highest line intensity in the infrared spectra of the molecule (Tables III-6 and III-7).

The mode with the highest infrared intensity was calculated to have a PED of 94% antisymmetric -C=C=O stretch. This is very interesting because the antisymmetric -C=C=O stretching mode (S_5) has the greatest induced dipole moment upon its vibration. This is very consistent with the same vibration of the -N=C=O group in chloro- and fluorocarbonyl isocyanate [72,88]. On the other hand, the symmetric -C=C=O stretch (S_6) was assigned to the calculated line at 1332 cm^{-1} with PED value of 40% in the spectrum of the *trans*-formyl ketene.

The C-C stretch S_4 (62% PED) of the *cis* conformer was calculated at 943 cm^{-1} (DFT-B3LYP). This mode was predicted to be highly mixed in the case of the *trans* conformer. Additionally, the four CCO bending modes were calculated to be mixed with others for both conformers, but their assignments were clear based on PED values. The lowest A" vibrational mode in the spectra of formyl ketene is the asymmetric torsion. This mode (ν_{15}) is predicted to be at 221 and 152 cm^{-1} in the spectra of the *cis* and the *trans* conformers respectively.

From the calculations, it was obvious upon comparison that all frequencies in the RHF spectra are much higher than those in the MP2 and the DFT/B3LYP spectra. The MP2 and the DFT do not differ too much in the region of the frequencies below 2000 cm^{-1}. Most of the DFT lines are slightly below the respective MP2 lines. However, a few appear also to be shifted slightly upward by DFT. It is clear from the comparison that MP2 does not shift downwards the CH stretches from their RHF values appreciably, but DFT does.

Furthermore, comparative studies on different molecules have been published in the literature (see reference [89] and references therein). Calculations on 32 different molecules using a 6-31G* basis and the BLYP functional in DFT show that, while bond lengths and angles are given slightly better by MP2 than by DFT (compared to experiment), dipole moments, harmonic frequencies and atomization energies are given better by DFT than by MP2 [25]. The mean absolute errors reported in that study on 32 molecules [90] are 0.020 Å (DFT) and 0.014 Å (MP2) for bond lengths, 2.33° (DFT) and 1.78° (MP2) for bond angles, 0.251 D (DFT) and 0.277 D (MP2) for dipole moments, 73 cm^{-1} (DFT) and 99 cm^{-1} (MP2) for harmonic frequencies, and 5.6 Kcal/mol (DFT) and 22.4 Kcal/mol (MP2) for atomization energies. Note that for that study a 6-31G* basis and DFT/BLYP were applied, while we used the improved 6-311++G** and DFT/B3LYP. Furthermore, note that while MP2 frequencies were generally too high, the DFT/BLYP values were mostly too low. Finally, a comparison between the calculated potential energy distribution values calculated by DFT-B3LYP/6-311++G** basis set and those obtained by RHF/6-31G* basis set, clearly shows a noticeable change. Therefore, one should use the data obtained by the higher level of calculations to obtain more reliable PED results. Thus, we decided to use the PED values given by the DFT for the future work in this thesis.

TABLE III-1: **Structural Parameters, Total Dipole Moment, and Rotational Constants of *Cis* and *Trans* Conformers of Formyl Ketene.**

Parameter	HF/6-311++G**		MP2/6-311++G**		B3LYP/6-311++G**	
	cis	*trans*	*cis*	*trans*	*cis*	*trans*
Bond Lengths (Å)						
r (C_1-C_2)	1.461	1.462	1.463	1.463	1.466	1.465
r (C_2-C_3)	1.325	1.319	1.339	1.335	1.328	1.324
r (C_3-O_4)	1.123	1.127	1.159	1.162	1.150	1.154
r (C_2-H_5)	1.072	1.073	1.082	1.083	1.082	1.083
r (C_1-O_6)	1.189	1.185	1.222	1.219	1.212	1.211
r (C_1-H_7)	1.093	1.096	1.106	1.109	1.107	1.107
Bond Angles (deg)						
($C_1C_2C_3$)	119.2	120.3	118.3	120.0	120.6	121.4
($C_2C_3O_4$)	179.5	179.7	178.8	178.8	179.0	178.6
($C_1C_2H_5$)	123.0	121.6	123.1	121.3	121.3	120.0
($C_2C_1O_6$)	125.0	123.7	125.2	123.4	125.9	123.3
($C_2C_1H_7$)	113.9	115.5	113.6	115.4	112.9	115.5
($C_3C_2C_1O_6$)	0.0	180.0	0.0	180.0	0.0	180.0

TABLE III-1: **Continue**

Parameter	HF/6-311++G**		MP2/6-311++G**		B3LYP/6-311++G**	
	cis	*trans*	*cis*	*trans*	*cis*	*trans*
Dipole Moment (Debye)						
μ_t	3.7	2.6	4.1	2.6	3.5	2.4
Rotational Constants (MHz)						
A	15531	43738	14538	42281	15219	43498
B	3602	2520	3591	2454	3485	2459
C	2924	2383	2880	2319	2836	2328

TABLE III-2: **Computed Total Energies, Zero-Point Corrections (Hartrees), Relative Energy, and Rotational Barriers (kcal/mol) in Formyl Ketene.**

HF/6-311++G**			MP2/6-311++G**			B3LYP/6-311++G**		
cis	*trans*	*TS*	*cis*	*trans*	*TS*	*cis*	*trans*	*TS*
Total energy								
-264.53222	-264.53144	-264.51290	-265.31934	-265.31917	-265.30033	-266.01211	-266.01263	-265.99252
Relative energy	0.4895			0.1067			0.3263	
Cis-trans barrier	12.1235			11.9290			12.2929	
Trans-cis barrier	11.6340			11.8223			12.6192	
Sum of total and zero point energies								
-264.48598	-264.48535	-264.46781	-265.27656	-265.27647	-265.25879	-265.96937	-265.96999	-265.95112
Zero-point correction								
0.04624	0.04609	0.04509	0.04278	0.04270	0.04154	0.04274	0.04264	0.04140
Corrected relative energy	0.3953			0.0565			0.3891	
Corrected cis-trans barrier	11.4019			11.1509			11.4521	
Corrected trans-cis barrier	11.0065			11.0944			11.8411	

TABLE III-3: **Calculated Potential Constants (kcal/mol) for the Asymmetric Torsion in Formyl Ketene.**

Potential Constants	6-311++G**		
	HF	MP2	DFT
V_1	0.887	0.456	0.165
V_2	11.854	11.875	12.546
V_3	-0.399	-0.326	-0.291
V_4	0.030	-0.180	-0.304
V_5	0.000	-0.023	0.103
V_6	0.002	-0.012	0.170

TABLE III-4: **Internal Coordinate Definitions [a] for Formyl Ketene.**

No.	Coordinate		Definition
1	C_1-C_2	stretch	R
2	C_2-C_3	stretch	P
3	C_3-O_4	stretch	Q
4	C_1-O_6	stretch	S
5	C_1-H_7	stretch	T
6	C_2-H_5	stretch	D
7	$C_1C_2C_3$	bend	β
8	$C_2C_3O_4$	bend	σ
9	$C_2C_1O_6$	bend	ε
10	$C_2C_1H_7$	bend	ϕ
11	$H_7C_1O_6$	bend	θ
12	$C_1C_2H_5$	bend	ρ
13	$C_3C_2H_5$	bend	δ
14	C_2=C_3=O_4	wag	χ
15	$H_7C_1C_2O_6$	wag	ω
16	$H_5C_1C_2C_3$	wag	π
17	$O_6C_1C_2C_3$	torsion	τ
	$H_7C_1C_2C_3$	torsion	

[a] For atom denotation see Figure III-1.

TABLE III-5: **Symmetry Coordinates for Formyl Ketene.**

Species	Description		Symmetry Coordinate [a]
A'	C-H	stretch	$S_1 = D$
	$C\text{-}H_{ald}$	stretch	$S_2 = T$
	C=O	stretch	$S_3 = S$
	C-C	stretch	$S_4 = R$
	C=C=O	antisymmetric stretch	$S_5 = P - Q$
	C=C=O	symmetric stretch	$S_6 = P + Q$
	C=C-H	in-plane bend	$S_7 = \rho - \delta$
	$C\text{-}H_{ald}$	in-plane bend	$S_8 = \phi - \theta$
	C-C=O	in-plane bend	$S_9 = \phi + \theta - 2\varepsilon$
	C=C-C	in-plane bend	$S_{10} = 2\beta - \rho - \delta$
	C=C=O	in-plane bend	$S_{11} = \sigma$
A''	C=C-H	out-of-plane bend (wag)	$S_{12} = \pi$
	$C\text{-}H_{ald}$	out-of-plane bend (wag)	$S_{13} = \omega$
	C=C=O	out-of-plane bend (wag)	$S_{14} = \chi$
	CHO	Asymmetric torsion	$S_{15} = \tau$

[a] Not normalized.

TABLE III-6: **Calculated Vibrational Frequencies (cm^{-1}) at HF/6-311++G**, MP2/6-311++G**, and B3LYP/6-311++G** Levels for the *Cis* Conformer of Formyl Ketene.**

Symm.	No.	HF					MP2		B3LYP		PED[b]
		Freq.	Scaled[a]	IR Int.	Raman Act.	Depol. Ratio	Freq.	IR Int.	Freq.	IR Int.	
A'	ν_1	3376	3038	10.3	75.5	0.2	3268	13.7	3204	12.0	99% C-H str. (S_1).
	ν_2	3147	2832	92.7	143.1	0.3	2999	103.4	2923	104.5	100% C-H_{ald} str. (S_2).
	ν_3	2386	2147	1258.2	16.0	0.7	2219	690.3	2230	852.3	94% C=C=O antisym. str. (S_5).
	ν_4	1927	1734	429.8	32.6	0.4	1712	262.6	1738	346.9	89% C=O str. (S_3).
	ν_5	1535	1381	17.9	5.9	0.2	1431	2.4	1418	10.0	87% C-H_{ald} in-plane bend (S_8).
	ν_6	1507	1356	279.8	15.7	0.2	1399	215.2	1389	220.3	32% C=C=O sym. str. (S_6), 32%C-C=O in-plane bend (S_7), 23% C-C str. (S_4).
	ν_7	1201	1081	19.4	17.4	0.2	1108	3.5	1120	1.7	55% C=C-H in-plane bend (S_7), 34% C=C=O sym. str. (S_6).
	ν_8	1023	921	39.2	5.8	0.03	962	42.8	943	40.1	62% C-C str. (S_4), 11% C=C=O sym. str. (S_6).
	ν_9	867	780	59.9	9.2	0.3	797	35.8	799	49.7	42% C=C-C in-plane bend (S_{10}), 20% C-C=O in-plane

TABLE III-6: **Continue.**

Symm.	No.	HF					MP2		B3LYP		PED[b]
		Freq.	Scaled[a]	IR Int.	Raman Act.	Depol. Ratio	Freq.	IR Int.	Freq.	IR Int.	
											bend (S_9), 18% C=C=O in-plane bend, (S_{11}), 13% C=C=O sym. str. (S_6),
	ν_{10}	524	472	15.6	1.2	0.2	463	4.2	462	2.5	49% C=C=O in-plane bend (S_{11}), 39% C=C-C in-plane bend (S_{10}).
	ν_{11}	163	147	3.9	3.0	0.6	142	2.7	146	3.1	68% C-C=O in-plane bend (S_9), 21% C=C=O in-plane bend (S_{11}), 10% C=C-C in-plane bend (S_{10}).
A"	ν_{12}	1131	1018	4.4	5.1	0.8	998	0.0	1006	0.4	97% C=C-H wag (S_{12}).
	ν_{13}	681	613	55.8	2.4	0.8	576	2.5	599	38.8	76% C-H_{ald} wag (S_{13}), 18% C=C=O wag (S_{14}).
	ν_{14}	595	535	43.4	0.7	0.8	498	66.1	563	26.3	82% C=C=O wag (S_{14}), 13% C-H_{ald} wag (S_{13}).
	ν_{15}	235	211	9.6	1.0	0.8	208	10.1	221	6.3	92% CHO asym. tor. (S_{15}), 11% C-H_{ald} wag (S_{13}).

[a] Scaled Frequencies are obtained with factors of 0.9 for all modes. Infrared intensities and Raman activities are calculated in Km mol^{-1} and $Å^4$ amu^{-1} respectively.

[b] PED values are obtained by using calculated frequencies at B3LYP level.

TABLE III-7: **Calculated Vibrational Frequencies (cm^{-1}) at HF/6-311++G**, MP2/6-311++G**, and B3LYP/6-311++G** Levels for the *Trans* Conformer of Formyl Ketene.**

Symm.	No.	HF					MP2		B3LYP		PED[b]
		Freq.	Scaled[a]	IR Int.	Raman Act.	Depol. Ratio	Freq.	IR Int.	Freq.	IR Int.	
A'	ν_1	3366	3029	17.5	69.4	0.2	3254	22.4	3196	19.7	100% C-H str. (S_1).
	ν_2	3114	2803	76.4	91.1	0.4	2964	82.1	2915	84.1	100% C-H_{ald} str. (S_2).
	ν_3	2373	2136	1298.4	18.2	0.7	2211	750.0	2220	889.1	95% C=C=O antisym. str. (S_5).
	ν_4	1949	1754	770.8	73.0	0.3	1725	419.9	1746	574.3	90% C=O str. (S_3).
	ν_5	1577	1419	20.5	1.6	0.5	1462	9.6	1448	12.1	71% C-H_{ald} in-plane bend (S_8), 10% C=C=O sym. str. (S_6).
	ν_6	1444	1300	42.6	19.3	0.2	1330	50.6	1332	43.3	40% C=C=O sym. str. (S_6), 22% C-H_{ald} in-plane bend (S_8), 22% C=C-H in-plane bend (S_7), 10% C-C str. (S_4).
	ν_7	1202	1082	119.7	17.9	0.5	1136	123.6	1121	60.9	54% C=C-H in-plane bend (S_7), 27% C-C str. (S_4), 11% C=C=O sym. str. (S_6).
	ν_8	1185	1066	68.1	11.0	0.1	1092	21.0	1087	97.6	28% C-C str. (S_4), 23% C=C=O sym. str. (S_6), 14%

TABLE III-7: **Continue.**

Symm.	No.	HF					MP2		B3LYP		PED[b]
		Freq.	Scaled[a]	IR Int.	Raman Act.	Depol. Ratio	Freq.	IR Int.	Freq.	IR Int.	
											C=C-C in-plane bend (S_{10}), 12% in-plane bend (S_9), 11% C=C=O in-plane bend (S_{11}), 10% C=C-H in-plane bend (S_7).
	ν_9	679	611	6.8	4.3	0.1	614	6.9	616	13.4	49% C=C=O in-plane bend (S_{11}), 21% C-C=O in-plane bend (S_9), 21% C-C str. (S_4).
	ν_{10}	537	483	14.5	2.8	0.2	496	12.4	498	14.4	70% C=C-C in-plane bend (S_{10}).
	ν_{11}	192	173	18.9	1.7	0.6	169	10.3	173	11.9	66% C-C=O in-plane bend (S_9), 29% C=C=O in-plane bend (S_{11}).
A"	ν_{12}	1120	1008	2.6	3.5	0.7	997	0.0	998	0.0	99% C=C-H wag (S_{12}).
	ν_{13}	688	619	99.3	3.5	0.7	599	47.1	642	65.6	103% C=C=O wag (S_{14}).
	ν_{14}	644	580	3.6	2.0	0.7	550	30.6	572	6.1	97% C-H_{ald} (S_{13}).
	ν_{15}	162	146	11.8	0.4	0.7	144	4.7	152	8.5	94% CHO asym. tor. (S_{15}).

[a] Scaled Frequencies are obtained with factors of 0.9 for all modes. Infrared intensities and Raman activities are calculated in Km mol^{-1} and $Å^4$ amu^{-1} respectively.

[b] PED values are obtained by using calculated frequencies at B3LYP level.

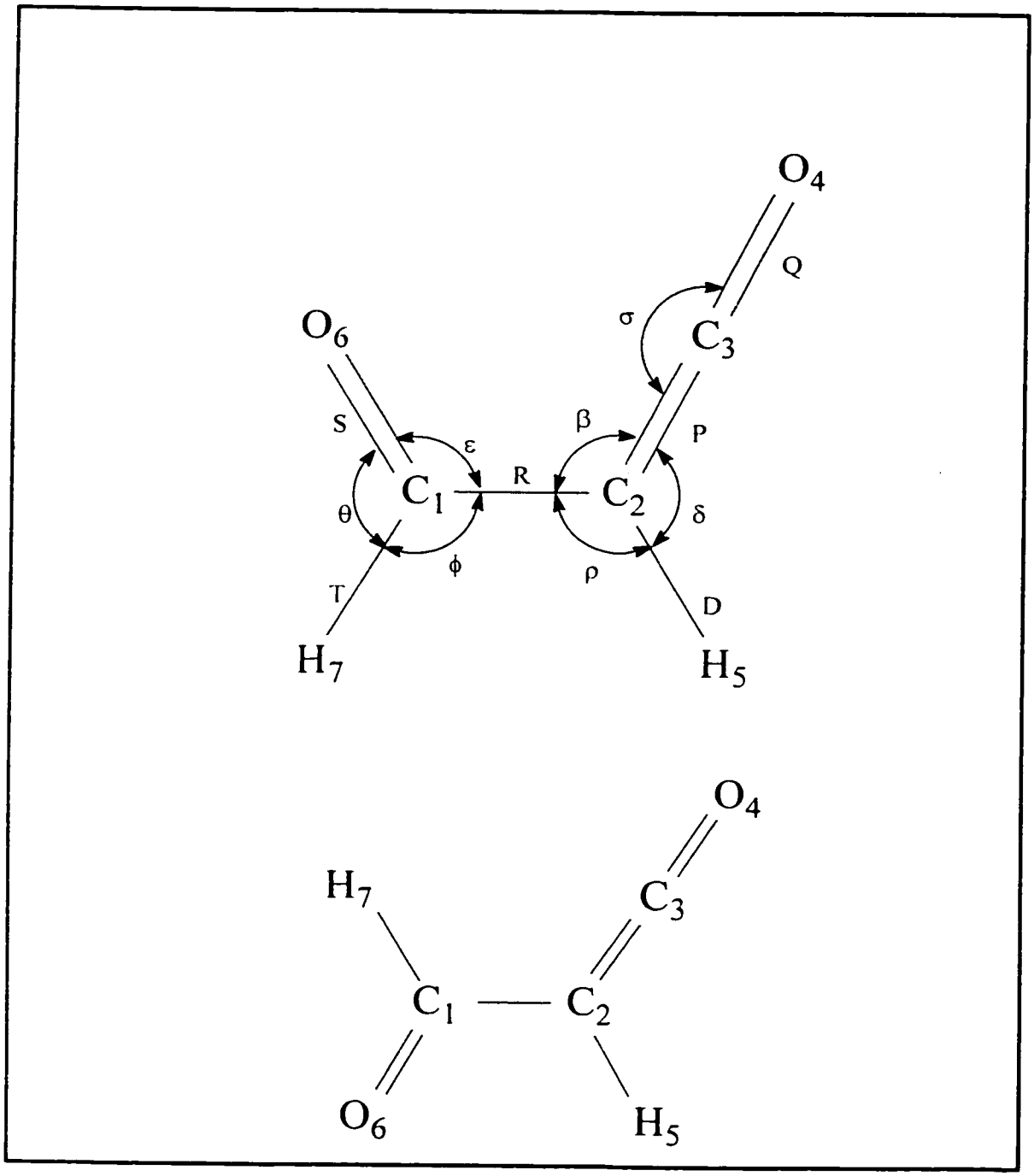

FIGURE III-1: **Atom Numbering for Formyl Ketene in the *Cis* (Upper) and the *Trans* (Lower) Conformations, with the Internal Coordinates Shown on the *Cis* Conformation.**

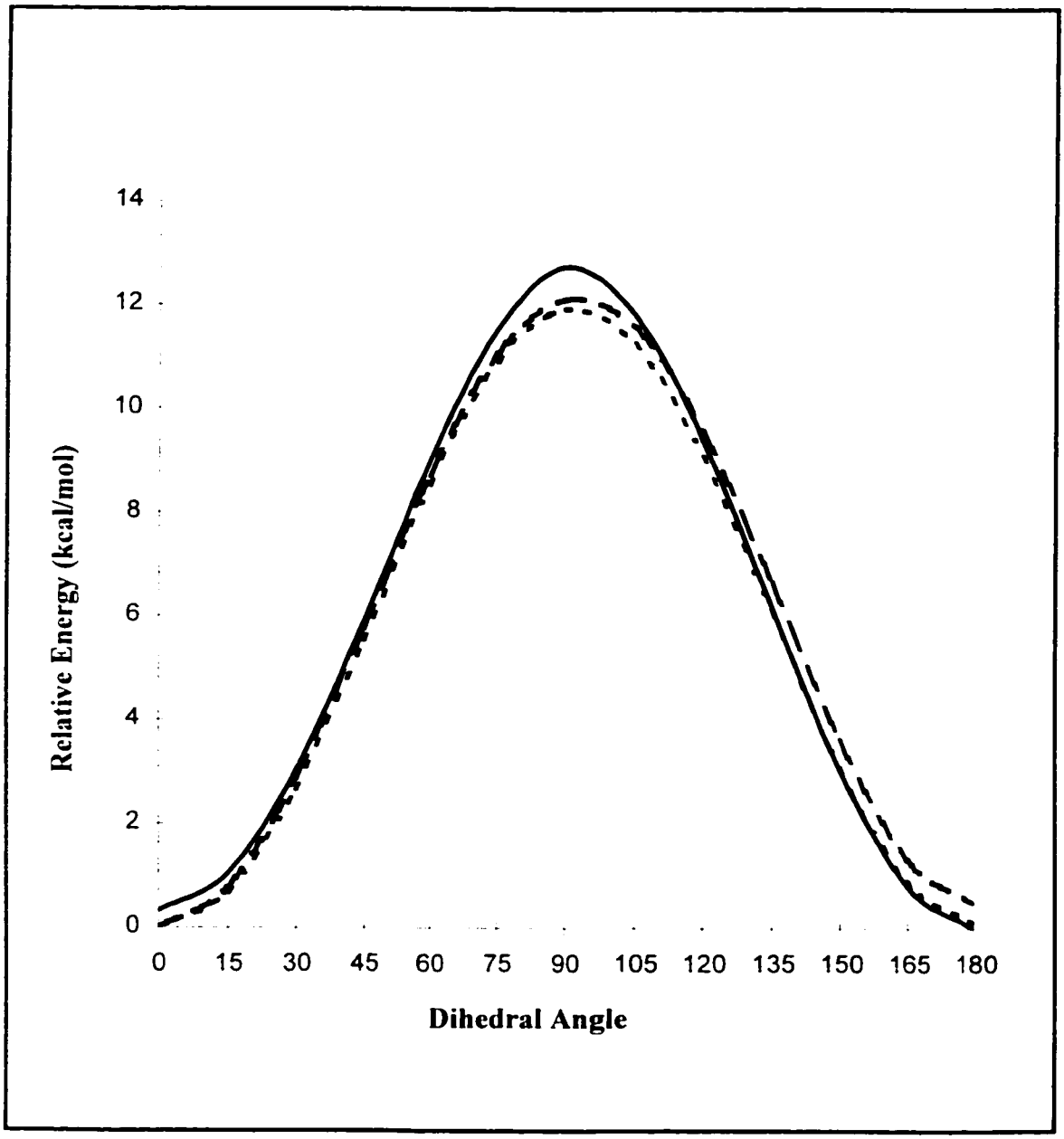

FIGURE III-2: **Potential Function for the Asymmetric Torsion in Formyl Ketene as Determined by Ab Initio Calculations at HF/6-311++G** (Dashed Line), MP2/6-311++G** (Dotted Line) and B3LYP/6-311++G** (Solid Line).**

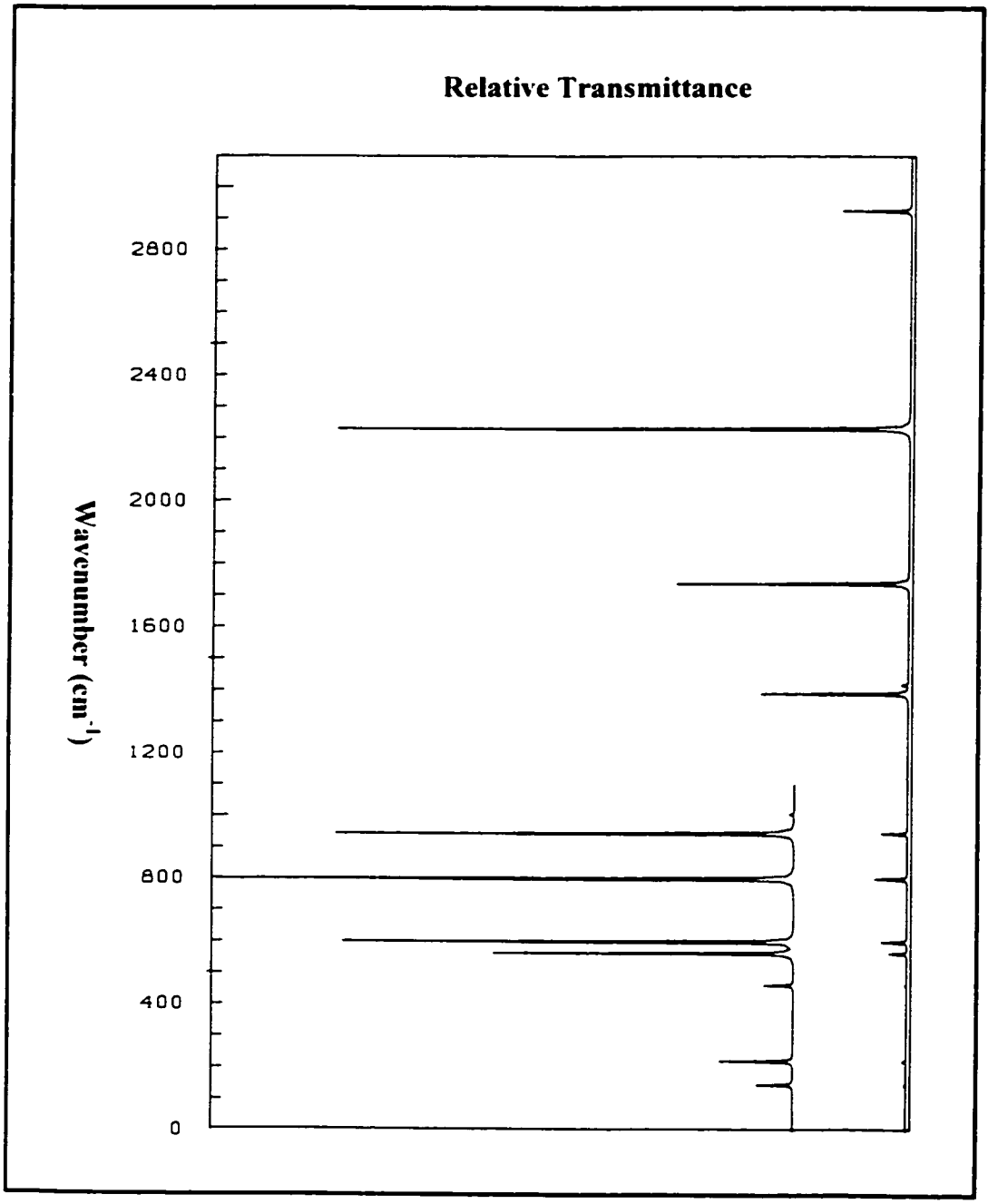

FIGURE III-3: **Calculated Vibrational Infrared Spectrum of the Mixture of the *Cis* and the *Trans* Conformers of Formyl Ketene at 300 K at the DFT-B3LYP/6-311++G** Level.**

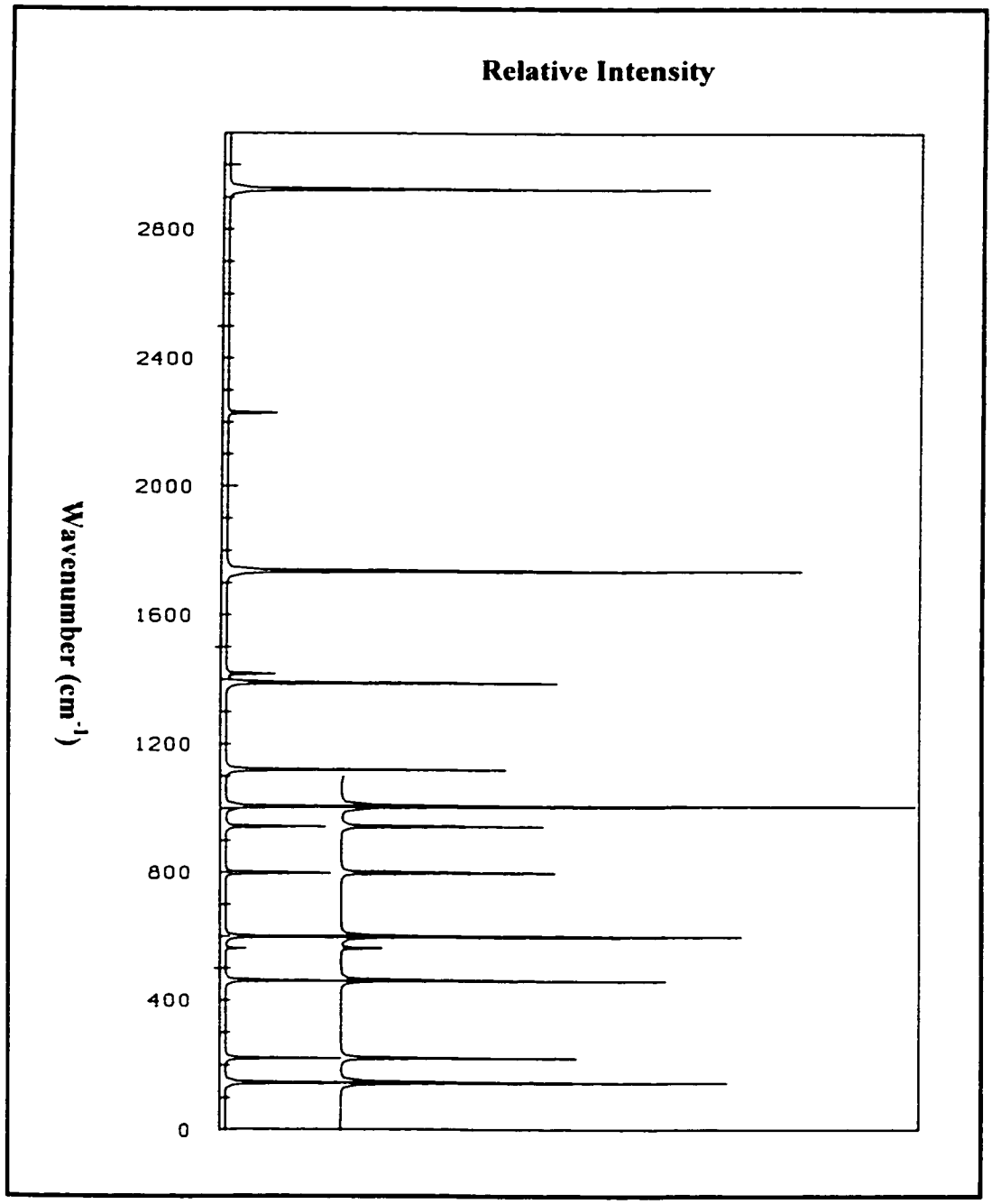

FIGURE III-4: **Calculated Vibrational Raman Spectrum of the Mixture of the *Cis* and the *Trans* Conformers of Formyl Ketene at 300 K at the DFT-B3LYP/6-311++G** Level.**

CHAPTER 4

DENSITY FANCTIONAL CALCULATIONS OF VIBRATIONAL WAVENUMBERS AND DERIVED POTENTIAL ENERGY DISTRIBUTIONS FOR FLUORO- AND CHLOROCARBONYL KETENE

4.1 INTRODUCTION

The structural stabilities of some saturated and unsaturated organic compounds of the general formula R–CXO, where X is a halogen atom, have been the subject of a number of investigations for many years. The importance of these compounds in synthetic chemistry has attracted the attention to study their conformational behavior.

A series of haloacetyl halides was studied experimentally by infrared and microwave methods, as well as theoretically using ab initio analysis [12-16]. The halogen-halogen interaction was found to be the main factor that controls the stability of these molecules. They were found to have the *trans* conformation to be the least energetic form. Only fluoroacetyl fluoride [15] and fluoroacetyl chloride [14] have the *cis* conformer to be

the second minimum in the potential scan, while all of the other haloacetyl halides [15,16] have the *gauche* conformer as the high-energy conformer.

Propinoyl fluoride [87], chloride [91] and bromide [92] were found to exist in the s-*trans* ⇔ *gauche* equilibrium, with the s-*trans* form being more stable than the *gauche* conformation in the three molecular systems. In the case of 3,3,3-trifluoropropinoyl fluoride [93], three possible conformations (*cis*, *trans* and *gauche*) were predicted to be the stable forms, whereas only the *cis* conformer was found to be the stable form in 3,3,3-trichloropropinoyl chloride [93].

The stability of propenoyl halides [17,82,94-97] were also studied and compared to the saturated analogues. For example, in propenoyl fluoride, chloride and bromide [94], the *cis*-to-*trans* rotational barriers were determined from the far-infrared spectra to be of a relatively higher energy as compared to the saturated ones [87,91,92], with the planar forms being the thermodynamically preferred conformations. This was attributed to the π-conjugation in the planar unsaturated acetyl halides. Moreover, by employing ab initio calculations at 6-31G* level, the structural stability of 2,3-butadienoyl fluoride and chloride [82] and cyanoacetyl fluoride and chloride [17] we studied and found that they are stable in the planar *cis* and *trans* forms due to conjugation.

Furthermore, ketenes containing CHO or CXO groups, where X is a halogen atom, were the subject of many studies by synthetic chemists [37,47,98-102]. An interesting example is the chlorocarbonyl ketene [103-106] which was generated by the thermolysis of malonyl dichloride and isolated in argon and xenon cryogenic matrices [105], and was also produced from the flash vacuum pyrolysis of cyclic lactones in acetone [104]. The interconversion between the two stable conformers of chlorocarbonyl ketene could take

place by irradiation at $\lambda \geq 330\,nm$ [105]. The 1,3-shift of the chloride atom in the molecule was verified experimentally using the ^{13}C NMR spectroscopy to be of a relatively moderate shift barrier [106]. The experimental infrared spectra of each conformer were obtained separately, and it was shown that the s-*trans* conformer is more stable than the s-*cis* one [105]. However, the vibrational assignment given in that work was not fully conclusive, especially for some of the skeletal modes in the system.

Therefore, we investigated the structural stability of chlorocarbonyl ketene and compared it to that of fluorocarbonyl ketene. The zero-point corrections were included in the calculation of the energies of the ground and the transition states at the DFT-B3LYP/6-311++G** level. We also carried out normal coordinate analyses by utilizing ab initio density functional calculations and derived the potential energy distributions (PED) among symmetry coordinates for the stable conformers of the two molecules. The complete vibrational assignments of nearly all the normal modes were made based on the calculated PED values for both systems in their ground states. The results of the work are presented herein.

4.2 AB INITIO CALCULATIONS

The GAUSSIAN 98 program [65], running on an IBM RS/6000 43P model 260 workstation, was used to carry out the LCAO-MO-SCF DFT-B3LYP calculations. The extended 6-311++G** basis set was employed at the Density Functional B3LYP level to optimize the structures and predict the energies and dipole moments of fluorocarbonyl ketene

and chlorocarbonyl ketene in their stable conformations. From full energy optimization, the *cis* and the *trans* conformations were found to be the energy minima for both molecular systems (Figure IV-1). The optimized structural parameters of the molecules in the two stable conformations are shown in Tables IV-1 and IV-2 and compared to the experimental values for the corresponding propenoyl fluoride [107] and chloride [108,109]. The optimized structural parameters were used to compute their vibrational frequencies at the DFT-B3LYP/6-311++G** level of calculation. Normal coordinate calculations were then carried out to derive the potential energy distributions for the molecules in their stable conformations.

4.2.1 Asymmetric Torsional Potential Functions

The potential scan for the internal rotation about the C-C single bond in the two molecules was obtained by allowing the OCCC dihedral angle (ϕ) to vary from 0° (*cis* position) to 180° (*trans* position). Full geometry optimizations at each of the fixed dihedral angles (ϕ) of 15°, 30°, 45°, 60°, 75°, 90°, 105°, 120°, 135°, 150°, and 165° were carried out at DFT-B3LYP/6-311++G** level of calculation in both systems. The zero-point correction, the barrier to interconversion and the corrected relative energies in fluorocarbonyl ketene and chlorocarbonyl ketene were calculated and presented in Table IV-3. The torsional potential was represented as a Fourier cosine series in the dihedral angle (ϕ): $V(\phi) = V_0 + \sum(V_n/2)[1-\cos(n\phi)]$, where V_0 is the relative energy of the *cis* conformation and the potential coefficients from V_1 to V_6 are considered adequate to describe the potential function. The

results of the energy optimizations were used to calculate the six coefficients by least-squares fitting for the systems (Table IV-4). The potential functions of fluorocarbonyl ketene and chlorocarbonyl ketene are shown in Figure IV-2.

4.2.2 Vibrational Frequencies and Normal Coordinate Analyses

Both fluoro- and chlorocarbonyl ketene in their stable planar conformations have C_s symmetry. There are 15 vibrational modes spanning the irreducible representations: 11 A' and 4 A". In the Raman spectra of the liquid, the A' modes should be polarized whereas the A" modes should be depolarized.

Normal coordinate analyses were carried out for the stable conformers of the molecules to provide a complete assignment of the fundamental vibrational frequencies. A computer program was written for this purpose by following Wilson's method [71]. The cartesian coordinates for the stable conformers together with the normal modes (in cartesian coordinates) and the frequencies from the GAUSSIAN 98 output were used as an input in the program. A complete set of internal coordinates (Table IV-5 and Figure IV-1) was used to form symmetry coordinates (Table IV-6) in the molecular systems. The potential energy distribution (PED) for each normal mode among the symmetry coordinates was calculated and is given in Tables IV-7 – IV-10.

A complete vibrational assignment of the fundamentals was proposed. The assignments were made based on calculated PED, infrared band intensities, Raman line activities, depolarization ratios and comparison with experimental values for similar molecules. The data of the vibrational assignments are listed in Tables IV-7 – IV-10.

4.2.3 Calculation of Vibrational Spectra

To calculate the Raman spectra we used the frequencies ν_j, the scattering activities S_j and the depolarization ratios ρ_j as calculated on DFT-B3LYP level (6-311++G** basis set for all). The procedure explained in Chapter two was used [72,73]. For the infrared spectrum we used the intensities as given by the DFT-B3LYP/6-311++G** calculations and converted them to relative transmittance.

The Boltzmann Distribution was then used to superimpose the spectra of the *cis* and the *trans* conformers of fluorocarbonyl ketene and chlorocarbonyl ketene. The total line intensity was calculated using equation (2-36). The degeneracy factor (g_i) value for fluoro- and chlorocarbonyl ketene in their planar *cis* and *trans* conformations is unity, and the temperature ($T = 300$ K) was used. The calculated vibrational infrared and Raman spectra of the fluorocarbonyl ketene mixture (26% *cis* and 74% *trans*) are shown in Figures IV-3 and IV-4, while the spectra of the chlorocarbonyl ketene mixture (26% *cis* and 74% *trans)* at 300 K are shown in Figures IV-5 and IV-6.

4.3 DISCUSSION

The interesting chemical reactivity of ketenes and their usefulness in synthetic chemistry [37,47,98-106] have recently prompted us to investigate the conformational and structural behavior of formyl ketene. In formyl ketene, as discussed in the previous

chapter, the molecule was predicted to exist as a *cis-trans* mixture. The two planar conformations in formyl ketene were predicted to be approximately of the same stability. The stability of formyl ketene was predicted to be governed by the dominant conjugation property that maintains the planar conformation and restricts the rotation around the C-C single bond.

We found from ab initio calculations at the DFT-B3LYP level that both fluorocarbonyl ketene and chlorocarbonyl ketene exist as a mixture of the *cis* and the *trans* planar conformations. The *trans* form in the two ketenic systems (the halogen atom eclipses the ketenic hydrogen) is predicted to be the lowest energy minima. This result is consistent with the experimental data from the IR analysis for chlorocarbonyl ketene [105]. The π-π interaction between the CXO group and the ketenic group –C=C=O in fluoro- and chlorocarbonyl ketene greatly stabilizes the planar forms with a relatively high *trans*-to-*cis* rotational barrier (11.7 and 11.8 kcal/mol in fluoro- and chlorocarbonyl ketene, respectively). The comparison shows that there is no difference between the calculated potential scan of the two molecules in Figure IV-2. This is basically because of the significant domination of the conjugation effect over the steric force.

We also calculated the vibrational frequencies of the stable conformations of the two molecules and plotted the IR and Raman spectra in Figures IV-3 – IV-6. Some vibrations were clearly pure and assigned on the basis of the PED values as shown in Tables IV-7 – IV-10. Other modes were predicted to be mixed with neighboring ones. We used the observed IR frequencies obtained for chlorocarbonyl ketene [105] and the observed Raman frequencies for the corresponding fluoro- [72] and chlorocarbonyl isocyanate [88] and

propenoyl halides [94], for comparison and to assist in making the assignment of the mixed vibrational modes.

There is only one C-H stretching mode associated with the ketenic C-H in fluoro- and chlorocarbonyl ketene. This stretch was predicted to have the highest Raman activity in the Raman spectra of the molecules. The C-H stretch in fluorocarbonyl ketene was calculated at 3216 cm^{-1} for the two conformers while, in chlorocarbonyl ketene, this stretch was calculated at 3227 cm^{-1} for the *cis* and 3191 for the *trans* form. The antisymmetric –C=C=O stretching mode was calculated to have the highest infrared intensity in the two molecules, which is consistent with experimental results observed for chlorocarbonyl ketene [105]. It has a very small degree of mixing with other modes in both molecules (95% PED for all of the four conformers).

The C=O stretching mode (S_3) was directly assigned to the wavenumber with the second highest line intensity in the IR spectra of the two molecules. The mode was calculated at 1855 and 1882 cm^{-1} for the *cis* and *trans*-fluorocarbonyl ketene, respectively. The calculated frequencies are in fair agreement with the experimental Raman frequencies obtained for fluorocarbonyl isocyanate (1848 cm^{-1}) as shown in Tables IV-6 and IV-7.

The –C=C=O symmetric stretching (S_5), the C=C–H in-plane bending (S_7) and the C–C stretching (S_2) vibrational modes in fluorocarbonyl ketene were predicted to be strongly coupled with each other at ν_4, ν_5 and ν_6, and their assignments were difficult based on the calculated PED values. However, the assignment of these three modes in the chlorocarbonyl derivative is quite clear as compared to the fluoro analogue. From the PED values, ν_5 and ν_6 could be assigned to the C=C–H in-plane bend and the C–C stretch, respectively. Then, the

–C=C=O symmetric stretch could be assigned to ν_4. The calculated PEDs of the two conformers in chlorocarbonyl ketene were of a great help to clarify the assignment of the corresponding experimental IR bands that were found to have a high degree of coupling [105]. The frequencies at which the above three wavenumbers were calculated agreed with the observed IR frequencies of the same molecule in the *cis* and the *trans* conformers (Tables IV-9 and IV-10).

The assignment of the C-Cl and the C-F stretching modes in the molecules was made based on the calculated PED values as well as the computed Raman activities. The C-Cl stretching mode should be assigned to the wavenumber of the highest Raman activity below 1000 cm^{-1}, which is in this case ν_8. The wavenumber ν_8 was calculated to be at 512 cm^{-1} (22% PED) in the *cis* and 576 cm^{-1} (38% PED) in the *trans*-chlorocarbonyl system. The corresponding mode in chlorocarbonyl ketene [105] was observed in the IR spectrum at 587 cm^{-1}, which supports our assignment of such a mode. The C-F stretching mode was assigned based on the calculated PEDs to ν_7 (946 cm^{-1} in the *cis* and 824 cm^{-1} in the *trans*). Tables IV-7 – IV-10 show that the C-F stretching mode was of a higher calculated IR intensity as compared to the corresponding C-Cl mode as one expects due to the greater induced dipole moment in the C-F bond as compared to the C-Cl one.

The CClO deformation in the chloro derivative was calculated to be higher in frequency than the CClO rocking vibrational mode. While the calculated frequencies of the corresponding fundamental vibrations associated with the CFO moiety in the fluoro derivative showed the reversed order. The experimental frequencies show the same trend as one moves from chlorocarbonyl isocyanate [88] to fluorocarbonyl isocyanate [72] or from

propenoyl chloride to propenoyl fluoride [94] (Tables IV-7 – IV-10). The in-plane C=C–C bending mode in the two carbonyl systems was directly assigned based on the PED values to ν_{11}. This leaves the C=C=O in-plane bending mode to be assigned to ν_7 and ν_8 in chloro- and fluorocarbonyl ketene, respectively.

The C–Cl and C–H wagging vibrations were calculated to be depolarized and mixed with each other at ν_{12} (706 cm^{-1}) in the *trans*-chlorocarbonyl ketene. The experimental frequency of the C–Cl wag was observed at 684 cm^{-1} in the infrared spectrum of the *trans*-chlorocarbonyl ketene, hence ν_{12} could be assigned with confidence to the C–Cl wag. Furthermore, the C–H wagging vibration could be assigned based on the calculated PEDs to ν_{14}. The –C=C=O out-of-plane bending vibrational mode was predicted to have a very low degree of mixing and directly assigned, from the derived PED, to ν_{13} in both fluoro- and chlorocarbonyl ketene.

The lowest vibrational modes in the spectra of the two ketenic systems were the asymmetric torsions. In fluorocarbonyl ketene, the asymmetric torsion was calculated at 112 and 115 cm^{-1} for the *cis* and *trans* conformers, respectively, while in chlorocarbonyl ketene it was predicted at 93 cm^{-1} for the *cis* and 116 cm^{-1} for the *trans* form. The calculated asymmetric torsion in the investigated systems is noticed to be consistent with the corresponding ones in propenoyl halide systems [94]. In propenoyl fluoride, the CFO torsion was observed at 101 and 117 cm^{-1} for the *cis* and the *trans* forms respectively, while it was 95 cm^{-1} for the *cis* and 108 cm^{-1} for the *trans*-prpenoyl chloride.

Finally, from the DFT calculations the planar conformations in the two molecular systems were predicted to be the stable form with a relatively high rotational barrier and a

small relative energy. We provided reliable vibrational assignments for the normal modes of the stable conformers of fluoro- and chlorocarbonyl ketene based on the normal coordinate analysis. The calculated PED values gave a resonable assignment for most of the bending and stretching modes.

TABLE IV-1: **Calculated structural Parameters, Total Dipole Moment, and Rotational Constants for the *Cis* and the *Trans* Conformations of Fluorocarbonyl Ketene.**

Parameter	B3LYP/6-311++G**		Microwave [a]	
	cis	*trans*	*cis*	*trans*
Bond Length (Å)				
$r(C_1\text{-}C_2)$	1.450	1.447	1.48	1.49
$r(C_2\text{-}C_3)$	1.328	1.328	1.35	1.35
$r(C_3\text{-}O_4)$	1.148	1.149		
$r(C_2\text{-}H_5)$	1.081	1.081	1.085[b]	1.085[b]
$r(C_1\text{-}O_6)$	1.189	1.185	1.18	1.18
$r(C_1\text{-}F_7)$	1.368	1.379	1.35	1.35
Bond Angle (deg)				
$(C_1C_2C_3)$	119.6	121.7	119.9	121.8
$(C_2C_3O_4)$	181.0	181.0		
$(C_1C_2H_5)$	122.1	119.6		
$(C_2C_1O_6)$	129.7	128.6	128.2	127.0
$(C_2C_1F_7)$	109.5	110.9	110.1	111.3
$(C_1C_2C_3O_4)$	0.0	180.0		
Dipole Moment (Debye)				
μ_t	3.4	3.2		
Rotational Constants (MHz)				
A	10866	10478		
B	2163	2348		
C	1804	1918		

[a] Data obtained for propenoyl fluoride from ref [107].

[b] Assumed values from ref [107].

TABLE IV-2: **Calculated Structural Parameters, Total Dipole Moment, and Rotational Constants for the *Cis* and the *Trans* Conformations of Chlorocarbonyl Ketene.**

Parameter	B3LYP/6-311++G**		Electron Diffraction [a]	Microwave [b]
	cis	*trans*	*cis*	*trans*
Bond Length (Å)				
$r(C_1\text{-}C_2)$	1.451	1.445	1.484	1.476
$r(C_2\text{-}C_3)$	1.331	1.330	1.339	1.345
$r(C_3\text{-}O_4)$	1.148	1.148		
$r(C_2\text{-}H_5)$	1.080	1.084		1.084
$r(C_1\text{-}O_6)$	1.190	1.186	1.192	1.192
$r(C_1\text{-}Cl_7)$	1.820	1.838	1.772	1.816
Bond Angle (deg)				
$(C_1C_2C_3)$	118.8	123.4	123.4	122.6
$(C_2C_3O_4)$	180.5	182.9		
$(C_1C_2H_5)$	122.7	118.8		
$(C_2C_1O_6)$	128.4	127.2	125.2	127.2
$(C_2C_1Cl_7)$	111.1	112.8	111.8	116.3
$(C_1C_2C_3O_4)$	0.0	180.0		
Dipole Moment (Debye)				
μ_t	3.4	3.1		
Rotational Constants (MHz)				
A	9405	4845		
B	1464	2203		
C	1267	1514		

[a] Data obtained for propenoyl chloride from ref [108].

[b] Data obtained for propenoyl chloride from ref [109].

TABLE IV-3: **Computed Total Energies, Zero-Point Corrections (Hartrees), Relative Energies, and Rotational Barriers (kcal/mol) in Fluorocarbonyl Ketene and Chlorocarbonyl Ketene.**

	B3LYP/6-311++G**					
	Fluorocarbonyl ketene			Chlorocarbonyl ketene		
	cis	*trans*	*TS*[a]	*cis*	*trans*	*TS*[b]
Total energy	-365.30433	-365.30536	-365.28570	-725.65017	-725.65113	-725.63130
Relative energy		0.64633			0.60241	
Cis-trans barrier		11.69051			11.48111	
Trans-cis barrier		12.33685			12.44352	
Zero-point correction	0.03565	0.03568	0.03462	0.03405	0.03402	0.03293
Sum of total and zero-point energies	-365.26868	-365.26968	-365.25108	-725.61612	-725.61711	-725.59836
Corrected relative energy		0.62751			0.62123	
Corrected *cis-trans* barrier		11.04418			11.14458	
Corrected *trans-cis* barrier		11.67169			11.76581	

[a] The CCCO dihedral angle of the *transition state* of fluorocarbonyl ketene was calculated to be 91.00°.

[b] The CCCO dihedral angle of the *transition state* of chlorocarbonyl ketene was calculated to be 91.24°.

TABLE IV-4: **Calculated Potential Constants (kcal mol^{-1}) for the Asymmetric Torsion in Fluorocarbonyl Ketene and Chlorocarbonyl Ketene.**

Potential Constants	B3LYP/6-311++G**	
	Fluorocarbonyl ketene	Chlorocarbonyl ketene
V_1	-0.008	0.056
V_2	12.186	12.279
V_3	-0.221	-0.269
V_4	-0.045	-0.120
V_5	0.195	0.181
V_6	0.210	0.217

TABLE IV-5: **Internal Coordinate Definitions [a] for Fluorocarbonyl Ketene (X=F) and Chlorocarbonyl Ketene (X=Cl).**

No.	Coordinate		Definition
1	C_1–C_2	stretch	R
2	C_2–C_3	stretch	P
3	C_3–O_4	stretch	Q
4	C_1–O_6	stretch	S
5	C_1–X_7	stretch	T
6	C_2–H_5	stretch	D
7	$C_1C_2C_3$	bend	β
8	$C_2C_3O_4$	bend	σ
9	$C_2C_1O_6$	bend	ε
10	$C_2C_1X_7$	bend	φ
11	$X_7C_1O_6$	bend	θ
12	$C_1C_2H_5$	bend	ρ
13	$C_3C_2H_5$	bend	δ
14	C_2=C_3=O_4	wag	χ
15	C_2–H_5	wag	π
16	C_1–X_7	wag	ω
17	$O_6C_1C_2C_3$	torsion	τ
	$X_7C_1C_2C_3$		

[a] See Figure IV-1 for atom denotation.

TABLE IV-6: **Symmetry Coordinates for Fluorocarbonyl Ketene (X=F) and Chlorocarbonyl Ketene (X=Cl).**

Species	Description		Symmetry Coordinate [a]
A'	C–H	stretch	$S_1 = D$
	C–C	stretch	$S_2 = R$
	C=O	stretch	$S_3 = S$
	C–X	stretch	$S_4 = T$
	C=C=O	symmetric stretch	$S_5 = P + Q$
	C=C=O	antisymmetric stretch	$S_6 = P - Q$
	C=C–H	in-plane bend	$S_7 = \rho - \delta$
	CXO	deformation (scissor)	$S_8 = \varepsilon + \varphi - 2\theta$
	CXO	rock	$S_9 = \varepsilon - \varphi$
	C=C=O	in-plane bend	$S_{10} = \sigma$
	C=C–C	in-plane bend	$S_{11} = 2\beta - \rho - \delta$
A''	C=C=O	out-of-plane bend (wag)	$S_{12} = \chi$
	C=C–H	out-of-plane bend (wag)	$S_{13} = \pi$
	C–X	out-of-plane bend (wag)	$S_{14} = \omega$
	Asymmetric torsion		$S_{15} = \tau$

[a] Not normalized.

TABLE IV-7: **Calculated Vibrational Frequencies (cm^{-1}) at B3LYP/6-311++G** Level for the *Cis* Conformer of Fluorocarbonyl Ketene.**

Symm.	Number	Frequency	IR Intensity [a]	Raman Activity	Depol. Ratio	Obs. [b]	PED [c]
A'	ν_1	3216	26.7	81.5	0.2		100% C-H str. (S_1)
	ν_2	2250	783.0	15.8	0.7	2158	95% C=C=O antisymm. str. (S_6)
	ν_3	1855	474.1	39.0	0.3	(1848)	90% C=O str. (S_3)
	ν_4	1420	224.1	9.8	0.2	1361	37% C=C=O symm. str. (S_5), 32% C=C-H in-plane bend (S_7), 23% C-C str. (S_2)
	ν_5	1126	34.8	10.7	0.2	1113	43% C=C-H in-plane bend (S_7), 43% C=C=O symm. str. (S_5)
	ν_6	1090	315.2	3.6	0.3	1004	29% C-C str. (S_2), 28% C-F str. (S_4), 21% C=C-H in-plane bend (S_7), 17% CFO def. (S_8)
	ν_7	946	68.9	6.7	0.1	826[d]	29% C-F str. (S_4), 21% C-C str. (S_2), 18% C=C-C in-plane bend (S_{11}), 12% CFO rock (S_9), 11% C=C=O in-plane bend (S_{10})
	ν_8	683	10.5	7.6	0.3		17% C=C=O in-plane bend (S_{10}), 36% C-F str. (S_4), 30% CFO def. (S_8)
	ν_9	520	8.1	2.2	0.1	(565)	41% CFO def. (S_8), 31% C=C=O in-plane bend (S_{10}), 19% C-C str. (S_2)
	ν_{10}	409	0.8	1.6	0.6	(494)	68% CFO rock (S_9), 16% C=C=O in-plane bend (S_{10})
	ν_{11}	143	3.9	3.3	0.7		65% C=C-C in-plane bend (S_{11}), 21% C=C=O in-plane bend (S_{10}), 14% CFO rock (S_9)

TABLE IV-7: **Continue.**

Symm.	Number	Frequency	IR Intensity [a]	Raman Activity	Depol. Ratio	Obs. [b]	PED [c]
A"	ν_{12}	749	50.6	0.4	0.8	(746)[e]	84% C-F wag (S_{14}), 16% C=C-H wag (S_{13})
	ν_{13}	581	14.9	1.2	0.8		85% C=C=O wag (S_{12})
	ν_{14}	550	19.1	0.2	0.8	531	78% C=C-H wag (S_{13}), 10% C=C=O wag (S_{12})
	ν_{15}	112	3.1	0.9	0.8	101[f]	96% asymm. torsion (S_{15})

[a] Infrared intensities and Raman activities are calculated in Km mol^{-1} and $Å^4$ amu^{-1}, respectively.

[b] Observed IR frequencies for *cis*-chlorocarbonyl ketene in argon matrix [105]; the values in brackets are Raman frequencies in the gas phase for fluorocarbonyl isocyanate [72].

[c] PED values are obtained by using calculated frequencies at B3LYP level.

[d] Observed IR frequencies in the liquid phase of *cis*-propenoyl fluoride [94].

[e] Observed in the Raman spectrum of the liquid [72].

[f] Observed IR frequencies in the gas phase of *cis*-propenoyl fluoride [94].

TABLE IV-8: **Calculated Vibrational Frequencies (cm^{-1}) at B3LYP/6-311++G** Level for the *Trans* Conformer of Fluorocarbonyl Ketene.**

Symm.	Number	Frequency	IR Intensity [a]	Raman Activity	Depol. Ratio	Obs. [b]	PED [c]
A'	ν_1	3216	26.6	74.6	0.2		100% C-H str. (S_1)
	ν_2	2248	809.8	16.9	0.7	2160	95% C=C=O antisymm. str. (S_6)
	ν_3	1882	748.2	70.4	0.3	(1848)	90% C=O str. (S_3)
	ν_4	1398	62.3	7.6	0.1	1376	44% C=C=O symm. str. (S_5), 27% C=C-H in-plane bend (S_7), 20% C-C str. (S_2)
	ν_5	1184	213.8	1.9	0.7	1125	32% C=C-H in-plane bend (S_7), 31% C-C str. (S_2), 15% C-F str. (S_4), 12% CFO def. (S_8)
	ν_6	1110	52.4	15.4	0.2	1051	37% C=C=O symm. str. (S_5), 34% C=C-H in-plane bend (S_7)
	ν_7	824	87.4	7.4	0.2	826[d]	74% C-F str. (S_4), 16% C-C str. (S_2)
	ν_8	698	9.0	7.5	0.2		26% C=C=O in-plane bend (S_{10}), 35% CFO def. (S_8), 18% C=C-C in-plane bend (S_{11})
	ν_9	531	6.1	2.6	0.2	(565)	67% CFO def. (S_8), 21% C-C str. (S_2), 13% C=C=O in-plane bend (S_{10})
	ν_{10}	419	1.0	2.0	0.7	(494)	65% CFO rock (S_9), 30% C=C=O in-plane bend (S_{10})
	ν_{11}	143	3.7	1.1	0.6		65% C=C-C in-plane bend (S_{11}), 18% C=C=O in-plane bend (S_{10}), 17% CFO rock (S_9)

TABLE IV-8: **Continue:**

Symm.	Number	Frequency	IR Intensity [a]	Raman Activity	Depol. Ratio	Obs. [b]	PED [c]
A"	ν_{12}	749	53.5	0.8	0.8	(746)[e]	77% C-F wag (S_{14}), 23% C=C-H wag (S_{13})
	ν_{13}	578	20.0	1.2	0.8		76% C=C=O wag (S_{12}), 18% C=C-H wag (S_{13})
	ν_{14}	564	8.4	0.1	0.8	558	61% C=C-H wag (S_{13}), 19% C=C=O wag (S_{12}), 16% C-F wag (S_{14})
	ν_{15}	115	4.4	0.2	0.8	117[f]	98% asymm. torsion (S_{15})

[a] Infrared intensities and Raman activities are calculated in Km mol^{-1} and $Å^4$ amu^{-1}, respectively.

[b] Observed IR frequencies for *trans*-chlorocarbonyl ketene in argon matrix [105]; the values in brackets are Raman frequencies in the gas phase for fluorocarbonyl isocyanate [72].

[c] PED values are obtained by using calculated frequencies at B3LYP level.

[d] Observed IR frequencies in the liquid phase of *cis*-propenoyl fluoride [94].

[e] Observed in the Raman spectrum of the liquid [72].

[f] Observed IR frequencies in the gas phase of *trans*-propenoyl fluoride [94].

TABLE IV-9: **Calculated Vibrational Frequencies (cm^{-1}) at B3LYP/6-311++G** Level for the *Cis* Conformer of Chlorocarbonyl Ketene.**

Symm.	Number	Frequency	IR Intensity [a]	Raman Activity	Depol. Ratio	Obs. [b]	PED [c]
A'	ν_1	3227	27.5	56.2	0.2		100% C-H str. (S_1)
	ν_2	2241	949.2	21.4	0.7	2158	95% C=C=O antisymm. str. (S_6)
	ν_3	1820	378.6	28.9	0.4	1748	92% C=O str. (S_3)
	ν_4	1391	255.8	16.4	0.1	1361	37% C=C=O symm. str. (S_5), 37% C=C-H in-plane bend (S_7), 19% C-C str. (S_2)
	ν_5	1125	5.2	14.0	0.3	1113	54% C=C-H in-plane bend (S_7), 37% C=C=O symm. str. (S_5)
	ν_6	1018	177.3	5.7	0.04	1004	57% C-C str. (S_2), 12% C=C=O symm. str. (S_5)
	ν_7	836	239.7	1.6	0.1	827	17% C=C=O in-plane bend (S_{10}), 22% CClO def. (S_8), 25% C=C-C in-plane bend (S_{11}), 18% CClO rock (S_9), 14% C-Cl str. (S_4)
	ν_8	512	31.8	14.3	0.2		22% C-Cl str. (S_4), 47% C=C=O in-plane bend (S_{10}), 11% C-C str. (S_2)
	ν_9	432	17.6	8.5	0.4	(448)	43% CClO def. (S_8), 53% C-Cl str. (S_4)
	ν_{10}	312	5.2	3.7	0.4	(410)	49% CClO rock (S_9), 22% CClO def. (S_8), 10% C-Cl str. (S_4)
	ν_{11}	134	3.4	1.6	0.5		60% C=C-C in-plane bend (S_{11}), 21% C=C=O in-plane bend (S_{10}), 19% CClO rock (S_9)

TABLE IV-9: **Continue:**

Symm.	Number	Frequency	IR Intensity [a]	Raman Activity	Depol. Ratio	Obs. [b]	PED [c]
A"	ν_{12}	677	38.0	1.1	0.8	660	69% C-Cl wag (S_{14}), 26% C=C-H wag (S_{13})
	ν_{13}	574	5.8	0.7	0.8		89% C=C=O wag (S_{12})
	ν_{14}	556	20.9	0.1	0.8	531	80% C=C-H wag (S_{13}), 18% C-Cl wag (S_{14})
	ν_{15}	93	2.8	0.3	0.8	95[d]	94% asymm. torsion (S_{15})

[a] Infrared intensities and Raman activities are calculated in Km mol^{-1} and $Å^4$ amu^{-1}, respectively.

[b] Observed IR frequencies for *cis*-chlorocarbonyl ketene in argon matrix [105]; the values in brackets are Raman frequencies in the gas phase for chlorocarbonyl isocyanate [88].

[c] PED values are obtained by using calculated frequencies at B3LYP level.

[d] Observed IR frequencies in the gas phase of *cis*-propenoyl chloride [94].

TABLE IV-10: **Calculated Vibrational Frequencies (cm^{-1}) at B3LYP/6-311++G** Level for the *Trans* Conformer of Chlorocarbonyl Ketene.**

Symm.	Number	Frequency	IR Intensity [a]	Raman Activity	Depol. Ratio	Obs. [b]	PED [c]
A'	ν_1	3191	21.3	115.1	0.2		100% C-H str. (S_1)
	ν_2	2243	784.0	14.5	0.7	2160	95% C=C=O antisymm. str. (S_6)
	ν_3	1851	669.8	59.1	0.4	1785	91% C=O str. (S_3)
	ν_4	1398	50.7	8.8	0.1	1376	44% C=C=O symm. str. (S_5), 30% C=C-H in-plane bend (S_7), 20% C-C str. (S_2)
	ν_5	1144	88.8	9.3	0.2	1125	61% C=C-H in-plane bend (S_7), 21% C-C str. (S_2), 11% C=C=O symm. str. (S_5)
	ν_6	1078	190.6	7.3	0.2	1051	27% C-C str. (S_2), 27% C=C=O symm. str. (S_5), 12% CClO rock (S_9), 11% C=C-C in-plane bend (S_{11})
	ν_7	632	5.0	6.0	0.6		41% C=C=O in-plane bend (S_{10}), 23% C=C-C in-plane bend (S_{11}), 16% CClO def. (S_8)
	ν_8	576	110.4	17.5	0.1	587	29% CClO def. (S_8), 38% C-Cl str. (S_4), 14% C-C str. (S_2), 12% CClO rock (S_9)
	ν_9	407	11.8	7.9	0.4	(448)	60% C-Cl str. (S_4), 32% CClO def. (S_8)
	ν_{10}	353	6.7	3.5	0.7	(410)	44% CClO rock (S_9), 35% C=C=O in-plane bend (S_{10}), 10% CClO def. (S_8)
	ν_{11}	131	1.7	1.9	0.7		60% C=C-C in-plane bend (S_{11}), 26% CClO rock (S_9), 11% C=C=O in-plane bend (S_{10})

TABLE IV-10: **Continue:**

Symm.	Number	Frequency	IR Intensity [a]	Raman Activity	Depol. Ratio	Obs. [b]	PED [c]
A"	ν_{12}	706	46.2	1.0	0.8	684	52% C-Cl wag (S_{14}), 48% C=C-H wag (S_{13})
	ν_{13}	577	11.7	0.8	0.8	558	86% C=C=O wag (S_{12})
	ν_{14}	528	9.0	0.1	0.8		49% C=C-H wag (S_{13}), 40% C-Cl wag (S_{14})
	ν_{15}	116	5.4	0.2	0.8	108[d]	98% asymm. torsion (S_{15})

[a] Infrared intensities and Raman activities are calculated in Km mol^{-1} and $Å^4$ amu^{-1}, respectively.

[b] Observed IR frequencies for *trans*-chlorocarbonyl ketene in argon matrix [105]; the values in brackets are Raman frequencies in the gas phase for chlorocarbonyl isocyanate [88].

[c] PED values are obtained by using calculated frequencies at B3LYP level.

[d] Observed IR frequencies in the gas phase of *trans*-propenoyl chloride [94].

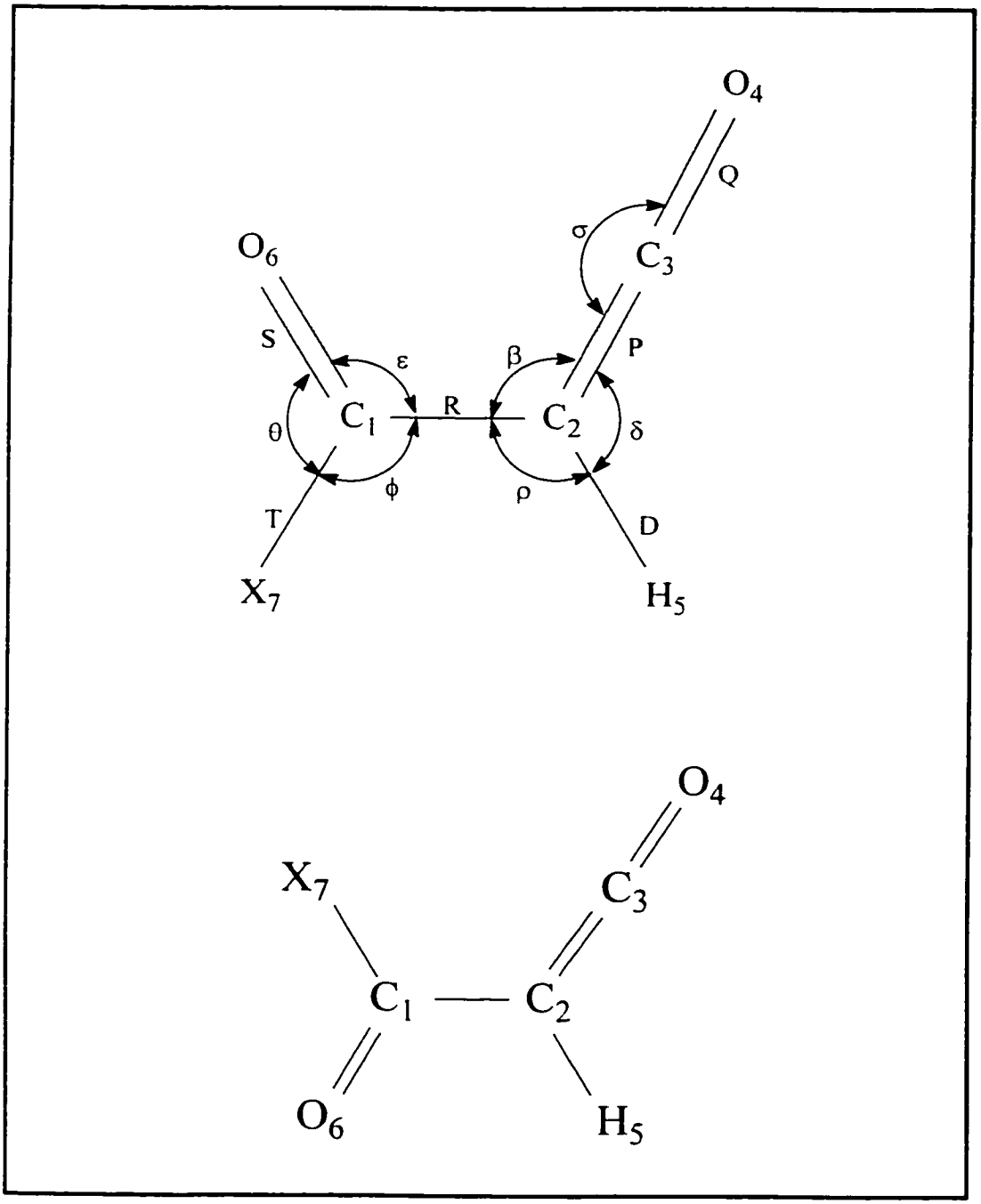

FIGURE IV-1: **Atom Numbering for Fluorocarbonyl Ketene (X=F) and for Chlorocarbonyl Ketene (X=Cl) in the *Cis* (Upper) and the *Trans* (Lower) Conformations, with the Internal Coordinates Shown on the *Cis* Conformation.**

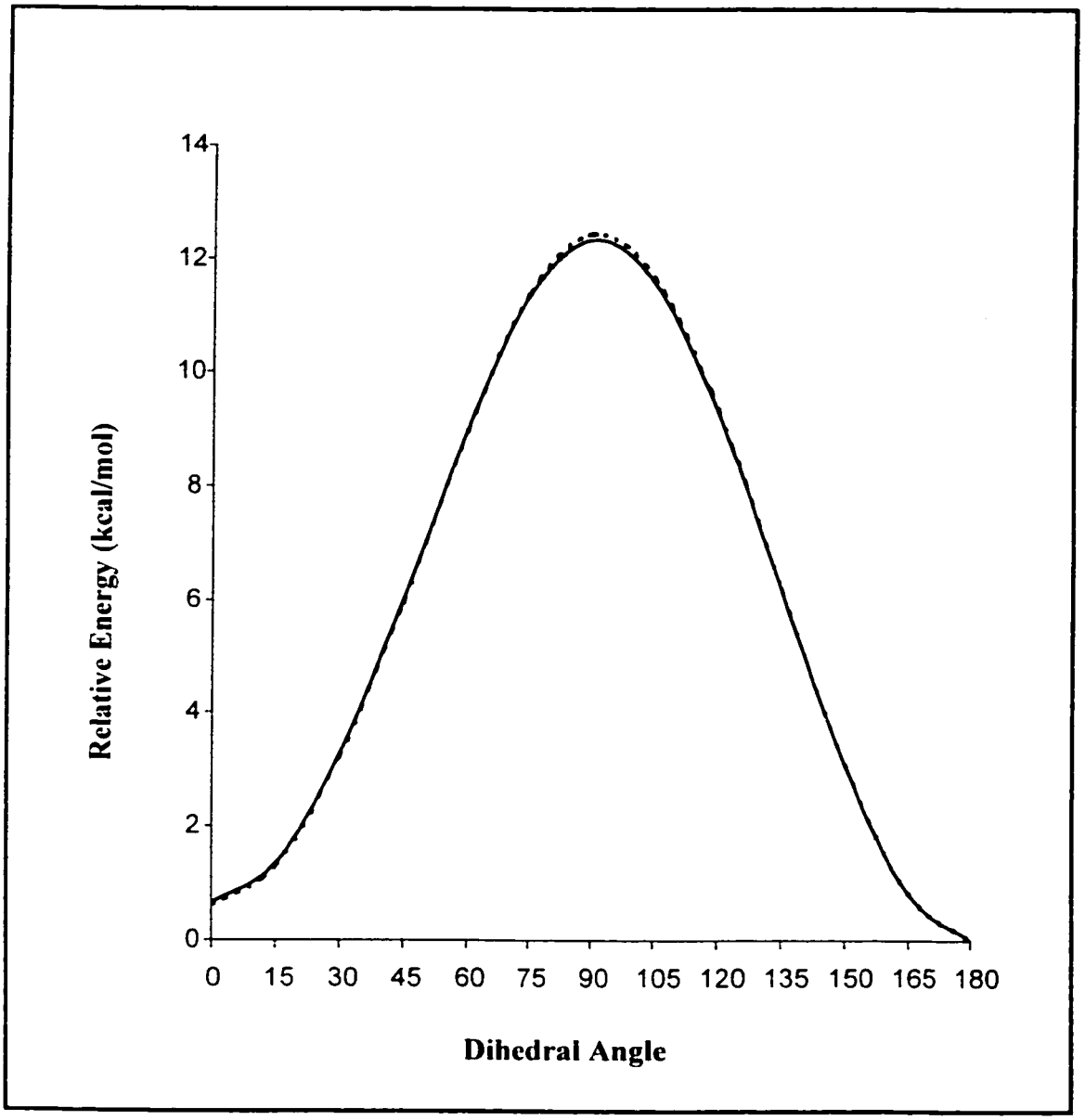

FIGURE IV-2: **Potential Curve for the Internal Rotation in Fluorocarbonyl Ketene (Solid Line) and Chlorocarbonyl Ketene (Dashed Line) as Determined by Ab Initio Calculations at B3LYP/6-311++G** Level.**

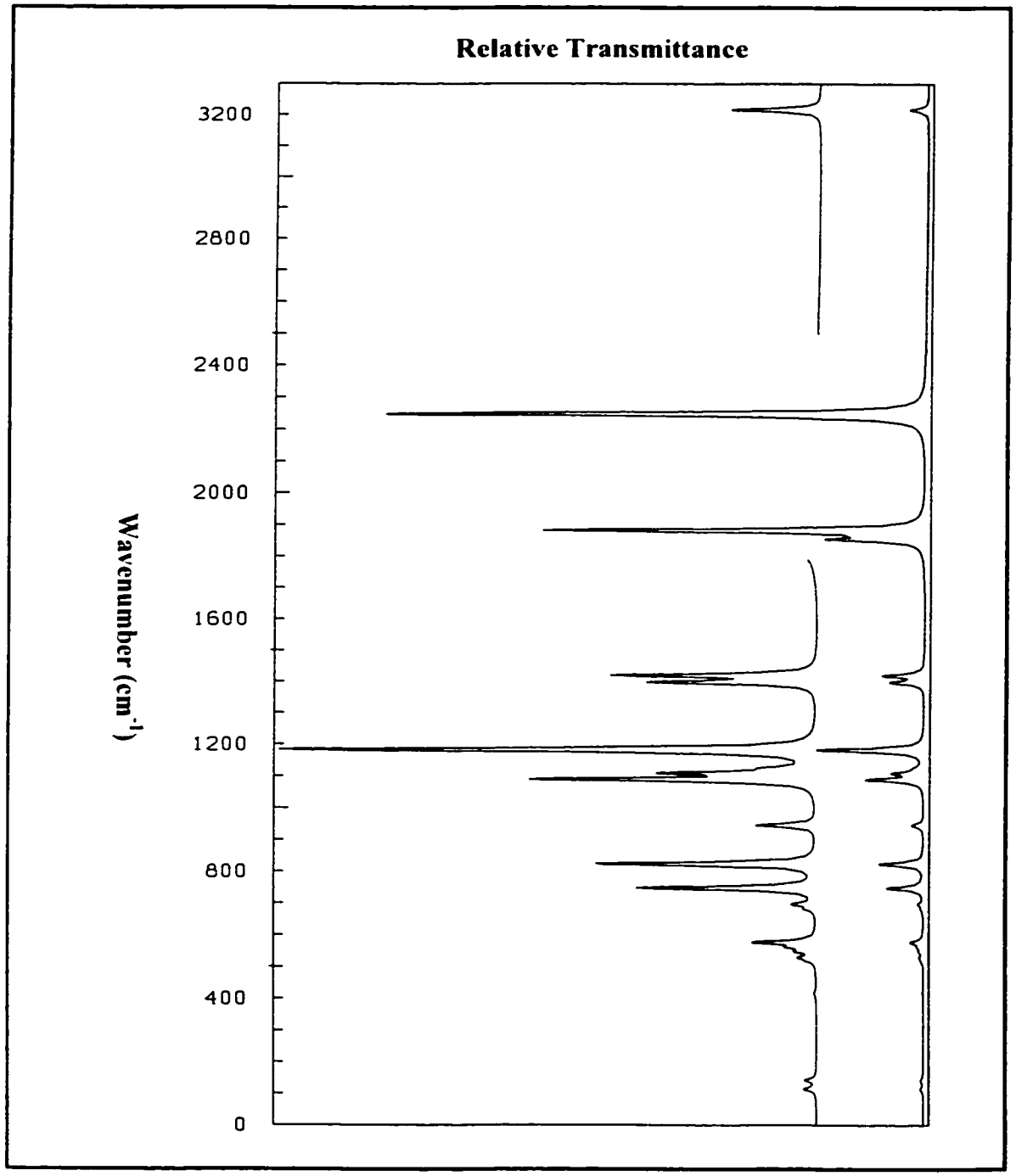

FIGURE IV-3: **Calculated Vibrational Infrared Spectrum of Fluorocarbonyl Ketene at 300 K at the DFT-B3LYP/6-311++G** Level.**

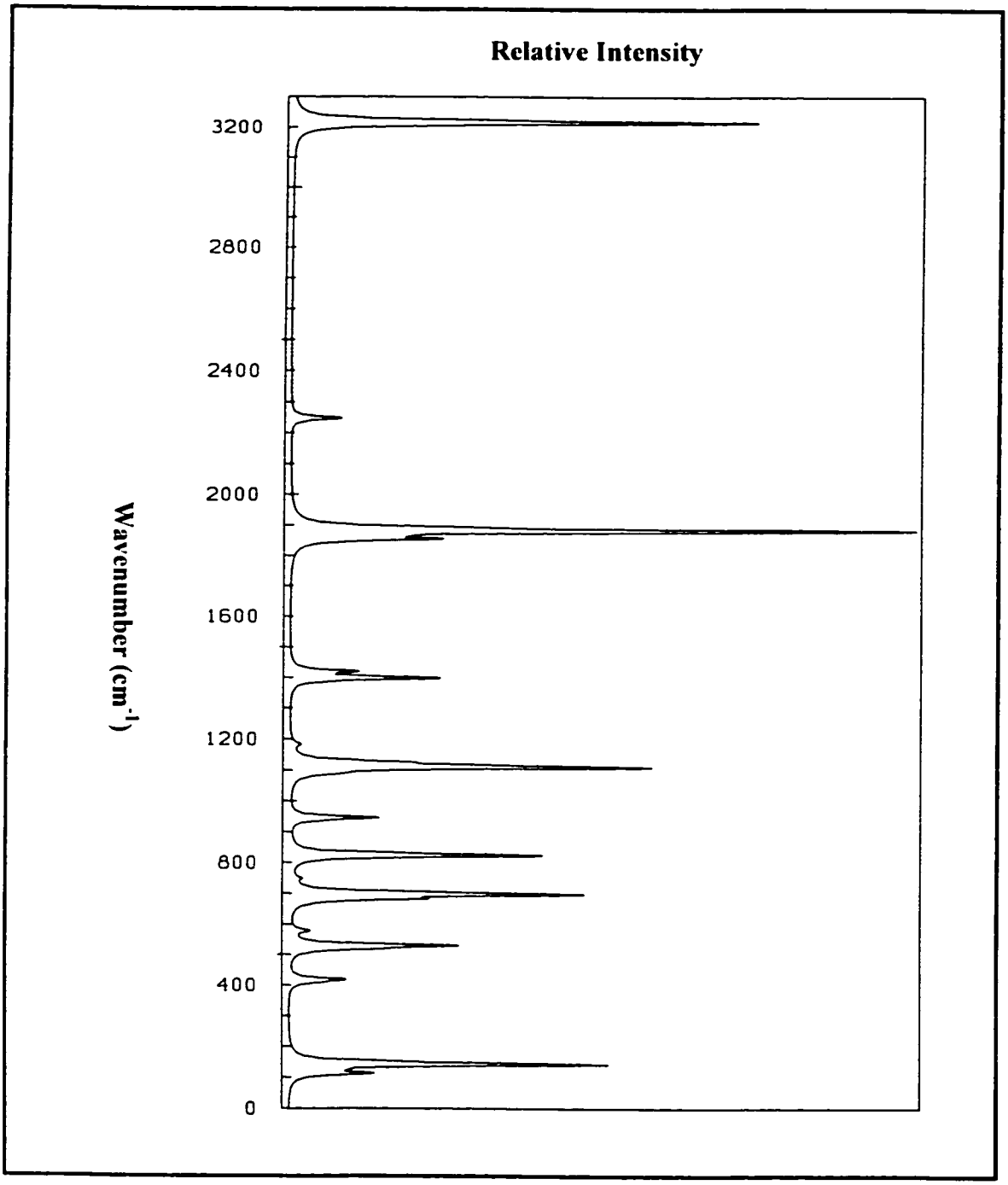

FIGURE IV-4: **Calculated Vibrational Raman Spectrum of Fluorocarbonyl Ketene at 300 K at the DFT-B3LYP/6-311++G** Level.**

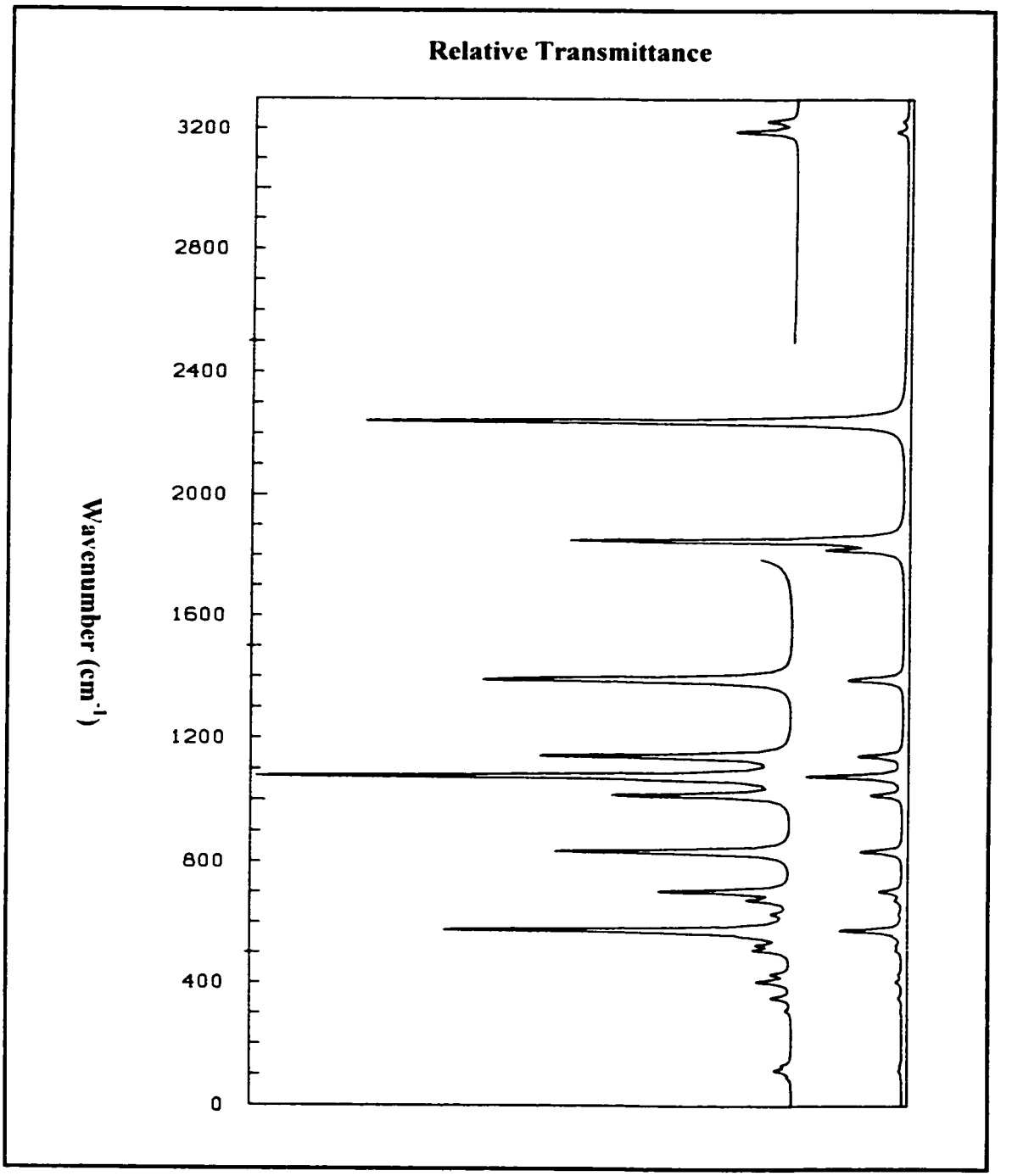

FIGURE IV-5: **Calculated Vibrational Infrared Spectrum of Chlorocarbonyl Ketene at 300 K at the DFT-B3LYP/6-311++G** Level.**

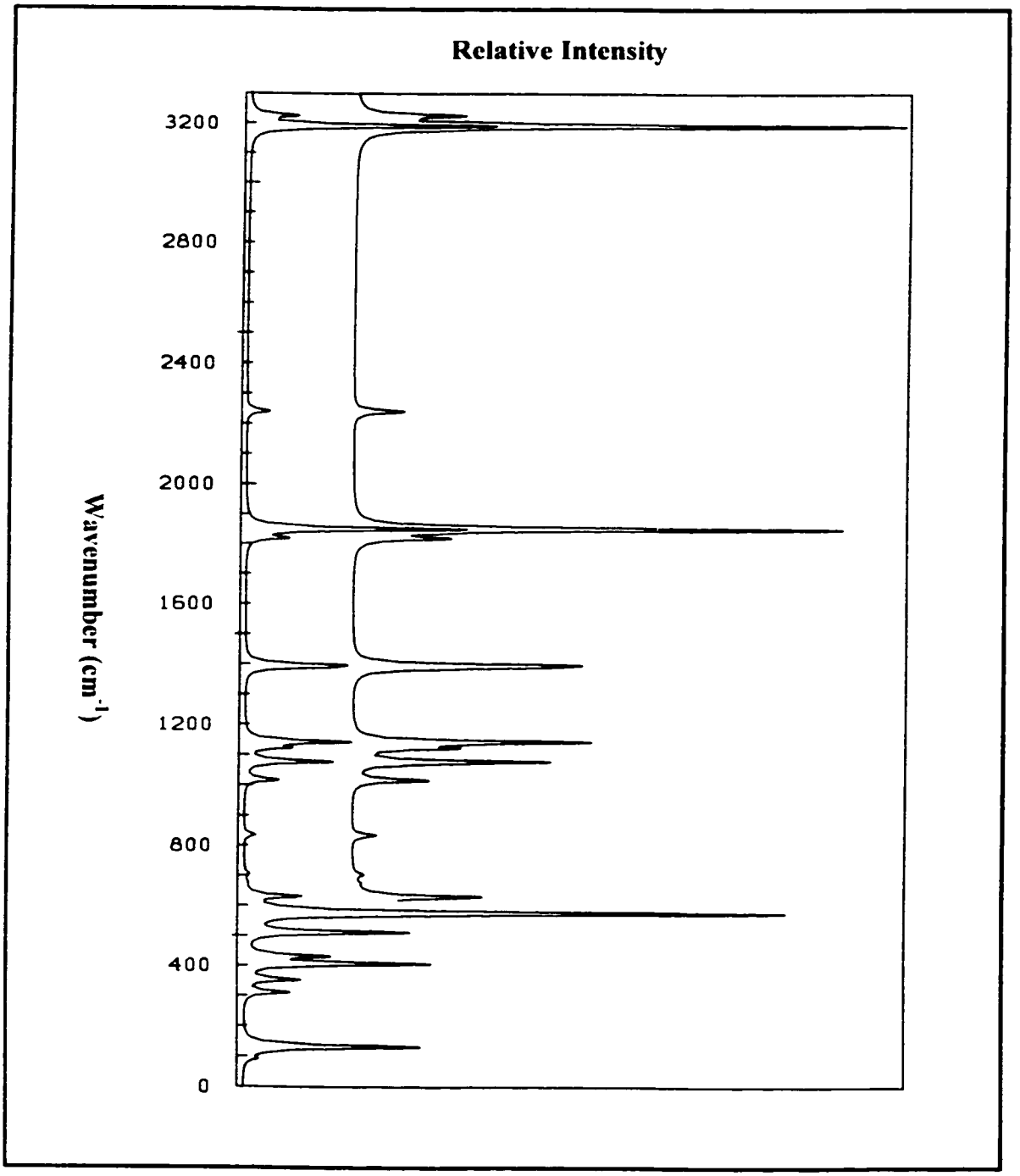

FIGURE IV-6: **Calculated Vibrational Raman Spectrum of Chlorocarbonyl Ketene at 300 K at the DFT-B3LYP/6-311++G** Level.**

CHAPETR 5

C-C AND C-N ROTATIONAL BARRIERS IN VINYL KETENE AND VINYL ISOCYANATE

5.1 INTRODUCTION

The chemical reactivity and the distinguished electronic structure of many unsaturated molecular systems were of a great interest for many years [36,74,77-82,94-97,134]. In such systems, the planar s-*cis* and s-*trans* conformations were predicted to be the stable forms due to π conjugation [36,77-82]. When this conjugation is absent in other saturated analogues, it was found that the rotation around the C-C or the C-N single bond is less hindered with relatively lower energetic barriers as compared to unsaturated ones [17,80,81,83,110,111].

Conjugated ketenes were of a particular interest in synthetic chemistry and are considered as important reactants for many types of reactions [103,112-114]. Vinyl ketene is one of the important conjugated ketenes. It was prepared experimentally [115-120] and characterized by different spectroscopic techniques, such as microwave [118], photoelectron [119], infrared [120], mass [117,121] and low-temperature infrared [121]

spectroscopy. Vinyl ketene was found to be stable in the gas phase at very low temperatures. The *trans*-vinyl ketene was generated by pyrolysis of vinylacetic anhydride. The derived rotational constants from the microwave study indicated a planar molecule [118]. Many studies on the conformational stability of vinyl ketene showed that it mostly exists in the s-*trans* form. Moreover, the s-*cis* conformation of the molecule was not detected and, as a result, only theoretical investigations shed some light on the less stable conformer [122]. The reactivity and the energetic behavior of the transition structure of vinyl ketene were also predicted by molecular orbital calculation [122-124]. The transition state was calculated to be much higher in energy as compared to the ground state conformers [122,123]. However, no conclusive analysis of the vibrational infrared and Raman spectra of the molecule has been reported.

As a continuation of these studies we investigated the structural stability of vinyl ketene and compared it to that of vinyl isocyanate which has been recently used in cycloaddition reactions [125,126] and polymer synthesis [127,128]. The zero-point corrections were included in the calculation of the energies of ground and transition states at the DFT-B3LYP/6-311++G** level. We also carried out normal coordinate analyses by utilizing ab initio density functional calculations and derived the potential energy distributions (PED) among symmetry coordinates for the stable conformers of the two molecules. The vibrational assignments of the normal modes were made based on the calculated PED values for both systems in their ground states. The results of the work are presented herein.

5.2 AB INITIO CALCULATIONS

The GAUSSIAN 98 program [65], running on an IBM RS/6000 43P model 260 workstation, was used to carry out the LCAO-MO-SCF DFT-B3LYP calculations. The extended 6-311++G** basis set was employed at the Density Functional B3LYP level to optimize the structures and predict the energies and dipole moments of vinyl ketene and vinyl isocyanate in their stable conformations. From full energy optimization, the *cis* and the *trans* conformations were found to be the energy minima for both molecular systems (Figure V-1). The optimized structural parameters of the molecules in the two stable conformations are shown in Tables V-1 and V-2. In addition, the optimized geometrical parameters of vinyl ketene were compared to the corresponding values obtained from experimental data for acrolein [75]. The calculated dipole moment and rotational constants of vinyl ketene were compared to the observed ones for the same molecule obtained from the microwave data [118]. The optimized structural parameters were used to compute their vibrational frequencies at the DFT-B3LYP/6-311++G** level of calculation. Normal coordinate calculations were then carried out to derive the potential energy distributions for the molecules in their stable conformations.

5.2.1 Asymmetric Torsional Potential Functions

The potential scan for the internal rotation about the C-C and the C-N single bond was obtained by allowing the OCCC and the OCNC dihedral angles (ϕ) in the two molecules to vary from 0° (*cis* position) to 180° (*trans* position). Full geometry optimizations at each of

the fixed dihedral angles (ϕ) of 15°, 30°, 45°, 60°, 75°, 90°, 105°, 120°, 135°, 150°, and 165° were carried out at DFT-B3LYP/6-311++G** level of calculation in both systems. The zero-point correction, the barrier to interconversion and the corrected relative energies in vinyl ketene and vinyl isocyanate were calculated and presented in Table V-3. The torsional potential was represented as a Fourier cosine series in the dihedral angle (ϕ): $V(\phi) = V_0 + \sum(V_n/2)[1-\cos(n\phi)]$, where V_0 is the relative energy of the *cis* conformation and the potential coefficients from V_1 to V_6 are considered adequate to describe the potential function. The results of the energy optimizations were used to calculate the six coefficients by least-squares fitting for the systems (Table V-4). The potential functions of vinyl ketene and vinyl isocyanate are shown in Figure V-2.

5.2.2 Vibrational Frequencies and Normal Coordinate Analyses

Both vinyl ketene and vinyl isocyanate in their planar stable conformations have the C_s symmetry. In vinyl ketene there are 21 vibrational modes spanning the irreducible representations: 15 A' and 6 A", while, in vinyl isocyanate, only 18 vibrational modes span the irreducible representations: 13 A' and 5 A". The A' modes should be polarized whereas the A" modes be depolarized in the Raman spectra of the liquid.

Normal coordinate analyses were carried out for the stable conformers of the molecules in order to provide a complete assignment of the fundamental vibrational frequencies. A computer program was written for this purpose by following Wilson's method [71]. The cartesian coordinates for the stable conformers together with the normal modes (in cartesian coordinates) and the frequencies from the GAUSSIAN 98 output were

used as an input in the program. A complete set of internal coordinates (Tables V-5 and V-6, and Figures V-1 and V-2) was used to form symmetry coordinates (Tables V-7 and V-8) in our molecular systems.

The potential energy distribution (PED) for each normal mode among the symmetry coordinates was calculated and is given in Tables V-9 - V-12. A complete vibrational assignment of the fundamentals was proposed. The assignments were made based on calculated PED, infrared band intensities, Raman line activities and depolarization ratios. The data of the vibrational assignments are listed in Tables V-9 - V-12.

5.2.3 Calculation of Vibrational Spectra

To calculate the Raman spectra we used the frequencies ν_j, the scattering activities S_j and the depolarization ratios ρ_j as calculated on DFT-B3LYP level (6-311++G** basis set for all). For the plots we used a grid of a step size of 10 cm^{-1}, but not when a spectral line appears between two consecutive grid points. In this case we inserted 12 points with step size of 0.5 cm^{-1} into this interval which include the exact location of the center of the line. For the infrared spectrum we used the intensities as given by the DFT-B3LYP/6-311++G** calculations and converted them to relative transmittance. The Boltzmann Distribution was used to superimpose the spectra of the *cis* and the *trans* conformers of vinyl ketene and vinyl isocyanate. The degeneracy factor (g_i) value for the vinyl ketene and the vinyl isocyanate in their planar *cis* and *trans* conformations is unity. The temperature $T = 300\ K$ was used. The calculated vibrational Raman and infrared spectra of the vinyl ketene mixture (6% *cis* and

94% *trans*) are shown in Figures V-3 and V-4, while the spectra of the vinyl isocyanate mixture (15% *cis* and 85% *trans)* are shown in Figures V-5 and V-6.

5.3 DISCUSSION

The structural stabilities of acrolein (propenal) [74,130] and some of its halo derivatives [94-97] were the subject of many studies in the past few years. The rotational barriers in these unsaturated aldehydes were determined from ab initio calculation to be high with the *cis* and the *trans* conformers to be the low energy forms. For example, the barrier for *trans* to *cis* interconversion was calculated to be 6.4 kcal/mol for acrolein [74] and was determined from the far-infrared spectra to be 5.7 kcal/mol for propenoyl fluoride, 5.1 kcal/mol for propenoyl chloride [94] and 5.0 kcal/mol for 2-chloropropenoyl fluoride [96].

As we have mentioned earlier, the conjugation effect in the above molecular systems considerably restricts the rotation around the C-C single bond. As a result, relatively high rotational barriers were predicted in the unsaturated aldehydes as compared to the saturated analogues [87,131,132]. For propanal, the saturated form of acrolein, the *cis* and the *gauche* conformations were found to be the stable forms [132]. The halo derivatives of propanal, propinoyl fluoride [87] and propinoyl chloride [131], were predicted to exist as a mixture of *trans* and *gauche* conformers. The calculated *trans* to *gauche* barrier was 2.1 kcal/mol for the fluoro derivative [87] and 3.2 kcal/mol for the chloro one [131].

From the DFT calculation, we found that both vinyl ketene and vinyl isocyanate exist as a mixture of the *cis* and the *trans* planar conformations. The *trans* form in vinyl ketene (the vinyl group eclipses the ketenic hydrogen) and in vinyl isocyanate (the vinyl group eclipses the lone pair of the nitrogen atom) are the most stable minima. The two hydrogen atoms in vinyl ketene, and the hydrogen atom and the lone pair in vinyl isocyanate eclipse each other in the *cis* form. This relatively destabilizes the molecule in the *cis* conformation as compared to the *trans* conformation. The situation is clear from the predicted high relative energy between the two conformers in both molecules as shown in Figure V-2 and Table V-3.

In the vinyl systems under investigation, the π-π interaction between the vinyl group CH_2=CH– and the ketenic group –C=C=O in vinyl ketene or the isocyanato group –N=C=O in vinyl isocyanate, greatly stabilizes the planar forms with a relatively high rotational barrier. Moreover, the C-N barrier in vinyl isocyanate was predicted to be much lower in energy than the C–C barrier in vinyl ketene (Table V-3). The significant difference between the two rotational barriers is due to the decrease in the partial π character of the C–N bond in the isocyanate as compared to that of the C–C bond in the ketene. This difference is the result of the electronegativity change as we go from the C–N bond in vinyl isocyanate to the corresponding C–C one in vinyl ketene. A similar variation was noticed when the energy barrier in formyl ketene was compared to that in formyl isocyanate [134].

We calculated the vibrational frequencies of the stable conformations of the two molecules and plotted the IR and Raman spectra in Figures V-3 - V-6. In general, the derived PED values could be used to provide good assignments for most of the vibrational modes as

one could see from Tables V-9 - V12. Moreover, some of the modes were predicted to be mixed with other modes.

The vibrational modes of the highest frequencies in vinyl ketene and vinyl isocyanate were calculated to be the C-H stretches. There are four C-H stretching modes predicted to appear on the vinyl ketene spectra, and three corresponding modes were found in the vinyl isocyanate spectra. The CH_2 antisymmetric stretches were calculated to have the highest frequencies; 3230 cm^{-1} in the *trans*-vinyl ketene and 3254 cm^{-1} in *trans*-vinyl isocyanate. The ketenic C-H stretch was predicted to be slightly higher in frequency than the vinylic one in both conformers of vinyl ketene, as shown in Tables V-9 and V-10. The vinylic C-H stretching mode in vinyl isocyanate was calculated at 3191 cm^{-1} for the *cis* and 3150 cm^{-1} for the *trans* form.

The antisymmetric –C=C=O and –N=C=O stretching modes were calculated to have the highest infrared intensities in the two molecules, which is consistent with experimental results observed for chlorocarbonyl ketene [105] and ethyl isocyanate [133]. They have a small degree of mixing with other modes in both conformers. The PED values of 97% and 98% were calculated for the antisymmetric stretching –C=C=O mode of vinyl ketene and for the antisymmetric stretching –N=C=O mode of vinyl isocyanate, respectively. Moreover, the highest line activity in the Raman spectra were calculated at 1671 cm^{-1} for vinyl ketene and 1691 cm^{-1} for vinyl isocyanate in their *trans* conformations. These vibrations could be assigned to the stretching C=C vibration in the molecules based on the calculated PED. The corresponding C=C vibration in acrolein was observed at 1625 cm^{-1} [129], which supports our assignment of such a mode in the vinyl systems.

The vinylic C-H in-plane bending modes could be assigned based on the calculated PEDs to ν_9 (1324 cm^{-1}) in vinyl ketene and ν_8 (1336 cm^{-1}) in vinyl isocyanate. The wagging C-H mode of vinyl ketene, however, was predicted to have a higher frequency (1009 cm^{-1}) as compared to the corresponding one in vinyl isocyanate (981 cm^{-1}). The ketenic C-H out-of-plane bending mode in vinyl ketene was calculated to be at 563 cm^{-1}. This agrees very well with the experimental frequency obtained for the same vibrational mode of chloroformyl ketene in the argon matrix experiment (Table V-9).

The assignment of the other four vibrational modes associated with the CH_2 group in both molecules was straightforward from the calculated PED values as shown in Tables V-9 – V-12. The polarized CH_2 deformation modes in vinyl ketene and isocyanate in the *cis* and *trans* forms were predicted to be of higher frequencies as compared to the other CH_2 vibrational modes. The polarized CH_2 deformation in vinyl ketene was calculated to have a frequency of 1451 and 1471 cm^{-1} for the *cis* and the *trans* forms, respectively. This mode was calculated at 1431 cm^{-1} for the *cis*- and 1413 cm^{-1} for the *trans*-vinyl isocyanate. On the other hand, the vibrational frequencies of the corresponding depolarized modes were calculated to be much lower as compared to the polarized ones.

The assignment of some of the vibrational modes related to the *trans* conformation of vinyl ketene was not clear based on the derived PED. The –C=C=O symmetric stretch, the C–C stretch and the ketenic C–H in-plane bend were predicted to strongly couple with each other at ν_8, ν_{10} and ν_{11}. The IR study of chloroformyl ketene in the argon matrix [105] helped us in the assignment of the ketenic C–H in-plane bending mode. The mode was observed at 1125 cm^{-1}; a value that is very close to the frequency of ν_{11} in vinyl ketene. Thus, the ketenic

C–H in-plane bending mode could be assigned with confidence to ν_{11}. Therefore, from the PED values, ν_{10} could be assigned to the stretching C–C mode, hence the –C=C=O symmetric stretch was left to be assigned to ν_8. The C–N stretching and the symmetric –N=C=O stretching modes in vinyl isocyanate were directly assigned, based on the PED values, to ν_{10} and ν_6, respectively.

Many skeletal bending modes in the two molecules were predicted to mix with each other. However, their assignments were made clear with the help of the calculated PEDs (Tables V-9 - V12). For instance, the out-of-plane bending –C=C=O vibration in vinyl ketene was calculated at 510 cm^{-1} with 60% PED for the *cis* form and 514 cm^{-1} with 83% PED for the *trans* form. In vinyl isocyanate, the –N=C=O out-of-plane bending mode was calculated at 585 cm^{-1} for the *cis* and 577 cm^{-1} for the *trans* with a PED value of 96% for the both conformations.

The lowest vibrational modes in the spectra of the two vinyl systems were the asymmetric torsions, except the *cis* conformer of the isocyanate in which the lowest vibration at 110 cm^{-1} was predicted to associate with the in-plane C–N=C bending mode. In vinyl ketene, the asymmetric torsion was calculated at 82 and 132 cm^{-1} for the *cis* and *trans* conformers, respectively, while in vinyl isocyanate it was predicted at 123 cm^{-1} for the *cis* and 93 cm^{-1} for the *trans* form.

Finally, we provided reliable vibrational assignments for the normal modes of the stable conformers of vinyl ketene and vinyl isocyanate based on the normal coordinate analysis. The calculated PED values gave a good assignment for most of the bending and stretching modes in the two systems.

TABLE V-1: **Calculated Structural Parameters, Total Dipole Moment, and Rotational Constants for the *Cis* and the *Trans* Conformations of Vinyl Ketene.**

Parameter	B3LYP/6-311++G**		Microwave [a]	
	cis	*trans*	*cis*	*trans*
Bond Length (Å)				
$r(C_1\text{-}C_2)$	1.338	1.338	1.339	1.341
$r(C_2\text{-}C_3)$	1.464	1.458	1.479	1.468
$r(C_3\text{-}C_4)$	1.316	1.320		
$r(C_4\text{-}O_5)$	1.160	1.161		
$r(C_1\text{-}H_6)$	1.085	1.085	1.099	1.089
$r(C_1\text{-}H_7)$	1.082	1.082	1.081	1.081
$r(C_2\text{-}H_8)$	1.086	1.086	1.087	1.084
$r(C_3\text{-}H_9)$	1.084	1.085		
Bond Angle (deg)				
$(C_1C_2C_3)$	128.0	124.6	121.4	120.3
$(C_2C_3C_4)$	125.0	123.6		
$(C_3C_4O_5)$	179.9	180.4		
$(C_2C_1H_6)$	122.7	122.0	118.5	119.8
$(C_2C_1H_7)$	120.5	120.8	121.6	122.2
$(C_1C_2H_8)$	118.7	119.1	121.0	122.4
$(C_3C_2H_8)$	113.3	116.3	117.6	117.3
$(H_6C_1H_7)$	116.7	117.2	120.0	118.0
$(C_2C_3H_9)$	120.0	120.8		
$(C_2C_3C_4O_5)$	0.0	180.0	0.0	180.0
Dipole Moment (Debye)				
μ_t	1.4	1.0		(0.97)
Rotational Constants (MHz)				
A	14481	40768		(39557)
B	3259	2375		(2393)
C	2660	2244		(2256)

[a] Data was obtained for acrolein from ref [75], and data between brackets was obtained from microwave experiment for vinyl ketene, see ref [118].

TABLE V-2: **Calculated Structural Parameters, Total Dipole Moment, and Rotational Constants for the *Cis* and the *Trans* Conformations of Vinyl Isocyanate.**

Parameter	B3LYP/6-311++G**	
	cis	*trans*
Bond Length (Å)		
$r(C_1\text{-}C_2)$	1.333	1.331
$r(C_2\text{-}N_3)$	1.393	1.394
$r(N_3\text{-}C_4)$	1.203	1.204
$r(C_4\text{-}O_5)$	1.170	1.170
$r(C_1\text{-}H_6)$	1.084	1.083
$r(C_1\text{-}H_7)$	1.082	1.082
$r(C_2\text{-}H_8)$	1.083	1.086
Bond Angle (deg)		
$(C_1C_2N_3)$	125.7	122.5
$(C_2N_3C_4)$	142.2	139.6
$(N_3C_4O_5)$	173.7	173.8
$(C_2C_1H_6)$	122.4	121.6
$(C_2C_1H_7)$	119.6	119.9
$(C_1C_2H_8)$	121.5	121.7
$(C_2N_3C_4O_5)$	0.0	180.0
Dipole Moment (Debye)		
μ_t	2.3	2.3
Rotational Constants (MHz)		
A	22179	65232
B	2957	2412
C	2609	2326

TABLE V-3: **Computed Total Energies, Zero-Point Corrections (Hartrees), Relative Energies, and Rotational Barriers (kcal/mol) in Vinyl Ketene and Vinyl Isocyanate.**

	B3LYP/6-311++G**					
	Vinyl ketene			Vinyl isocyanate		
	cis	*trans*	*TS*[a]	*cis*	*trans*	*TS*[b]
Total energy	-230.06870	-230.07151	-230.06143	-246.14897	-246.15046	-246.14746
Relative energy		1.76330			0.93499	
Cis-trans barrier		4.56200			0.94754	
Trans-cis barrier		6.32530			1.88253	
Zero-point correction	0.06590	0.06605	0.06540	0.05558	0.05545	0.05516
Sum of total and zero-point energies	-230.00280	-230.00546	-229.99603	-246.09339	-246.09501	-246.09230
Corrected relative energy		1.66918			1.01657	
Corrected *cis-trans* barrier		4.24824			0.68399	
Corrected *trans-cis* barrier		5.91741			1.70055	

[a] The CCCO dihedral angle of the *transition state* of vinyl ketene was calculated to be 97.17°.

[b] The CNCO dihedral angle of the *transition state* of vinyl isocyanate was calculated to be 78.60°.

TABLE V-4: **Calculated Potential Constants (kcal/mol) for the Asymmetric Torsion in Vinyl Ketene and Vinyl Isocyanate.**

Potential Constants	B3LYP/6-311++G**	
	Vinyl ketene	Vinyl isocyanate
V_1	0.091	-0.597
V_2	5.864	1.676
V_3	-0.708	0.244
V_4	0.417	0.383
V_5	0.530	0.308
V_6	0.537	0.268

Table V-5: **Internal Coordinate Definitions [a] for Vinyl Ketene.**

No.	Coordinate		Definition
1	C_1-C_2	stretch	R
2	C_2-C_3	stretch	X
3	C_3-C_4	stretch	S
4	C_4-O_5	stretch	Q
5	C_2-H_8	stretch	T
6	C_3-H_9	stretch	D
7	C_1-H_6	stretch	P_1
8	C_1-H_7	stretch	P_2
9	$C_1C_2C_3$	bend	β_1
10	$C_3C_2H_8$	bend	β_2
11	$C_1C_2H_8$	bend	β_3
12	$C_2C_3C_4$	bend	γ
13	$C_3C_4O_5$	bend	σ
14	$C_4C_3H_9$	bend	δ
15	$C_2C_3H_9$	bend	ρ
16	$H_6C_1H_7$	bend	α_1
17	$C_2C_1H_6$	bend	α_2
18	$C_2C_1H_7$	bend	α_3
19	C_3=C_4=O_5	wag (out-of-plane bend)	χ
20	C_2-H_8	wag (out-of-plane bend)	ω
21	C_3-H_9	wag (out-of-plane bend)	π
22	$(H_6C_1C_2C_3 - H_7C_1C_2C_3)$	torsion	ξ_1
23	$(H_6C_1C_2C_3 + H_7C_1C_2C_3)$	torsion	ξ_2
24	$C_1C_2C_3H_9$ $C_1C_2C_3C_4$	Asymmetric torsion	τ

[a] See Figure V-1 for atom denotation.

TABLE V-6: **Internal Coordinate Definitions [a] for Vinyl Isocyanate.**

No.	Coordinate	Definition	
1	C_1-C_2	stretch	R
2	C_2-N_3	stretch	X
3	N_3-C_4	stretch	S
4	C_4-O_5	stretch	Q
5	C_1-H_6	stretch	P_1
6	C_1-H_7	stretch	P_2
7	C_2-H_8	stretch	T
8	$C_1C_2N_3$	bend	β_1
9	$N_3C_2H_8$	bend	β_2
10	$C_1C_2H_8$	bend	β_3
11	$C_2N_3C_4$	bend	γ
12	$N_3C_4O_5$	bend	σ
13	$H_6C_1H_7$	bend	α_1
14	$C_2C_1H_6$	bend	α_2
15	$C_2C_1H_7$	bend	α_3
16	N=C=O	wag	χ
17	C_2-H_8	wag (out-of-plane bend)	ω
18	$(H_6C_1C_2N_3 - H_7C_1C_2N_3)$	torsion	ξ_1
19	$(H_6C_1C_2N_3 + H_7C_1C_2N_3)$	torsion	ξ_2
20	$C_1C_2N_3C_4$	Asymmetric torsion	τ
	$H_8C_2N_3C_4$		

[a] See Figure V-2 for atom denotation.

***TABLE V-7:* Symmetry Coordinates for Vinyl Ketene.**

Species	Description		Symmetry Coordinate [a]
A'	C_1=C_2	stretch	$S_1 = R$
	C–C	stretch	$S_2 = X$
	C_2–H_8	stretch	$S_3 = T$
	C_3–H_9	stretch	$S_4 = D$
	C=C=O	symmetric stretch	$S_5 = S + Q$
	C=C=O	antisymmetric stretch	$S_6 = S - Q$
	C=C=O	in-plane bend	$S_7 = \sigma$
	C_2–H_8	in-plane bend	$S_8 = \beta_2 - \beta_3$
	C_3–H_9	in-plane bend	$S_9 = \rho - \delta$
	C_1=C_2–C_3	in-plane bend	$S_{10} = 2\beta_1 - \beta_2 - \beta_3$
	C_2–C_3=C_4	in-plane bend	$S_{11} = 2\gamma - \rho - \delta$
	CH_2	symmetric stretch	$S_{12} = P_1 + P_2$
	CH_2	antisymmetric stretch	$S_{13} = P_1 - P_2$
	CH_2	deformation	$S_{14} = 2\alpha_1 - \alpha_2 - \alpha_3$
	CH_2	wag	$S_{15} = \alpha_2 - \alpha_3$
A''	C=C=O	wag (out-of-plane bend)	$S_{16} = \chi$
	C_2–H_8	wag (out-of-plane bend)	$S_{17} = \omega$
	C_3–H_9	wag (out-of-plane bend)	$S_{18} = \pi$
	CH_2	deformation I	$S_{19} = \xi_1$
	CH_2	deformation II	$S_{20} = \xi_2$
	Asymmetric torsion		$S_{21} = \tau$

[a] Not normalized.

TABLE V-8: **Symmetry Coordinates for Vinyl Isocyanate.**

Species	Description		Symmetry Coordinate [a]
A'	C=C	stretch	$S_1 = R$
	C–N	stretch	$S_2 = X$
	C_2–H_8	stretch	$S_3 = T$
	N=C=O	symmetric stretch	$S_4 = S + Q$
	N=C=O	antisymmetric stretch	$S_5 = S - Q$
	N=C=O	in-plane bend	$S_6 = \sigma$
	C_2–H_8	in-plane bend	$S_7 = \beta_2 - \beta_3$
	C=C–N	in-plane bend	$S_8 = 2\beta_1 - \beta_2 - \beta_3$
	C–N=C	in-plane bend	$S_9 = \gamma$
	CH_2	symmetric stretch	$S_{10} = P_1 + P_2$
	CH_2	antisymmetric stretch	$S_{11} = P_1 - P_2$
	CH_2	deformation	$S_{12} = 2\alpha_1 - \alpha_2 - \alpha_3$
	CH_2	wag	$S_{13} = \alpha_2 - \alpha_3$
A''	N=C=O	wag (out-of-plane bend)	$S_{14} = \chi$
	C_2–H_8	wag (out-of-plane bend)	$S_{15} = \omega$
	CH_2	deformation I	$S_{16} = \xi_1$
	CH_2	deformation II	$S_{17} = \xi_2$
	Asymmetric torsion		$S_{18} = \tau$

[a] Not normalized.

TABLE V-9: **Calculated Vibrational Frequencies (cm^{-1}) at B3LYP/6-311++G** Level for the *Cis* Conformer of Vinyl Ketene.**

Symm.	Number	Frequency	IR Intensity [a]	Raman Activity	Depol. Ratio	PED [b]
A'	ν_1	3225	9.2	80.3	0.5	94% CH_2 antisymm. str. (S_{13})
	ν_2	3182	7.1	128.1	0.2	95% C_3-H_9 str. (S_4)
	ν_3	3156	11.9	82.7	0.4	92% C_2-H_8 str. (S_3)
	ν_4	3135	5.3	66.1	0.1	95% CH_2 symm. str. (S_{12})
	ν_5	2200	860.7	25.6	0.4	97% C=C=O antisymm. str. (S_6)
	ν_6	1667	65.2	107.7	0.2	65% C_1=C_2 str. (S_1), 17% CH_2 def. (S_{14})
	ν_7	1451	13.6	35.9	0.3	74% CH_2 def. (S_{14}), 12% C_2-H_8 in-plane bend (S_8)
	ν_8	1424	31.1	49.6	0.2	38% C=C=O symm. str. (S_5), 32% C_3-H_9 in-plane bend (S_9), 16% C-C str. (S_2)
	ν_9	1334	0.2	21.3	0.2	58% C_2-H_8 in-plane bend (S_8), 17% C_1=C_2 str. (S_1), 11% CH_2 wag (S_{15})
	ν_{10}	1146	0.4	13.0	0.4	59% C_3-H_9 in-plane bend (S_9), 25% C=C=O symm. str. (S_5)
	ν_{11}	1060	8.4	5.7	0.6	67% CH_2 wag (S_{15}), 12% C_2-H_8 in-plane bend (S_8), 12% C=C=O symm. str. (S_5)
	ν_{12}	934	7.6	8.4	0.2	51% C-C str. (S_2), 13% C=C=O symm. str. (S_5), 10% C_2-C_3=C_4 in-plane bend (S_{11}), 10% C=C=O in-plane bend (S_7)
	ν_{13}	696	9.6	4.0	0.4	34% C=C=O in-plane bend (S_7), 24% C_2-C_3=C_4 in-plane bend (S_{11}), 13% C-C str. (S_2), 10% CH_2 wag (S_{15})
	ν_{14}	434	4.7	3.9	0.3	62% C_1=C_2-C_3 in-plane bend (S_{10}), 27% C=C=O in-plane bend (S_7)
	ν_{15}	144	1.4	8.6	0.6	62% C_2-C_3=C_4 in-plane bend (S_{11}), 25% C=C=O in-plane bend (S_7), 12% C_1=C_2-C_3 in-plane bend (S_{10})

TABLE V-9: **Continue.**

Symme.	Number	Frequency	IR Intensity [a]	Raman Activity	Depol. Ratio	PED [b]
A"	ν_{16}	1011	15.1	2.3	0.8	84% C_2-H_8 wag (S_{17}), 16% CH_2 def. II (S_{20})
	ν_{17}	896	56.7	9.6	0.8	98% CH_2 def. I (S_{19})
	ν_{18}	682	0.02	6.3	0.8	63% CH_2 def. II (S_{20}), 23% C_3-H_9 wag (S_{18}), 10% C_2-H_8 wag (S_{17})
	ν_{19}	557	57.5	1.7	0.8	45% C_3-H_9 wag (S_{18}), 36% C=C=O wag (S_{16}), 13% CH_2 def. II (S_{20})
	ν_{20}	510	10.4	0.8	0.8	60% C=C=O wag (S_{16}), 28% C_3-H_9 wag (S_{18})
	ν_{21}	82	0.3	0.6	0.8	90% asymm. torsion (S_{21})

[a] Infrared intensities and Raman activities are calculated in Km mol^{-1} and $Å^4$ amu^{-1} respectively.

[b] PED values are obtained by using calculated frequencies at B3LYP level.

TABLE V-10: **Calculated Vibrational Frequencies (cm^{-1}) at B3LYP/6-311++G** level for the *Trans* Conformer of Vinyl Ketene.**

Symm.	Number	Frequency	IR Intensity [a]	Raman Activity	Depol. Ratio	Obs. [b]	PED [c]
A'	ν_1	3230	10.2	82.4	0.6	3103	96% CH_2 antisymm. str. (S_{13})
	ν_2	3169	6.1	44.8	0.2		94% C_3-H_9 str. (S_4)
	ν_3	3148	4.6	164.1	0.3	3069	84% C_2-H_8 str. (S_3)
	ν_4	3139	7.5	53.5	0.1	2998	89% CH_2 symm. str. (S_{12})
	ν_5	2205	1103.5	16.4	0.3	(2160)	97% C=C=O antisymm. str. (S_6)
	ν_6	1671	102.3	212.6	0.2	1625	65% C_1=C_2 str. (S_1), 14% CH_2 def. (S_{14}) , 10% C_2-H_8 in-plane bend (S_8)
	ν_7	1471	3.9	56.0	0.3	1420	61% CH_2 def. (S_{14}), 12% C_2-H_8 in-plane bend (S_8)
	ν_8	1359	0.4	3.3	0.6	(1376)	30% C=C=O symm. str. (S_5), 23% C_1=C_2 str. (S_1), 23% CH_2 def. (S_{14}), 18% C_3-H_9 in-plane bend (S_9)
	ν_9	1324	1.5	48.6	0.3	1275	63% C_2-H_8 in-plane bend (S_8), 11% CH_2 wag (S_{15})
	ν_{10}	1185	18.9	42.4	0.4		32% C-C str. (S_2), 24% C_3-H_9 in-plane bend (S_9), 21% CH_2 wag (S_{15})
	ν_{11}	1117	13.1	11.1	0.2	(1125)	36% C_3-H_9 in-plane bend (S_9), 29% C=C=O symm. str. (S_5), 11% CH_2 wag (S_{15})
	ν_{12}	927	2.9	1.4	0.3	912	49% CH_2 wag (S_{15}), 26% C-C str. (S_2)
	ν_{13}	637	8.9	6.9	0.2		50% C=C=O in-plane bend (S_7), 21% C_2-C_3=C_4 in-plane bend (S_{11}), 17% C-C str. (S_2)
	ν_{14}	415	1.8	8.5	0.3	324	72% C_1=C_2-C_3 in-plane bend (S_{10})
	ν_{15}	172	4.0	1.5	0.6		63% C_2-C_3=C_4 in-plane bend (S_{11}), 27% C=C=O in-plane bend (S_7)

TABLE V-10: **Continue.**

Symm.	Number	Frequency	IR Intensity [a]	Raman Activity	Depol. Ratio	Obs. [b]	PED [c]
A"	ν_{16}	1009	20.3	1.0	0.8	972	82% C_2-H_8 wag (S_{17}), 19% CH_2 def. II (S_{20})
	ν_{17}	896	59.7	9.7	0.8	993	98% CH_2 def. I (S_{19})
	ν_{18}	711	0.7	2.9	0.8	959	48% CH_2 def. II (S_{20}), 33% C_3-H_9 wag (S_{18}), 11% C_2-H_8 wag (S_{17})
	ν_{19}	563	51.5	0.9	0.8	(558)	46% C_3-H_9 wag (S_{18}), 26% CH_2 def. II (S_{20}), 15% C=C=O wag (S_{16})
	ν_{20}	514	0.4	3.4	0.8		83% C=C=O wag (S_{16})
	ν_{21}	132	0.1	1.3	0.8	158	80% asymm. torsion (S_{21}), 18% C_3-H_9 wag (S_{18})

[a] Infrared intensities and Raman activities are calculated in Km mol^{-1} and $Å^4$ amu^{-1}, respectively.

[b] Observed infrared frequencies for *trans*-acrolein obtained in the gas phase [129]; the values in brackets are for *trans*-chloroformyl ketene obtained from a low-temperature infrared experiment in the argon matrix [105].

[c] PED values are obtained by using calculated frequencies at B3LYP level.

TABLE V-11: **Calculated Vibrational Frequencies (cm^{-1}) at B3LYP/6-311++G** Level for the *Cis* Conformer of Vinyl Isocyanate.**

Symm.	Number	Frequency	IR Intensity [a]	Raman Activity	Depol. Ratio	PED [b]
A'	ν_1	3245	6.3	75.5	0.5	96% CH_2 antisymm. str. (S_{11})
	ν_2	3191	8.9	114.5	0.3	96% C_2-H_8 str. (S_3)
	ν_3	3151	1.5	79.3	0.1	97% CH_2 symm. str. (S_{10})
	ν_4	2363	1375.7	18.8	0.1	98% N=C=O antisymm. str. (S_5)
	ν_5	1672	81.6	140.9	0.1	66% C=C str. (S_1), 14% CH_2 def. (S_{12})
	ν_6	1524	14.1	56.3	0.2	59% N=C=O symm. str. (S_4), 25% C-N str. (S_2)
	ν_7	1431	3.3	8.5	0.4	62% CH_2 def. (S_{12}), 31% C_2-H_8 in-plane bend (S_7)
	ν_8	1336	0.8	22.6	0.4	49% C_2-H_8 in-plane bend (S_7), 23% C=C str. (S_1), 14% CH_2 def. (S_{12})
	ν_9	1091	47.9	5.1	0.7	62% CH_2 wag (S_{13}), 14% C=C-N in-plane bend (S_8), 10% N=C=O symm. str. (S_4)
	ν_{10}	849	37.8	3.9	0.2	58% C-N str. (S_2), 23% N=C=O symm. str. (S_4), 15% CH_2 wag (S_{13})
	ν_{11}	635	36.2	0.7	0.7	83% N=C=O in-plane bend (S_6)
	ν_{12}	497	15.1	1.7	0.3	70% C=C-N in-plane bend (S_8), 11% CH_2 wag (S_{13}), 11% N=C=O in-plane bend (S_6)
	ν_{13}	110	4.1	9.4	0.6	96% C-N=C in-plane bend (S_9)

TABLE V-11: **Continue.**

Symm.	Number	Frequency	IR Intensity [a]	Raman Activity	Depol. Ratio	PED [b]
A"	ν_{14}	996	23.3	1.6	0.8	83% C_2-H_8 wag (S_{15}), 16% CH_2 def. II (S_{17})
	ν_{15}	906	55.9	5.0	0.8	99% CH_2 def. I (S_{16})
	ν_{16}	695	5.5	2.7	0.8	83% CH_2 def. II (S_{17}), 15% C_2-H_8 wag (S_{15})
	ν_{17}	585	23.2	0.4	0.8	96% N=C=O wag (S_{14})
	ν_{18}	123	2.3	0.7	0.8	95% asymm. torsion (S_{18})

[a] Infrared intensities and Raman activities are calculated in Km mol^{-1} and $Å^4$ amu^{-1} respectively.

[b] PED values are obtained by using calculated frequencies at B3LYP level.

TABLE V-12: **Calculated Vibrational Frequencies (cm^{-1}) at B3LYP/6-311++G** Level for the *Trans* Conformer of Vinyl Isocyanate.**

Symm.	Number	Frequency	IR Intensity [a]	Raman Activity	Depol. Ratio	PED [b]
A'	ν_1	3254	3.7	71.5	0.7	99% CH_2 antisymm. str. (S_{11})
	ν_2	3163	1.7	170.9	0.2	77% CH_2 symm. str. (S_{10}), 21% C_2-H_8 str. (S_3)
	ν_3	3150	11.9	25.4	0.6	77% C_2-H_8 str. (S_3), 22% CH_2 symm. str. (S_{10})
	ν_4	2364	1593.8	13.1	0.1	98% N=C=O antisymm. str. (S_5)
	ν_5	1691	166.4	194.0	0.1	65% C=C str. (S_1), 13% CH_2 def. (S_{12}) , 10% C_2-H_8 in-plane bend (S_7)
	ν_6	1506	4.8	80.2	0.3	57% N=C=O symm. str. (S_4), 23% C-N str. (S_2), 17% CH_2 def. (S_{12})
	ν_7	1413	7.3	2.1	0.3	54% CH_2 def. (S_{12}), 28% C_2-H_8 in-plane bend (S_7), 12% N=C=O symm. str. (S_4)
	ν_8	1340	2.8	27.8	0.4	56% C_2-H_8 in-plane bend (S_7), 19% C=C str. (S_1), 16% CH_2 def. (S_{12})
	ν_9	1114	14.9	3.1	0.7	55% CH_2 wag (S_{13}), 19% C=C-N in-plane bend (S_8), 12% C-N str. (S_2)
	ν_{10}	847	23.2	2.4	0.2	50% C-N str. (S_2), 26% CH_2 wag (S_{13}), 19% N=C=O symm. str. (S_4)
	ν_{11}	633	36.3	0.9	0.6	91% N=C=O in-plane bend (S_6)
	ν_{12}	455	4.5	10.2	0.4	76% C=C-N in-plane bend (S_8), 10% CH_2 wag (S_{13})
	ν_{13}	137	6.4	0.6	0.6	93% C-N=C in-plane bend (S_9)

TABLE V-12: **Continue.**

Symm.	Number	Frequency	IR Intensity [a]	Raman Activity	Depol. Ratio	PED [b]
A"	ν_{14}	981	25.5	1.3	0.8	81% C_2-H_8 wag (S_{15}), 19% CH_2 def. II (S_{17})
	ν_{15}	918	55.5	7.0	0.8	98% CH_2 def. I (S_{16})
	ν_{16}	703	7.7	1.9	0.8	80% CH_2 def. II (S_{17}), 18% C_2-H_8 wag (S_{15})
	ν_{17}	577	21.1	0.9	0.8	96% N=C=O wag (S_{14})
	ν_{18}	93	0.3	0.1	0.8	98% asymm. torsion (S_{18})

[a] Infrared intensities and Raman activities are calculated in Km mol^{-1} and $Å^4$ amu^{-1} respectively.

[b] PED values are obtained by using calculated frequencies at B3LYP level.

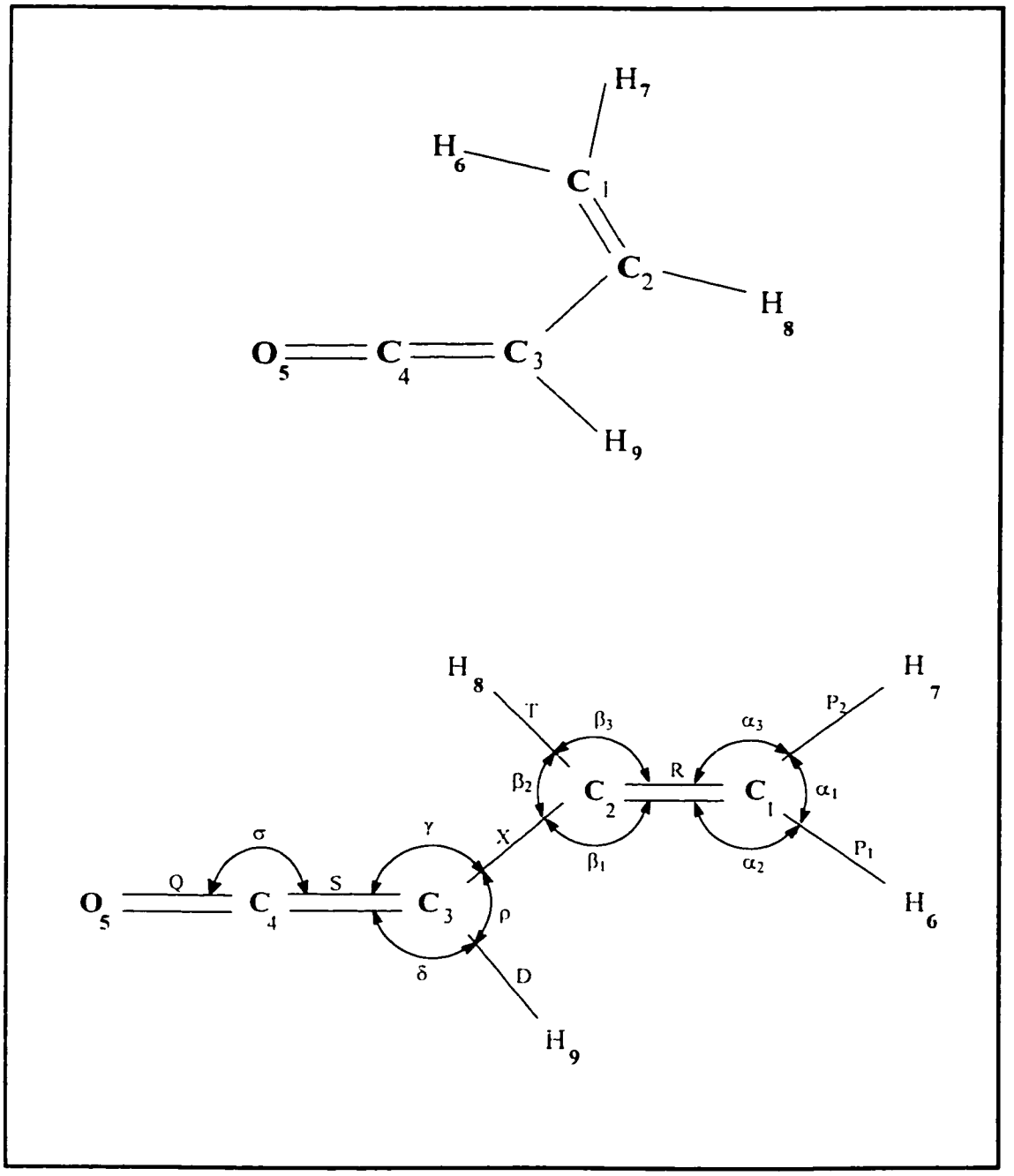

FIGURE V-1: **Atom Numbering for Vinyl Ketene in the *Cis* (Upper) and the *Trans* (Lower) Conformations, With the Internal Coordinates Shown on the *Trans* Conformation.**

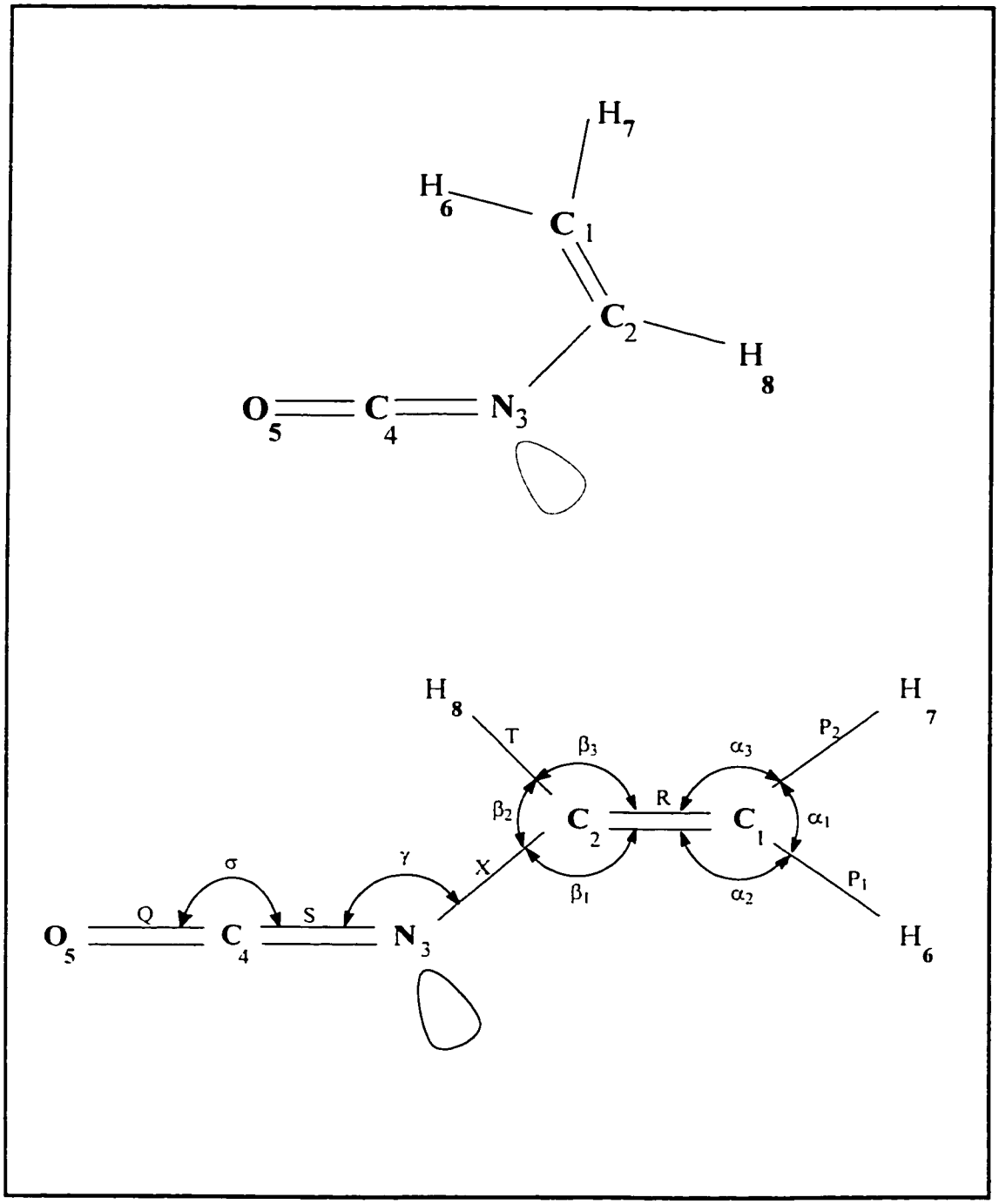

FIGURE V-2: **Atom Numbering for Vinyl Isocyanate in the *Cis* (Upper) and the *Trans* (Lower) Conformations, With the Internal Coordinates Shown on the *Trans* Conformation.**

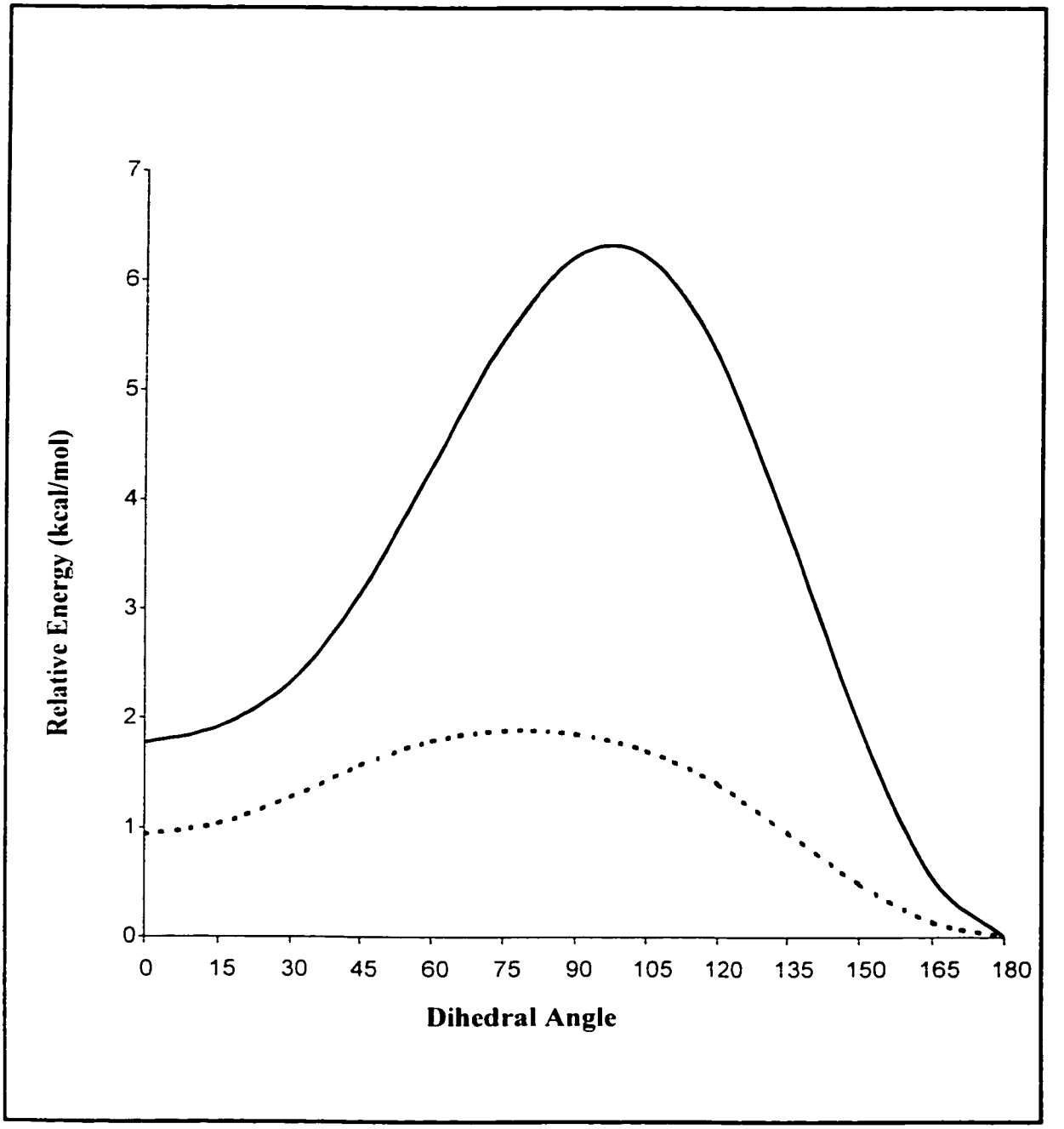

FIGURE V-3: **Potential Curve for the Internal Rotation in Vinyl Ketene (Solid Line) and Vinyl Isocyanate (Dashed Line) as Determined by Ab Initio Calculations at B3LYP/6-311++G** Level.**

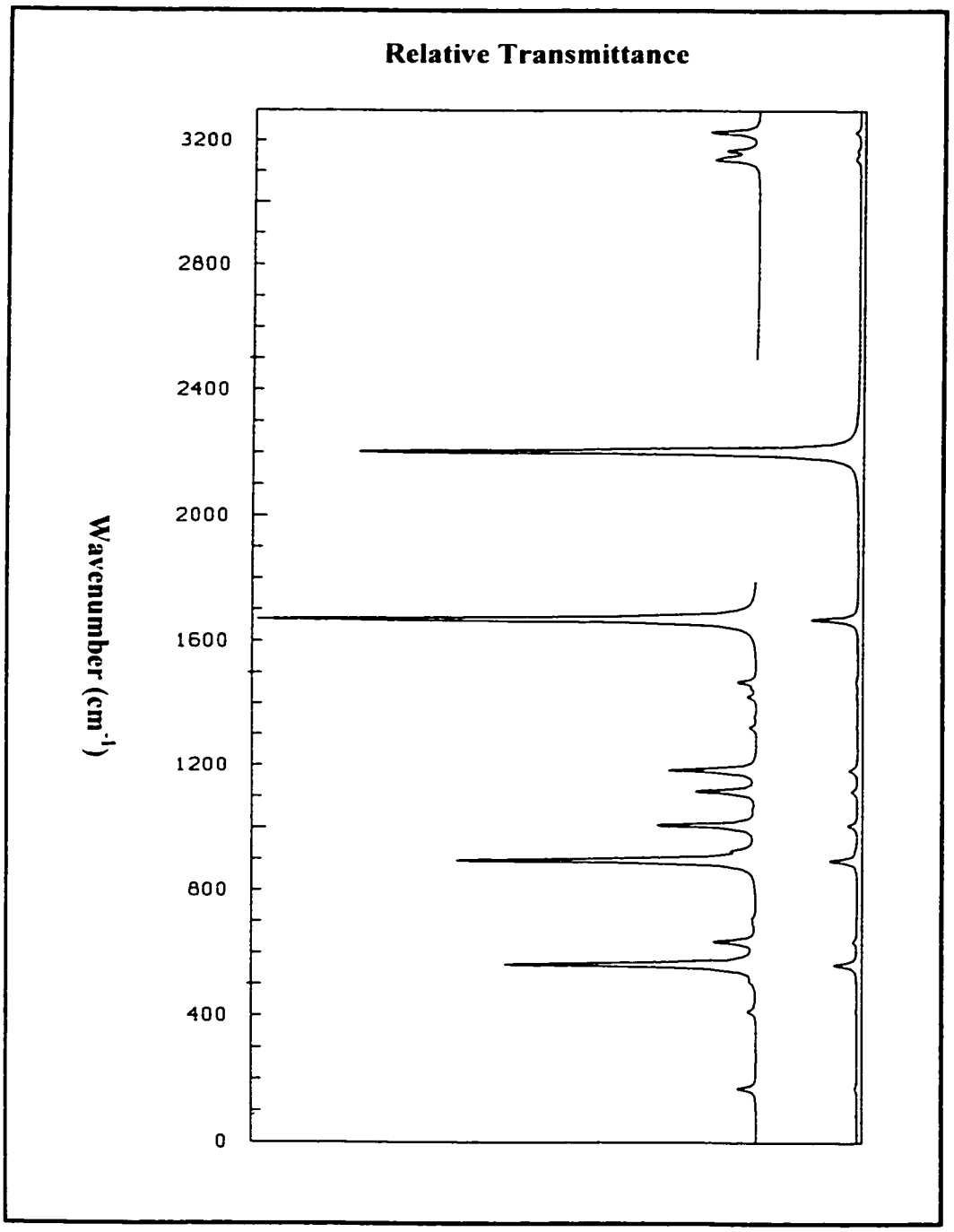

FIGURE V-4: **Calculated Vibrational Infrared Spectrum of Vinyl Ketene at 300 K at the DFT-B3LYP/6-311++G** Level.**

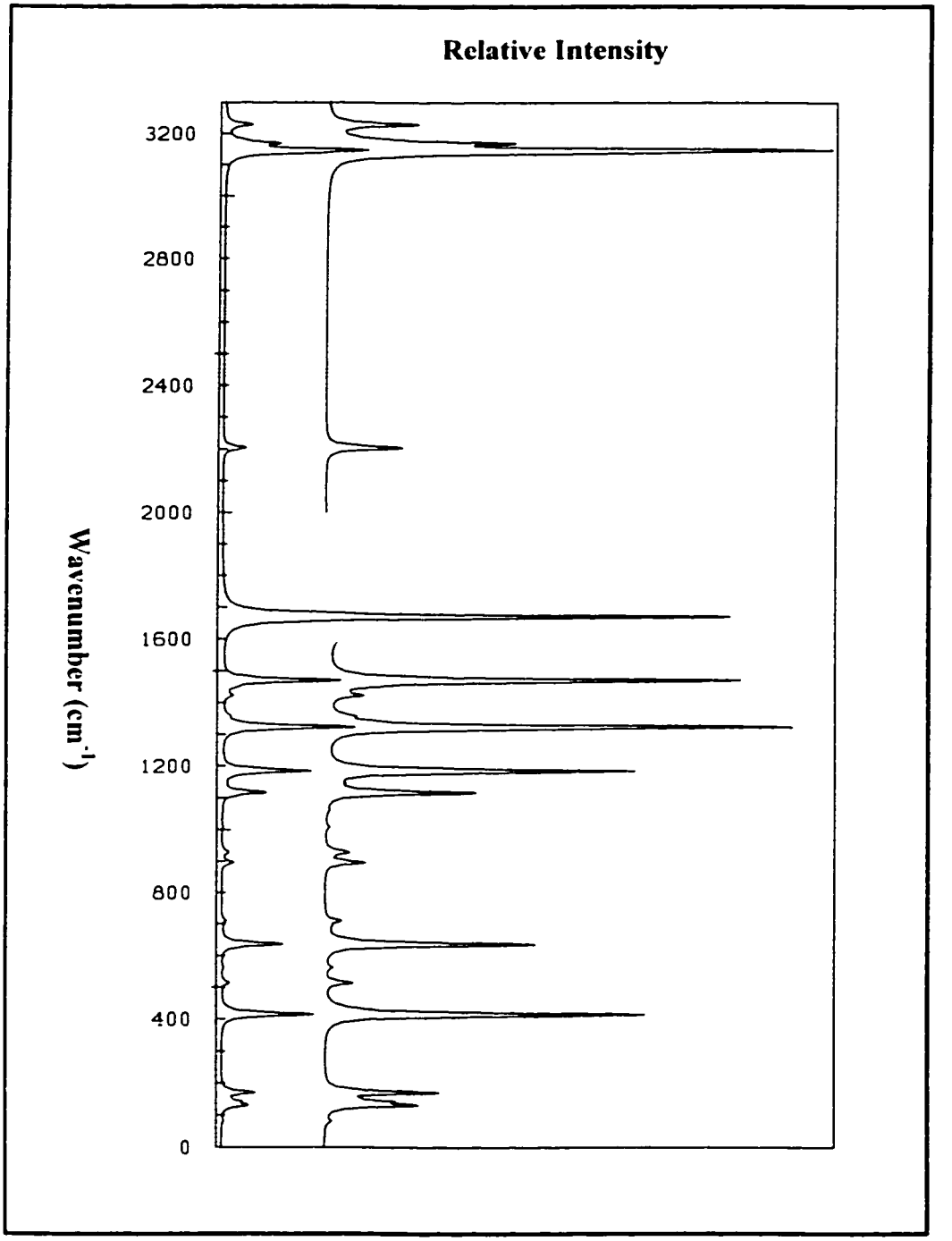

FIGURE V-5: **Calculated Vibrational Raman Spectrum of Vinyl Ketene at 300 K at the DFT-B3LYP/6-311++G** Level.**

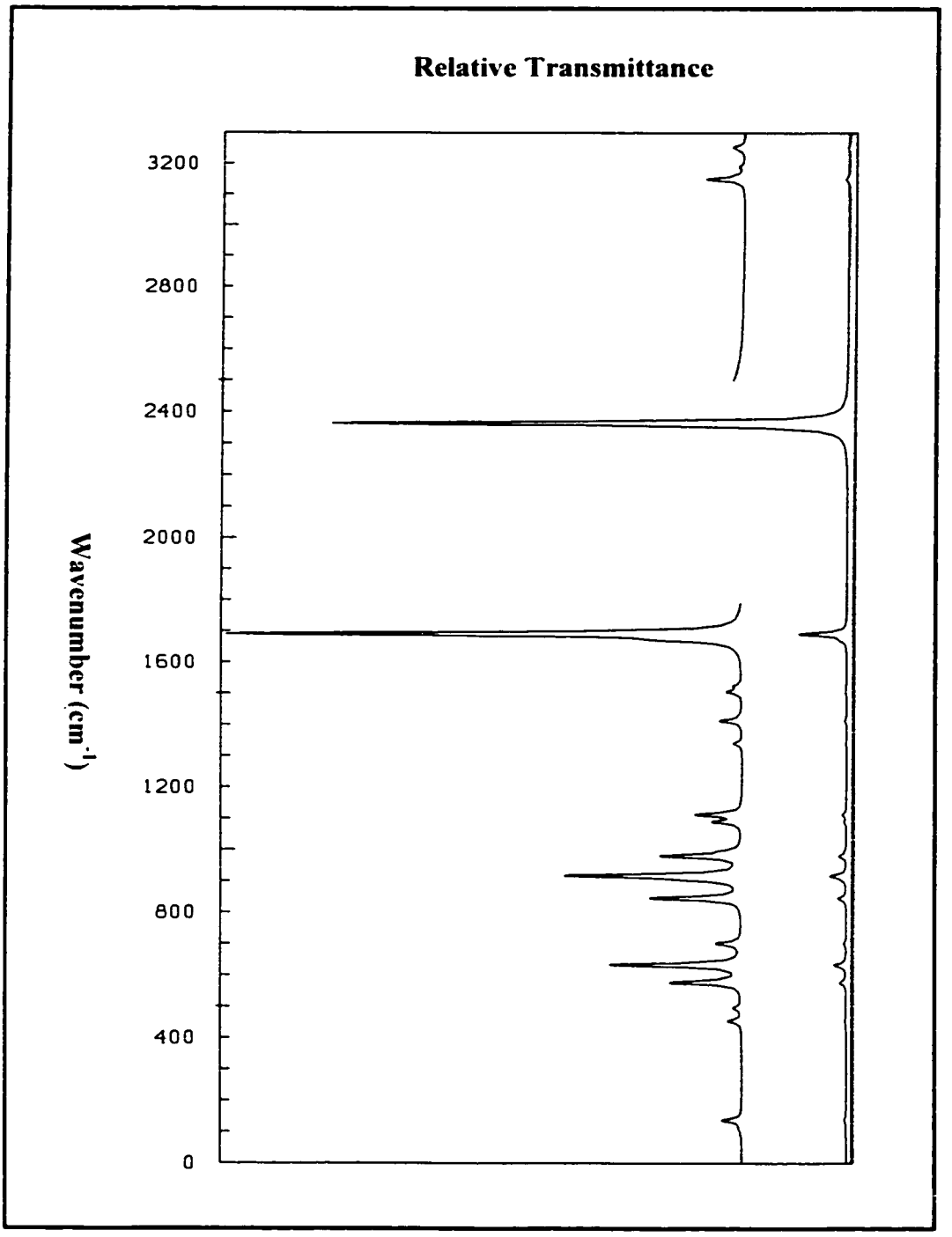

FIGURE V-6: **Calculated Vibrational Infrared Spectrum of Vinyl Isocyanate at 300 K at the DFT-B3LYP/6-311++G** Level.**

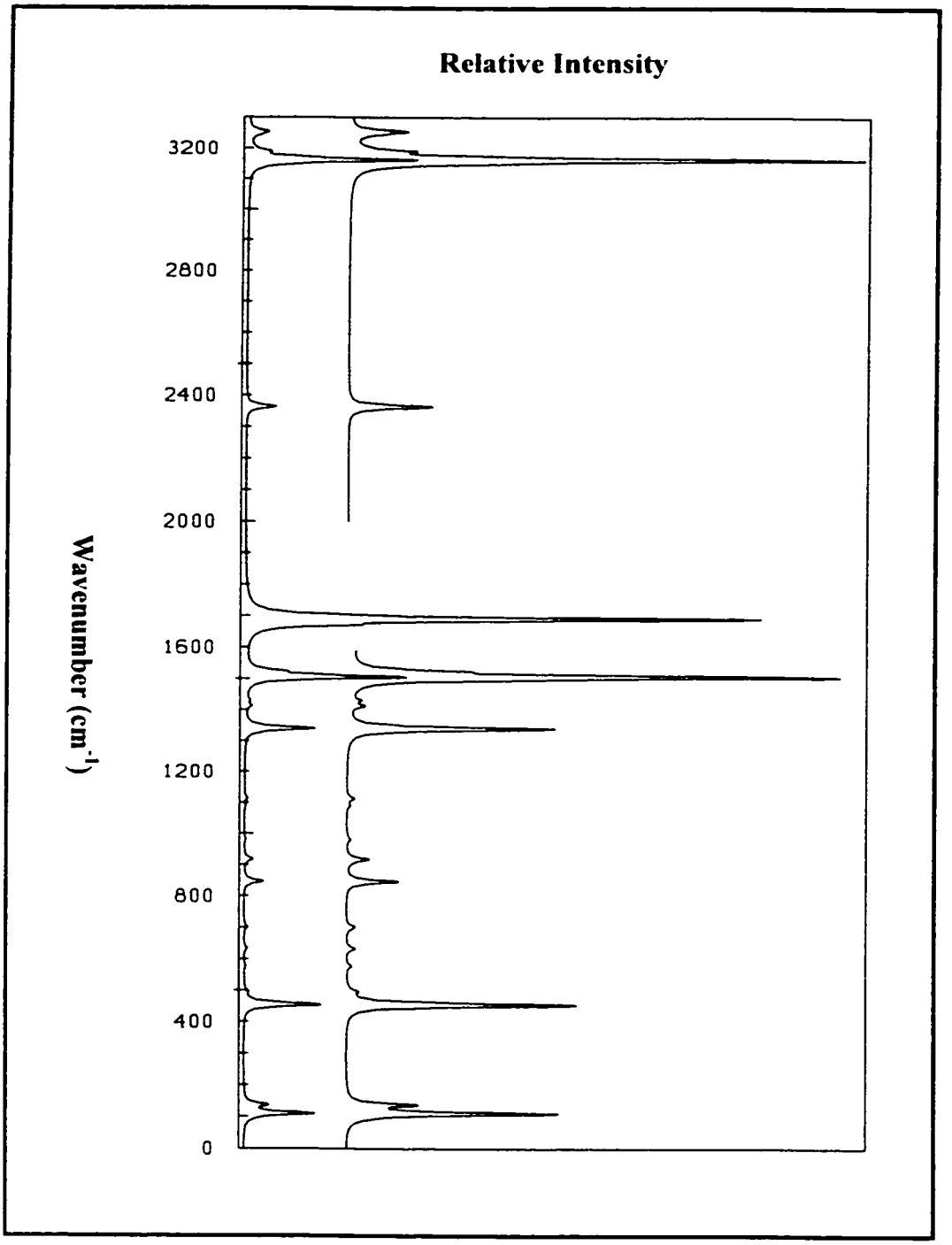

FIGURE V-7: **Calculated Vibrational Raman Spectrum of Vinyl Isocyanate at 300 K at the DFT-B3LYP/6-311++G** Level.**

CHAPTER 6

VIBRATIONAL ASSIGNMENTS AND DERIVED POTENTIAL ENERGY DISTRIBUTIONS FOR TRI- AND DIFLUOROMETHYL KETENE BY DENSITY FUNCTIONAL CALCULATIONS

6.1 INTRODUCTION

The interesting electronic structure and chemical reactivity of ketenes have been demonstrated in the literature [40-45,122,135]. Many simple substituted ketenic molecules were isolated experimentally, characterized, and used to produce other ketenic and organic systems [37,47,98-102,103,105]. The importance of ketenes as well as aldehydes [5,17,20,30,36,74-83,130] and isocyanates [72,83,88,110,111,133,134,136-145] in synthetic chemistry has attracted the attention to study their properties and structural stabilities for many years.

When conjugation was the predominant force, as in acrolein [74,130], formyl ketene and formyl isocyanate [134], the molecules were determined to exist as a mixture of the planar *cis* and *trans* conformations. In these compounds, it was clear that the π-π interaction between the C=O bond and vinyl –C=C–, the ketene –C=C=O or the isocyanate –N=C=O

groups greatly stabilizes the planar forms with a relatively high rotational barrier. On comparison, the rotational barrier around the C-N bond in the isocyanates is much lower in energy than the C–C barrier in the vinyl derivatives and ketenes. This significant difference between the two rotational barriers is due to the difference in the strength of the partial π character of the C–N bond as compared to that of the C–C bond. This difference is indeed the result of the electronegativity change as going from the C–C bond to the C–N one.

In the case of halomethyl isocyanates, the molecules were found to exist only in one conformation with minimum interaction between the halogen atom and the lone-pair [110,111]. For example, chloromethyl isocyanate was found to have only the *gauche* (or the near-*cis*) conformation, in which the chlorine atom is staggered to the nitrogen lone pair, to be the stable conformation [110]. Difluoromethyl isocyanate was also predicted to exist in the *trans* conformation in which the hydrogen atom eclipses the electron lone-pair [111]. In haloacetaldehyde systems [5,20], it was found that the planar s-*trans* conformation (the halogen atom eclipses the aldehydic hydrogen) is the form of the lowest energy. The steric effect (the repulsive force between the halogen atom and the carbonyl group) would destabilize the *cis* form of the molecule.

The 3,3,3-trifluoromethyl ketene was reported as an important intermediate [146,147]. The rate of hydration of the molecule was experimentally observed using UV spectroscopy [147]. Moreover, the reactivity of trifluoromethyl ketene was studied using the molecular orbital methods, and the substituent effect of the CF_3 group in the system was theoretically compared to a series of other substituents [135]. As a continuation of these studies, we investigated the structure of 3,3,3-trifluoromethyl ketene and 3,3-difluoromethyl ketene to understand the nature of forces that control the conformational behavior of such

important molecular systems. We carried out normal coordinate calculations by utilizing ab initio density functional calculations and derived the potential energy distributions among symmetry coordinates. The vibrational assignments of the normal modes were made for both molecules.

6.2 AB INITIO CALCULATIONS

The GAUSSIAN 98 program [65] running on an IBM RS/6000 43P model 260 workstation, was used to carry out the LCAO-MO-SCF DFT-B3LYP calculations. The extended 6-311++G** basis set was employed to optimize the structures and predict the energies and dipole moments of trifluoromethyl ketene and difluoromethyl ketene in their stable conformations. The calculations were extended to the Density Functional B3LYP level. From full energy optimization the *cis* conformation in trifluoromethyl ketene was found to be the energy minimum for the system, whereas both the *cis* and the *gauche* conformations were the stable conformers in difluoromethyl ketene (Figure VI-1). The calculated structural parameters in the molecules are shown in Tables VI-1 and VI-2. Moreover, the optimized geometrical parameters of trifluoromethyl ketene were compared to the corresponding values obtained from experimental data for trifluoroacetaldehyde [148] as shown in Table VI-1. The optimized structural parameters were used to compute their vibrational frequencies at the DFT-B3LYP/6-311++G** level of calculation. Normal coordinate calculations were then carried out to derive the potential energy distributions for the molecules in their stable conformations.

6.2.1 Torsional Potential Functions

The potential scans for the internal rotation about the C-C single bond were obtained by allowing the OCCC dihedral angle (ϕ) to vary from 0° (*cis* position) to 180° (*trans* position). Full geometry optimizations at each of the fixed dihedral angles (ϕ) of 15°, 30°, 45°, 60°, 75°, 90°, 105°, 120°, 135°, 150°, and 165° were carried out at DFT-B3LYP/6-311++G** level of calculations in both systems. The barrier to interconversion and the relative energies in difluoromethyl ketene were calculated and shown in Table VI-3. The torsional potential was represented as a Fourier cosine series in the dihedral angle (ϕ): $V(\phi) = V_0 + \sum(V_n/2)[1-\cos(n\phi)]$, where V_0 is the relative energy at the *cis* conformation, and the potential coefficients from V_1 to V_6 are considered adequate to describe the potential function. The results of the energy optimizations were used to calculate the six coefficients by least-squares fitting for the systems (Table VI-4). The potential functions of trifluoromethyl ketene and difluoromethyl ketene are shown in Figure VI-2.

6.2.2 Vibrational Frequencies and Normal Coordinate Analyses

Both trifluoromethyl ketene and difluoromethyl ketene in their *cis* conformations have C_s symmetry. The 18 vibrational modes span the irreducible representations: 12 A' and 6 A". The A' modes should be polarized while the A" modes be depolarized in the Raman spectra of the liquid. However, the *gauche* conformation in difluoromethyl ketene has C_1

symmetry. All the eighteen vibrational modes in difluoromethyl ketene belong to A representation and are polarized in Raman spectrum of the liquid.

Normal coordinate analyses were carried out for the stable conformers of the molecules in order to provide a complete assignment of the fundamental vibrational frequencies. A computer program was written for this purpose by following Wilson's method [71]. A complete set of internal coordinates (Tables VI-5, VI-6 and Figure VI-1) was used to form symmetry coordinates (Tables VI-7 and VI-8) in our molecular systems.

The potential energy distribution (PED) for each normal mode among the symmetry coordinates was calculated and is given in Tables VI-9, VI-10 and VI-11. A complete vibrational assignment of the fundamentals was proposed. The assignments were made based on calculated PED, infrared band intensities, Raman line activities and depolarization ratios. The data of the vibrational assignments are also given in Tables VI-9, VI-10 and VI-11.

6.2.3 Calculation of Vibrational Spectra

The frequencies ν_j, the scattering activities S_j and the depolarization ratios ρ_j as calculated at DFT-B3LYP level (6-311++G** basis set for all) were used to calculate the Raman spectra. Then, the Raman cross-sections ($\partial\sigma_j/\partial\Omega$), which are proportional to the intensities [72,73], are given in equation (2-31). For the plots we used a grid of a step size of 10 cm^{-1}, but not when a spectral line appears between two consecutive grid points. In this case we inserted 12 points with step size of 0.5 cm^{-1} into this interval which include the exact location of the center of the line.

For the infrared spectrum we used the intensities as given by the DFT-B3LYP/6-311++G** calculations and converted them to relative transmittance. The Boltzmann Distribution was then used to superimpose the spectra of the *cis* and the *gauche* conformers of difluoromethyl ketene. The g_l value for the trifluoro- and difluoromethyl ketene in the *cis* conformation is unity, whereas it is 2 for the nonplanar *gauche* conformer of the difluoro-derivative. Additionally, E_l represents the total energy of conformer l corrected with the corresponding zero-point energy. The label $l = 0$ is given to the lowest energy conformer. As previous, $T = 300\ K$ was used. The calculated vibrational Raman and infrared spectra of the *cis*-trifluoromethyl ketene are shown in Figures VI-3 and VI-4, while the spectra of the difluoromethyl ketene mixture (65% *cis* and 35% *gauche)* at 300 K are shown in Figures VI-5 and VI-6.

6.3 DISCUSSION

The interesting properties of organoisocyanate molecules [72,83,88,110,111,136-145] have recently prompted our group to investigate the conformational and structural stabilities of isocyanatoacetaldehyde, chloromethyl isocyanate, difluoromethyl isocyanate and formyl isocyanate. The conformational behavior of these compounds depends greatly on the extent of interactions between the substituent and both the π-system of the isocyanate group and the lone-pair on the nitrogen. In isocyanatoacetaldehyde the *cis-cis* conformation (isocyanate group eclipses the carbonyl group) was found to be the lowest energy form with the carbonyl oxygen being oriented away from the lone pair [83]. The potential surface

governing internal rotation about the C-N bond in chloromethyl isocyanate was calculated to be consistent with a single minimum corresponding to a structure having the chlorine atom *gauche* or near-*cis* to the -NCO moiety [110]. From a more recent study, difluoromethyl isocyanate was predicted to exist only in the *trans* conformation, again with minimum repulsive interaction between the fluorine atoms and the electron lone-pair on the nitrogen [111].

In the case of formyl isocyanate, the molecule was predicted to have a *cis* ⇔ *trans* conformational equilibrium [134]. The molecule was found to have the *cis* (carbonyl oxygen eclipses the isocyanato group) conformer as the lower energy form, with the carbonyl oxygen being away from the electron lone-pair on nitrogen. Similar conformational equilibrium was predicted for formyl ketene with a relatively higher rotational barrier. The conjugation stabilization force in such systems stabilizes the planar forms and considerably restricts the internal rotation of the -CHO group.

The electronic structure of trifluoromethyl ketene was very fascinating to us. On first sight, we expected that the *trans* conformer (a fluorine atom eclipses the ketenic hydrogen) should be more stable than the *cis* form (a fluorine atom eclipses the C=C=O moiety). However, closer inspection shows that actually the reverse was true. As shown in Table VI-12, the partially negatively charged F_6 atom in the *cis* conformer is calculated to be quite close to the partially positive C_3 atom. Moreover, in both conformers the repulsion between the negative F_6 and O_4 atoms is rather small due to the large distances between them. Thus C_3-F_6 and C_3-F_7(F_8) electrostatic attractions dominate the F-O_4 repulsion in both cases. The corresponding stabilization is larger in the *cis* conformer than in the trans one, because the absolute values of the charges are larger and the C-F distance is smaller in the *cis* form.

However, this simple electrostatic argument explains only why the *cis* is more stable than the *trans* form, not why *cis* is a minimum but *trans* a maximum in the potential curve (Figure VI-2). A closer look at the MO interactions in the system provides an explanation for that result.

As it is well known, the interactions between two filled orbitals destabilize (Figure VI-7a), while those between a filled and an unfilled orbital stabilize (Figure VI-7b) a system. Candidates for such interactions in our system are the lone-pairs at fluorine, the σ,σ^* orbitals of the C-F bond and the π,π^* orbitals of the C=C π bond. Being flanked by a CF_3 group at one end and a C=O bond at the other, the C=C bond can be considered as quite electron deficient, making it an ideal system to interact with F lone-pairs or the σ orbitals of the C-F bond. However, as Figure VI-7c shows, in the *trans* conformer neither of them can efficiently overlap with the π^* orbital due to geometry, while in the *cis* form F_6 lies in the nodal plane of the π^* orbital (Figure VI-7d). Thus, there are no efficient stabilizing orbital interactions and we have to concentrate on the destabilizing ones. In the case of the destabilizing interactions there is a significant difference between the *cis* and the *trans* form. Again in the *cis* conformer the lone-pair at F_6 and the C-F_6 σ orbital are exactly in the nodal plane of the π orbital and they are symmetric with respect to this plane, while π is antisymmetric. Therefore, in the *cis* form there are no efficient destabilizing orbital interactions present as compared to that in the *trans* conformer. Furthermore, any arbitrary rotation away from the fully symmetric *cis* form destroys the symmetry of the C-F σ orbital or the F_6 lone-pair, increasing destabilizing interactions. Hence, *cis* must be a true energy minimum.

On the contrary, in the *trans* form, as shown in Figure VI-7e, there are destabilizing interactions present, and thus the *trans* conformer has to be thermodynamically less preferable than the *cis* form. Additionally, Figure VI-7e indicates that any rotation out of the fully symmetric *trans* form would reduce these destabilizing effects, and thus the *trans* form is a maximum in the potential curve. Given the fact, that the distances between the atoms indicate comparatively small effects due to the discussed orbital interactions, one would expect to find small barriers as predicted in our calculations. The difference in MO interactions between the two forms we have just viewed above surely dominate any electrostatic attractive interactions between the fluorine and the ketenic hydrogen atom because the latter ones are of roughly the same strength in both conformers.

An electron diffraction study for trifluoroacetaldehyde concluded that the *cis* conformation (fluorine eclipses the aldehyde group) was the preferred conformation for the system [148]. The results obtained from the electron diffraction experiment were reasonably consistent with the microwave study [149]. As a result this experimental conclusion fairly supports our prediction for the stability of trifluoromethyl ketene.

In the case of the difluoro derivative, the steric effects play a competitive role with the MO orbital interactions in determining the conformational stability in difluoromethyl ketene. The question which bond C-H_6 or C-F, eclipses the ketenic hydrogen (C-H_5) or the CCO group is also important, because the different effects of steric hindrance might out-balance those due to MO interactions. In difluoromethyl ketene the low minima are expected at such angles, where either CH_6 or CF eclipses the ketenic CCO group and the C-H_5 bond is staggered relative to the other two bonds of the difluoromethyl (CHF_2) rotor.

In the lowest energy *cis* conformation of difluoromethyl ketene, the small H_6 atom opposes the CCO group while the more bulky C-F bonds eclipse the C-H_5 bond. The second, lower energy *gauche* conformer with HCCC dihedral angle of 131° has the C-F_8 eclipsing the CCO moiety. It is higher in energy than the *cis* conformer, because here the bulky F_8 opposes the CCO group. However, although in both forms the ketenic CCO group is in an eclipsed position, the two are the lower energy forms, because they are the only forms where no destabilizing interactions between the fluorine lone-pairs and the π orbitals of the C=C double bond occur. In the *cis* case no lone pair points to the CC double bond, while in the higher *gauche* (HCCC is 120°) case the F_8 lone pair lies in the nodal plane of the C=C bond (see Figure VI-7d).

The other *gauche* conformer (HCCC is 60°) and the *trans* structure both suffer from the aforementioned destabilizing interactions. The *trans* form has two such interactions, while the high energy *gauche* structure has only one. Since these interactions are rather small in difluoromethyl ketene, not the *trans* form is higher in energy, but the *gauche* structure (HCCC of 60°). The reason for that is simply that the bulky C-F_7 bond eclipses C-H_5 in the case of the high energy *gauche* form, while in the *trans* case only C-H_6 is eclipsing C-H_5. While MO interactions would give the *gauche*-60 structure the lower energy, their effects are out-balanced by the larger steric hindrance in the *gauche* form, making it higher in energy than the *trans* structure. Since in both *gauche*-60 and *trans*, any rotation out of their respective positions would lower the destabilizing effects and finally drive them into one of the minima, the two structures are maxima, with *gauche*-60 being higher in energy than *trans*.

We calculated the vibrational wavenumbers and derived the PED values among symmetry coordinates in the low energy conformers of the two molecules. Some of the vibrations were clearly pure, and their assignments were easily made possible only based on the PED values as shown in Tables VI-9 – VI-11, and others were predicted to be mixed with neighboring modes.

The C-H stretching modes of the two molecules were calculated to have the highest Raman activities in the Raman spectra. Only one C-H stretching mode is in the Raman spectrum of trifluoromethyl ketene and was calculated to be at 3215 cm^{-1}. While in difluoromethyl ketene Raman spectrum there are two C-H stretches that were calculated at 3196 cm^{-1} for the ketenic C-H stretch and at 3100 cm^{-1} for the other C-H stretch for the *cis* conformer.

The highest calculated IR intensities in the tri- and difluoromethyl ketene IR spectra were assigned to the –C=C=O antisymmetric stretching vibrations with PED values of 97%. Furthermore, the C=C-C in-plane bending modes of the *cis* conformers of both molecules were calculated at 142 cm^{-1} for the trifluoro derivative and 173 cm^{-1} for the difluoro one.The –C=C=O symmetric stretching mode in the trifluoro system was of a clear assignment and was calculated at 1442 cm^{-1} with 43% PED. In the case of the difluoro derivative, the assignment of this –C=C=O mode was not straightforward based on the calculated PED and could be assigned to either ν_4 or ν_5. However, the –C=C=O symmetric stretching mode could be assigned to the ν_4 with the higher IR intensity as one might expect for such a vibration. Then, the assignment of ν_5 could be predicted from the PED values in Table VI-9 to the C-H_6 in-plane bending.

Several vibrational modes in trifluoromethyl ketene were calculated to be mixed with other modes. The assignments of such modes could be clarified with the help of the observed frequencies obtained from the gas phase Raman spectrum of trifluoroacetaldehyde (fluoral) [150]. For example, ν_4 in our trifluoro system could be referred to either the C-C stretching or the CF_3 symmetric stretching. In fluoral, the experimental frequency assigned to the CF_3 symmetric stretching mode was 1298 cm^{-1}. Therefore, ν_4 in trifluoromethyl ketene could be assigned to CF_3 symmetric stretching. Whereas, the C-C stretching vibration can be assigned with confidence to the 856 cm^{-1} frequency since the corresponding vibration in fluoral was observed at 841 cm^{-1}. Similarly, the CF_3 antisymmetric stretching mode and the C=C-H in-plane bending mode were calculated to couple with each other in ν_5 and ν_6. Experimentally, the CF_3 antisymmetric stretching mode was found at 1197 cm^{-1} [150] which is closer to the frequency of ν_5 in trifluoromethyl ketene (Table VI-9). Thus, ν_5 and ν_6 can be assigned to the antisymmetric CF_3 stretching and the in-plane C=C-H bending modes, respectively.

The assignment of some of the CF_3 vibrational modes below 1000 cm^{-1} was obvious from derived PED values. The calculated wavenumbers at 535 and 361 cm^{-1} were referred to the CF_3 antisymmetric deformation and the CF_3 rock, respectively. The CF_3 symmetric deformation in fluoral was observed at 707 cm^{-1}, hence the CF_3 symmetric deformation in trifluoromethyl ketene could be assigned to ν_8. This leaves us with the assignment of ν_{10} to the -C=C=O in-plane bending vibration.

The calculated PEDs for difluoromethyl ketene in the *cis* conformation represented excellent aid for the assignments of most of the skeletal vibrations (see Table VI-10). The wavenumbers ν_6, ν_7, ν_8, ν_9 and ν_{11} can with little doubt be assigned to the C=C-H in-plane

bending (55% PED), the C-C stretching (40% PED), the CF_2 symmetric stretching (60% PED), the C=C=O in-plane bending (41%PED) and the CF_2 deformation (47% PED), respectively. This should then assign ν_{10} at 565 cm^{-1} to the CF_2 rocking mode. The remaining wavenumber at 1332 cm^{-1} in the *cis* conformer of the difluoro system (ν_5) can be referred with confidence to the C-H_6 in-plane bending.

Many vibrational modes in the *gauche* form of the difluoro derivative, however, were difficult to be assigned only based on the calculated PEDs, especially for the region below 1000 cm^{-1} at which a large degree of coupling of many bending modes was found (Table VI-11). From the experimental IR frequencies of chlorocarbonyl ketene obtained in the xenon matrix [105], the C=C-H wag was observed at 531 cm^{-1} for the *cis* and 556 cm^{-1} for the *trans* conformers. The observed modes were weak in the IR spectrum. This information leads to the assignment of the C=C-H wag of the *gauche* difluoromethyl ketene to the depolarized wavenumber at 519 cm^{-1}. Therefore, from the calculated PEDs, the C=C=O in-plane bending was assigned to ν_{12}. Then, the CF_2 rock and the CF_2 twist could be assigned to ν_{11} and ν_{15}, respectively. This approximate assignment leads one to assign ν_8 at 1096 cm^{-1} to the symmetric CF_2 stretching.

Many of the bending modes of A" symmetry in the tri- and the difluoromethyl ketene spectra were calculated to have a very low degree of mixing and their assignments are shown in Tables VI-9 and VI-10. Among these modes only the C=C–H wag was of a low PED value in trifluoromethyl ketene. The C=C–H waging mode was predicted to be at 630 and 622 cm^{-1} in the triflouro and difluoro systems, respectively. The lowest vibrational mode in the spectra of the two molecules was the asymmetric torsion. The CF_3 asymmetric torsion in

the spectrum of trifluoromethyl ketene was calculated to be at 50 cm^{-1}, and the CHF_2 asymmetric torsion in the difluoro spectrum was predicted to be at 63 cm^{-1} in the *cis* form and 51 cm^{-1} in the *gauche* form. The asymmetric torsion modes were predicted to have a relatively small degree of contribution from the C=C–H waging mode as shown in Tables VI-9 – VI-11.

At the end of this chapter, we were able to provide reasonable vibrational assignments for the normal modes of the stable conformers of tri- and difluoromethyl ketene based on normal coordinate analysis. Good agreements were noticed when the calculated frequencies of trifluoromethyl ketene were compared to the experimental ones of fluoral, especially for the vibrational modes associated to the CF_3 moiety.

TABLE VI-1: **Calculated Structural Parameters, Total Dipole Moment and Rotational Constants for the *Cis* Conformation of Trifluoromethyl Ketene.**

Parameter [a]	B3LYP/6-311++G**	Electron Diffraction [b]
	cis	*cis*
Bond Length (Å)		
$r(C_1\text{-}C_2)$	1.484	1.540 ± 0.020
$r(C_2\text{-}C_3)$	1.317	
$r(C_3\text{-}O_4)$	1.154	
$r(C_2\text{-}H_5)$	1.081	1.09 (assumed to be constant)
$r(C_1\text{-}F_6)$	1.353	1.332 ± 0.007
$r(C_1\text{-}F_7)$	1.354	1.332 ± 0.007
$r(C_1\text{-}F_8)$	1.354	1.332 ± 0.007
Bond Angle (deg)		
$(C_1C_2C_3)$	121.656	
$(C_2C_3O_4)$	181.103	
$(C_1C_2H_5)$	119.160	
$(C_3C_2H_5)$	119.184	120.0 (assumed to be constant)
$(F_6C_1F_7)$	107.342	108.7 ± 1
$(F_6C_1F_8)$	107.342	108.7 ± 1
$(F_7C_1F_8)$	105.922	108.7 ± 1
$(C_3C_2C_1F_6)$	0.0	0.0
$(C_3C_2C_1F_7)$	120.510	
$(C_3C_2C_1F_8)$	-120.510	
Dipole Moment μ_t (Debye)	2.1	
Rotational Constants (MHz)		
A	5428	
B	1681	
C	1657	

[a] Calculated total energy, zero-point correction, and the sum of total and zero point energies (in Hartrees) of the *cis* conformer of trifluoromethyl ketene at DFT-B3LYP/6-311++G** level are -489.79721, 0.03794, and -489.75927, respectively.

[b] Data obtained for trifluoromethylacetaldehyde (fluoral), see ref[148].

TABLE VI-2: **Calculated Structural Parameters, Total Dipole Moment and Rotational Constants for the *Cis* and the *Gauche* Conformations of Difluoromethyl Ketene.**

Parameter	B3LYP/6-311++G**	
	cis	*gauche*
Bond Length (Å)		
$r(C_1\text{-}C_2)$	1.484	1.489
$r(C_2\text{-}C_3)$	1.314	1.316
$r(C_3\text{-}O_4)$	1.157	1.156
$r(C_2\text{-}H_5)$	1.083	1.082
$r(C_1\text{-}H_6)$	1.091	1.092
$r(C_1\text{-}F_7)$	1.377	1.380
$r(C_1\text{-}F_8)$	1.377	1.372
Bond Angle (deg)		
$(C_1C_2C_3)$	121.859	122.084
$(C_2C_3O_4)$	179.996	180.802
$(C_1C_2H_5)$	119.425	119.629
$(C_2C_1H_6)$	114.020	113.460
$(C_2C_1F_7)$	110.651	111.223
$(C_2C_1F_8)$	110.651	110.579
$(C_3C_2C_1H_6)$	0.0	131.508
$(C_3C_2C_1F_7)$	121.707	119.954
$(C_3C_2C_1F_8)$	-121.717	-121.680
Dipole Moment (Debye)		
μ_t	1.4	2.8
Rotational Constants (MHz)		
A	8815	7928
B	1906	2259
C	1690	1962

TABLE VI-3: **Computed Total Energies, Zero-Point Corrections (Hartrees), Relative Energies and Rotational Barriers (kcal/mol) in Difluoromethyl Ketene.**

	B3LYP/6-311++G**		
	cis	*gauche*[a]	*TS*[b]
Total energy	-390.51751	-390.51622	-390.51402
Relative energy		0.80949	
Cis-gauche barrier		2.19001	
Gauche-cis barrier		1.38052	
Zero-point correction	0.04634	0.04629	0.04599
Sum of total and zero-point energies	-390.47118	-390.46993	-390.46803
Corrected relative energy		0.78439	
Corrected *cis-gauche* barrier		1.97666	
Corrected *gauche-cis* barrier		1.19227	

[a] The CCCO dihedral angle of the *gauche* conformer was calculated to be 131.51°.

[b] The CCCO dihedral angle of the *transition state* was calculated to be 67.57°.

TABLE VI-4: **Calculated Potential Constants (kcal/mol) for the Three-Fold Symmetric Torsion in Trifluoromethyl Ketene and the Asymmetric Torsion in Difluoromethyl Ketene.**

Potential Constants	B3LYP/6-311++G**	
	Trifluoromethyl Ketene [a]	Difluoromethyl ketene
V_1		0.115
V_2		1.077
V_3	1.315	1.289
V_4		0.012
V_5		-0.021
V_6		-0.022

[a] All potential constants, except V_3, describing the symmetric torsion of the trifluoro-derivative are of negligible values.

TABLE VI-5: **Internal Coordinate Definitions [a] for Trifluoromethyl Ketene.**

No.	Coordinate		Definition
1	C_1-C_2	stretch	R
2	C_2-C_3	stretch	P
3	C_3-O_4	stretch	T
4	C_2-H_5	stretch	D
5	C_1-F_6	stretch	Q_1
6	C_1-F_7	stretch	Q_2
7	C_1-F_8	stretch	Q_3
8	$C_1C_2C_3$	bend	γ
9	$C_2C_3O_4$	bend	σ
10	$C_1C_2H_5$	bend	ρ
11	$C_3C_2H_5$	bend	δ
12	$C_2C_1F_6$	bend	α_1
13	$C_2C_1F_7$	bend	α_2
14	$C_2C_1F_8$	bend	α_3
15	$F_6C_1F_7$	bend	β_1
16	$F_6C_1F_8$	bend	β_2
17	$F_7C_1F_8$	bend	β_3
18	C_2=C_3=O_4	wag	χ
19	$H_5C_1C_2C_3$	wag	π
20	$F_6C_1C_2C_3$	(CF_3) torsion	τ
	$F_7C_1C_2C_3$		
	$F_8C_1C_2C_3$		

[a] See Figure VI-1 for atom denotation.

TABLE VI-6: Internal Coordinate Definitions [a] for Difluoromethyl Ketene.

No.	Coordinate		Definition
1	C_1-C_2	stretch	R
2	C_2-C_3	stretch	P
3	C_3-O_4	stretch	T
4	C_2-H_5	stretch	D
5	C_1-H_6	stretch	Q_1
6	C_1-F_7	stretch	Q_2
7	C_1-F_8	stretch	Q_3
8	$C_1C_2C_3$	bend	γ
9	$C_2C_3O_4$	bend	σ
10	$C_1C_2H_5$	bend	ρ
11	$C_3C_2H_5$	bend	δ
12	$C_2C_1H_6$	bend	α_1
13	$C_2C_1F_7$	bend	α_2
14	$C_2C_1F_8$	bend	α_3
15	$H_6C_1F_7$	bend	β_1
16	$H_6C_1F_8$	bend	β_2
17	$F_7C_1F_8$	bend	β_3
18	C_2=C_3=O_4	wag	χ
19	$H_5C_1C_2C_3$	wag	π
20	$H_6C_1C_2C_3$	(CHF_2) torsion	τ
	$F_7C_1C_2C_3$		
	$F_8C_1C_2C_3$		

[a] See Figure VI-1 for atom denotation.

***TABLE VI-7:* Symmetry Coordinates for Trifluoromethyl Ketene.**

Species	Description		Symmetry Coordinate [a]
A′	C-H	stretch	$S_1 = D$
	C-C	stretch	$S_2 = R$
	C=C=O	symmetric stretch	$S_3 = P + T$
	C=C=O	antisymmetric stretch	$S_4 = P - T$
	CF_3	symmetric stretch	$S_5 = Q_1 + Q_2 + Q_3$
	CF_3	antisymmetric stretch	$S_6 = 2Q_1 - Q_2 - Q_3$
	C=C-H	in-plane bend	$S_7 = \rho - \delta$
	C=C-C	in-plane bend	$S_8 = 2\gamma - \rho - \delta$
	C=C=O	in-plane bend	$S_9 = \sigma$
	CF_3	symmetric deformation	$S_{10} = \alpha_1 + \alpha_2 + \alpha_3 - \beta_1 - \beta_2 - \beta_3$
	CF_3	antisymmetric deformation	$S_{11} = \beta_1 + \beta_2 - 2\beta_3$
	CF_3	rock	$S_{12} = 2\alpha_1 - \alpha_2 - \alpha_3$
A″	C=C-H	out-of-plane bend (wag)	$S_{13} = \pi$
	C=C=O	out-of-plane bend (wag)	$S_{14} = \chi$
	CF_3	antisymmetric stretch	$S_{15} = Q_2 - Q_3$
	CF_3	antisymmetric deformation	$S_{16} = \beta_1 - \beta_2$
	CF_3	rock	$S_{17} = \alpha_2 - \alpha_3$
	CF_3	torsion	$S_{18} = \tau$

[a] Not normalized.

TABLE VI-8: **Symmetry Coordinates for Difluoromethyl Ketene.**

Species	Description		Symmetry Coordinate [a]
A′	$C\text{-}H_5$	stretch	$S_1 = D$
	C-C	stretch	$S_2 = R$
	C=C=O	symmetric stretch	$S_3 = P + T$
	C=C=O	antisymmetric stretch	$S_4 = P - T$
	CF_2	symmetric stretch	$S_5 = Q_2 + Q_3$
	$C\text{-}H_6$	stretch	$S_6 = Q_1$
	C=C-H	in-plane bend	$S_7 = \rho - \delta$
	C=C-C	in-plane bend	$S_8 = 2\gamma - \rho - \delta$
	C=C=O	in-plane bend	$S_9 = \sigma$
	CH_6	in-plane bend	$S_{10} = [\,(6)^{1/2} - 2\,]\,\beta_3 - [\,(6)^{1/2} + 2\,]\,\alpha_1 + \alpha_2 + \alpha_3 + \beta_1 + \beta_2$
	CF_2	deformation	$S_{11} = [\,(6)^{1/2} + 2\,]\,\beta_3 - [\,(6)^{1/2} - 2\,]\,\alpha_1 - \alpha_2 - \alpha_3 - \beta_1 - \beta_2$
	CF_2	rock	$S_{12} = \alpha_2 + \alpha_3 - \beta_1 - \beta_2$
A″	C=C-H	out-of-plane bend (wag)	$S_{13} = \pi$
	C=C=O	out-of-plane bend (wag)	$S_{14} = \chi$
	CF_2	antisymmetric stretch	$S_{15} = Q_2 - Q_3$
	$C\text{-}H_6$	out-of-plane bend	$S_{16} = \alpha_2 - \alpha_3 + \beta_1 - \beta_2$
	CF_2	twist	$S_{17} = \alpha_2 - \alpha_3 - \beta_1 + \beta_2$
	CHF_2	torsion	$S_{18} = \tau$

[a] Not normalized.

TABLE VI-9: **Calculated Vibrational Frequencies (cm^{-1}) at B3LYP/6-311++G** Level for the *Cis* Conformer of Trifluoromethyl Ketene.**

Symm.	No.	Frequency	IR Intensity [a]	Raman Activity	Depol. Ratio	Obs. [b]	PED [c]
A'	ν_1	3215	26.4	77.6	0.2	3160	100% C-H str. (S_1)
	ν_2	2252	714.5	12.6	0.7		97% C=C=O antisymm. str. (S_4)
	ν_3	1442	154.3	8.4	0.1		43% C=C=O symm. str. (S_3), 25% C=C-H in-plane bend (S_7), 24% C-C str. (S_2)
	ν_4	1235	256.3	0.4	0.7	1298	17% CF_3 symm. str. (S_5), 22% C-C str. (S_2), 17% CF_3 symm. def. (S_{10}), 17% C=C-H in-plane bend (S_7), 14% CF_3 antisymm. str. (S_6)
	ν_5	1136	265.2	6.5	0.3	1197	22% CF_3 antisymm. str. (S_6), 36% C=C=O symm. str. (S_3), 17% C=C-H in-plane bend (S_7), 11% CF_3 symm. str. (S_5)
	ν_6	1100	155.2	11.5	0.3		35% C=C-H in-plane bend (S_7), 34% CF_3 antisymm. str. (S_6)
	ν_7	856	12.1	6.5	0.1	841	45% CF_3 symm. str. (S_5), 21 % C-C str. (S_2), 10% CF_3 antisymm. str. (S_6), 10% C=C=O in-plane bend (S_9)
	ν_8	709	4.7	5.3	0.2	707	32% CF_3 symm. def. (S_{10}), 23% CF_3 symm. str. (S_5), 18% C=C=O in-plane bend (S_9), 12% C=C-C in-plane bend (S_8)
	ν_9	535	0.6	0.6	0.7	531	69% CF_3 antisymm. def. (S_{11}), 12% CF_3 antisymm. str. (S_6)
	ν_{10}	509	13.9	2.4	0.1		30% C=C=O in-plane bend (S_9), 33% CF_3 symm. def. (S_{10}), 27% C-C str. (S_2)
	ν_{11}	361	3.1	1.5	0.6	255	62% CF_3 rock (S_{12}), 17% CF_3 antisymm. def. (S_{11}), 11% C=C=O in-plane bend (S_9)
	ν_{12}	142	2.6	1.7	0.7		65% C=C-C in-plane bend (S_8), 19% C=C=O in-plane bend (S_9), 16% CF_3 rock (S_{12})

TABLE VI-9: **Continue.**

Symm.	No.	Frequency	IR Intensity [a]	Raman Activity	Depol. Ratio	Obs. [b]	PED [c]
A"	ν_{13}	1101	355.8	2.8	0.7	1194	77% CF_3 antisymm. str. (S_{15}), 13% CF_3 antisymm. def. (S_{16})
	ν_{14}	630	28.0	0.6	0.7		23% C=C-H wag (S_{13}), 31% CF_3 rock (S_{17}), 15% CF_3 antisymm. str. (S_{15}), 14% CF_3 torsion (S_{18})
	ν_{15}	547	2.5	1.3	0.7		88% C=C=O wag (S_{14})
	ν_{16}	508	9.4	1.3	0.7	529 [d]	56% CF_3 antisymm. def. (S_{16}), 22% C=C-H wag (S_{13}), 14% CF_3 torsion (S_{18})
	ν_{17}	324	12.6	0.7	0.7	320	60% CF_3 rock (S_{17}), 25% C=C-H wag (S_{13}), 15% CF_3 antisymm. def. (S_{16})
	ν_{18}	50	2.2	2.4	0.7	65	74% CF_3 torsion (S_{18}), 26% C=C-H wag (S_{13})

[a] Infrared intensities and Raman activities are calculated in Km mol^{-1} and $Å^4$ amu^{-1}, respectively.

[b] Observed Raman frequencies (cm^{-1}) in the gas phase for trifluoroacetaldehyde (fluoral) are obtained from reference [150].

[c] PED values are obtained by using calculated frequencies at B3LYP level.

[d] IR frequency.

TABLE VI-10: **Calculated Vibrational Frequencies (cm^{-1}) at B3LYP/6-311++G** Level for the *Cis* Conformer of Difluoromethyl Ketene.**

Symm.	No.	Frequency	IR Intensity [a]	Raman Activity	Depol. Ratio	PED [b]
A'	ν_1	3196	19.9	76.5	0.2	100% C-H_5 str. (S_1)
	ν_2	3100	24.8	73.5	0.2	100% C-H_6 str. (S_6)
	ν_3	2234	752.7	13.1	0.7	97% C=C=O antisymm. str. (S_4)
	ν_4	1466	108.6	4.2	0.1	24% C=C=O symm. str. (S_3), 34% C-H_6 in-plane bend (S_{10}), 15% C=C-H in-plane bend (S_7), 14% C-C str. (S_2), 13% CF_2 rock (S_{12})
	ν_5	1332	1.3	7.6	0.2	23% C-H_6 in-plane bend (S_{10}), 31% CF_2 rock (S_{12}), 29% C=C=O symm. str. (S_3), 13% C=C-H in-plane bend (S_7)
	ν_6	1143	7.8	7.5	0.6	55% C=C-H in-plane bend (S_7), 17% C-C str. (S_2), 16% C=C=O symm. str. (S_3)
	ν_7	1087	229.1	4.0	0.1	40% C-C str. (S_2), 18% C=C=O symm. str. (S_3), 15% CF_2 symm. str. (S_5)
	ν_8	1052	141.7	14.3	0.2	60% CF_2 symm. str. (S_5)
	ν_9	630	3.0	4.9	0.1	41% C=C=O in-plane bend (S_9), 17% C=C-C in-plane bend (S_8), 13% C-C str. (S_2), 12% CF_2 symm. str. (S_5), 10% CF_2 def. (S_{11})
	ν_{10}	565	3.4	0.8	0.6	26% CF_2 rock (S_{12}), 29% CF_2 def. (S_{11}), 18% C=C=O in-plane bend (S_9), 11% CF_2 symm. str. (S_5), 11% C-H_6 in-plane bend (S_{10})
	ν_{11}	426	22.2	2.2	0.3	47% CF_2 def. (S_{11}), 17% CF_2 rock (S_{12}), 15% C-H_6 in-plane bend (S_{10}), 14% C-C str. (S_2)
	ν_{12}	173	8.7	2.5	0.7	66% C=C-C in-plane bend (S_8), 28% C=C=O in-plane bend (S_9)

TABLE VI-10: **Continue.**

Symm.	No.	Frequency	IR Intensity [a]	Raman Activity	Depol. Ratio	PED [b]
A"	ν_{13}	1346	9.8	3.8	0.8	67% C-H_6 wag (S_{16}), 33% CF_2 twist (S_{17})
	ν_{14}	1008	274.0	4.2	0.8	94% CF_2 antisymm. str. (S_{15})
	ν_{15}	622	37.0	1.7	0.8	15% CF_2 twist (S_{17}), 33% C=C-H wag (S_{13}), 28% CHF_2 torsion (S_{18}), 11% C-H_6 wag (S_{16})
	ν_{16}	548	0.1	0.6	0.8	94% C=C=O wag (S_{14})
	ν_{17}	346	14.5	1.2	0.8	49% CF_2 twist (S_{17}), 28% C=C-H wag (S_{13}), 21% C-H_6 wag (S_{16})
	ν_{18}	63	4.1	2.3	0.8	65% CHF_2 torsion (S_{18}), 35% C=C-H wag (S_{13})

[a] Infrared intensities and Raman activities are calculated in Km mol^{-1} and $Å^4$ amu^{-1} respectively.

[b] PED values are obtained by using calculated frequencies at B3LYP level.

TABLE VI-11: **Calculated Vibrational Frequencies (cm^{-1}) at B3LYP/6-311++G** Level for the *Gauche* Conformer of Difluoromethyl Ketene.**

Symm.	No.	Frequency	IR Intensity [a]	Raman Activity	Depol. Ratio	PED [b]
A	ν_1	3206	16.9	84.9	0.2	100% C-H_5 str. (S_1)
	ν_2	3090	34.3	120.7	0.2	67% C-H_6 str. (S_6), 33% CF_2 symm. str. (S_5)
	ν_3	2239	753.6	12.2	0.7	97% C=C=O antisymm. str. (S_4)
	ν_4	1432	40.6	8.1	0.1	44% C=C=O symm. str. (S_3), 29% C=C-H in-plane bend (S_7), 16% C-C str. (S_2)
	ν_5	1380	102.1	4.2	0.7	51% C-H_6 in-plane bend (S_{10}), 19% C-H_6 wag (S_{16}), 14% CF_2 rock (S_{12})
	ν_6	1366	30.9	5.9	0.7	76% C-H_6 wag (S_{16}), 14% C-H_6 in-plane bend (S_{10})
	ν_7	1146	48.0	12.5	0.3	49% C=C-H in-plane bend (S_7), 13% C=C=O symm. str. (S_3)
	ν_8	1096	105.4	5.1	0.4	22% CF_2 symm. str. (S_5), 19% C=C=O symm. str. (S_3), 14% C=C-H in-plane bend (S_7), 10% C-H_6 str. (S_6)
	ν_9	1014	291.1	7.3	0.4	71% CF_2 antisymm. str. (S_{15}), 11% CF_2 symm. str. (S_5)
	ν_{10}	915	32.7	8.0	0.04	42% C-C str. (S_2), 16% CF_2 rock (S_{12}), 12% C=C=O symm. str. (S_3), 10% CF_2 symm. str. (S_5)
	ν_{11}	786	33.6	2.8	0.7	23% CF_2 rock (S_{12}), 21% C=C=O in-plane bend (S_9), 20% C=C-C in-plane bend (S_8)
	ν_{12}	598	29.2	3.2	0.2	11% C=C=O in-plane bend (S_9), 21% C=C-H wag (S_{13}), 21% C=C=O wag (S_{14})
	ν_{13}	548	3.1	2.8	0.5	59% C=C=O wag (S_{14}), 24% CF_2 def. (S_{11})

TABLE VI-11: **Continue.**

Symm.	No.	Frequency	IR Intensity [a]	Raman Activity	Depol. Ratio	PED [b]
A	ν_{14}	519	6.0	0.8	0.7	23% C=C-H wag (S_{13}), 29% CF_2 def. (S_{11}), 20% C=C=O wag (S_{14}), 10% CHF_2 torsion (S_{18}),
	ν_{15}	429	10.2	0.7	0.6	30% C=C=O in-plane bend (S_9), 20% CF_2 twist (S_{17}), 18% CF_2 rock (S_{12}), 10% C-H_6 in-plane bend (S_{10})
	ν_{16}	361	17.8	1.3	0.6	49% CF_2 twist (S_{17}), 28% C=C-H wag (S_{13}), 10% CF_2 rock (S_{12})
	ν_{17}	143	1.1	1.6	0.7	65% C=C-C in-plane bend (S_8), 20% C=C=O in-plane bend (S_9)
	ν_{18}	51	1.0	2.0	0.7	81% CHF_2 torsion (S_{18}), 18% C=C-H wag (S_{13})

[a] Infrared intensities and Raman activities are calculated in Km mol^{-1} and $Å^4$ amu^{-1}, respectively.

[b] PED values are obtained by using calculated frequencies at B3LYP level.

TABLE V-12: **Total Atomic Charges and Selected Non-Bonded Distances Calculated at B3LYP/6-311++G** Level for the *Cis* and the *Trans* Conformations of Trifluoromethyl Ketene and Difluoromethyl Ketene.**

Trifluoromethyl ketene			Difluoromethyl ketene		
Atom	*cis*	*trans* [a]	Atom	*cis*	*trans*
C_1	0.098	0.125	C_1	-0.261	-0.210
C_2	0.029	0.048	C_2	0.141	0.065
C_3	0.189	0.135	C_3	0.102	0.193
O_4	-0.179	-0.166	O_4	-0.181	-0.175
H_5	0.220	0.218	H_5	0.225	0.173
F_6	-0.164	-0.137	H_6	0.224	0.220
F_7	-0.099	-0.112	F_7	-0.125	-0.133
F_8	-0.099	-0.112	F_8	-0.125	-0.133
Non-bonded distance(Å)			Non-bonded distance(Å)		
F_6-C_3	2.678		H_6-C_3	2.624	
F_6-O_4	3.403		H_6-O_4	3.416	
F_8-C_3		2.976	F_8-C_3		2.963
F_8-C_3		3.818	F_8-O_4		3.793

[a] Transition state.

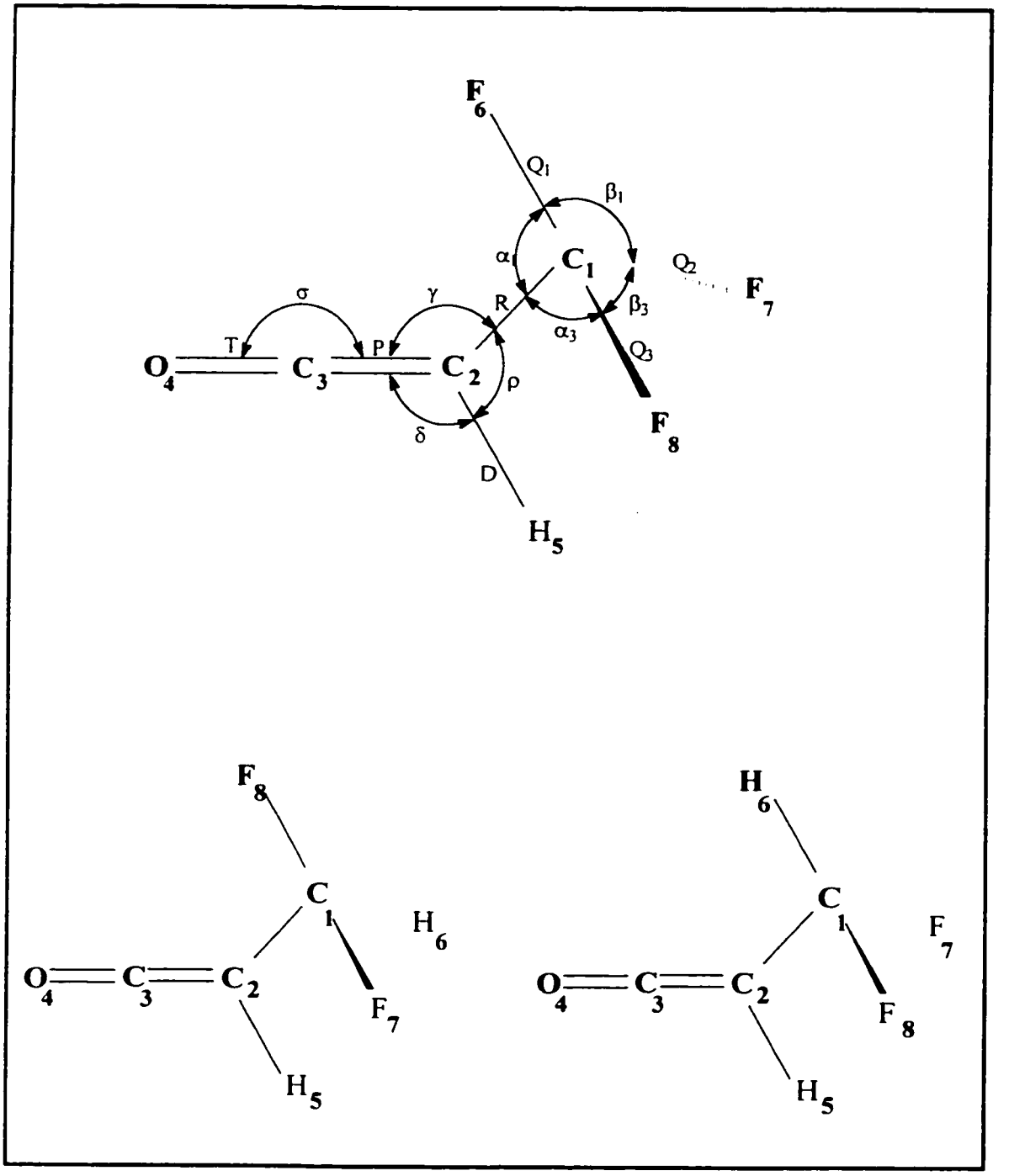

FIGURE VI-1: **Atom Numbering for *Cis*-Trifluoromethyl Ketene (Upper) and Difluoromethyl Ketene (Lower) in the *Cis* (Right) and the *Gauche* (Left) Conformations, with the Internal Coordinates Shown on the *Cis*-Trifluoromethyl Ketene**

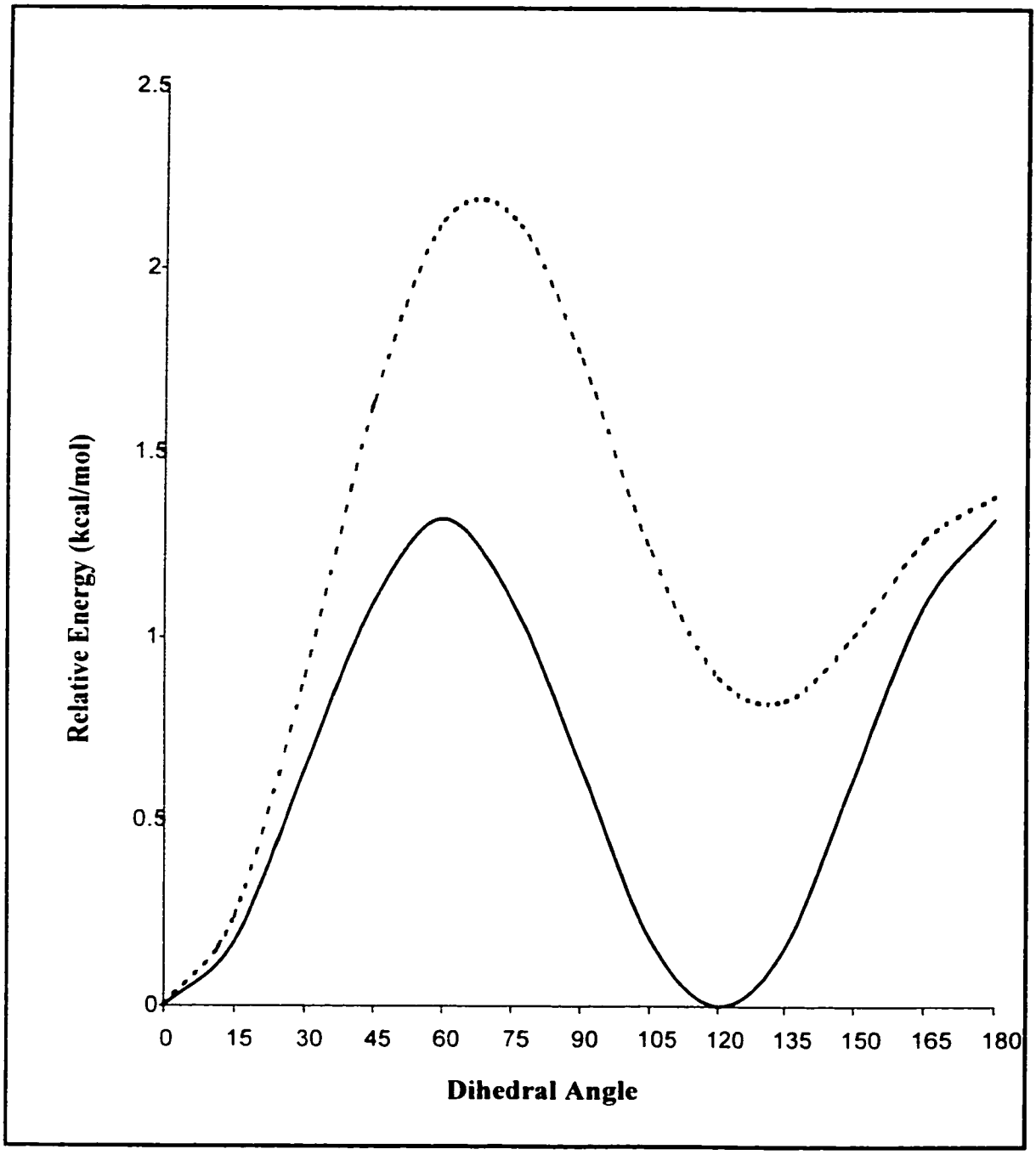

FIGURE VI-2: **Potential Curve for the Internal Rotation in Trifluoromethyl Ketene (Solid Line) and Difluoromethyl Ketene (Dashed Line) as Determined by Ab Initio Calculations at B3LYP/6-311++G** Level.**

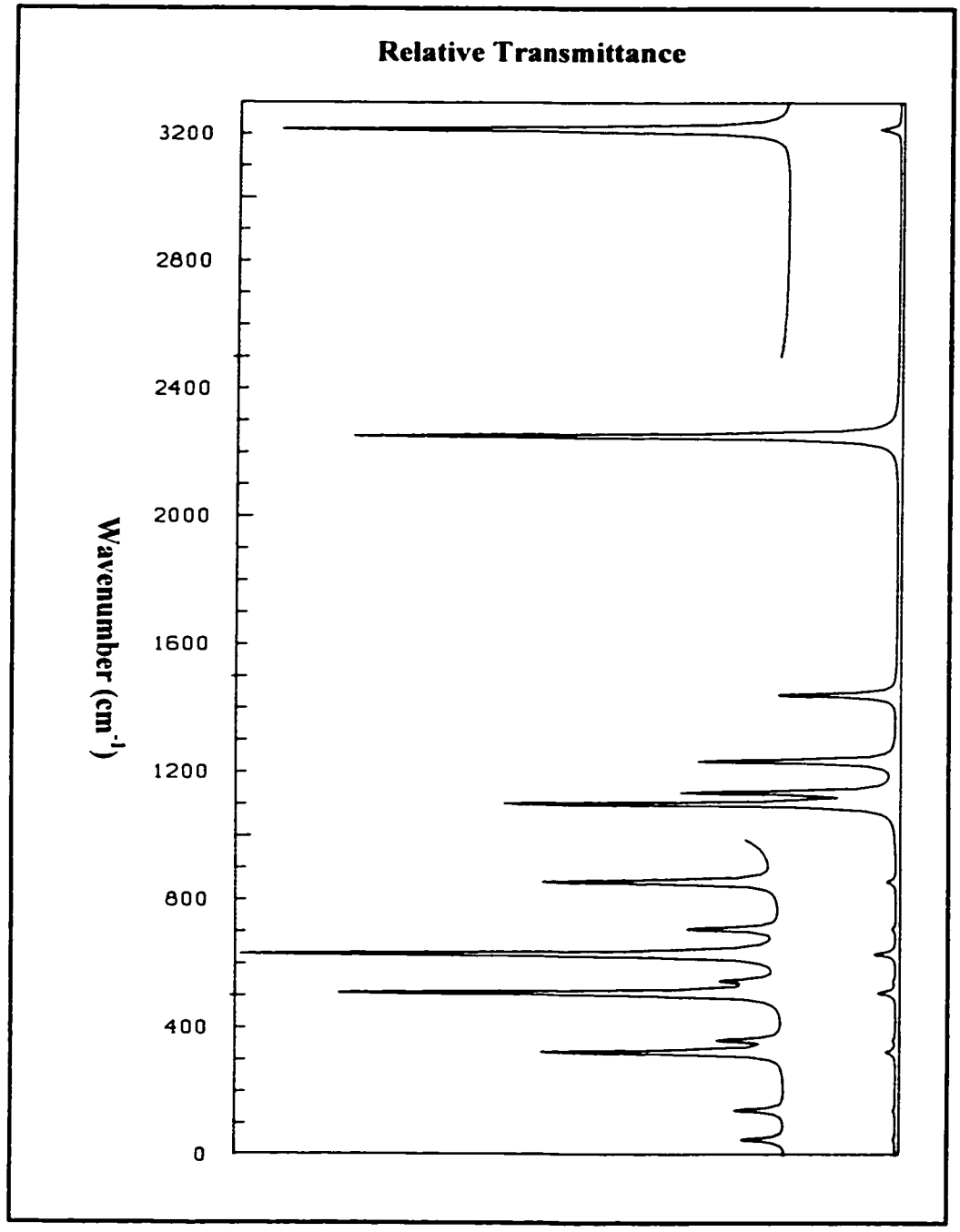

FIGURE VI-3: **Calculated Vibrational Infrared Spectrum of Trifluoromethyl Ketene at the DFT-B3LYP/6-311++G** Level.**

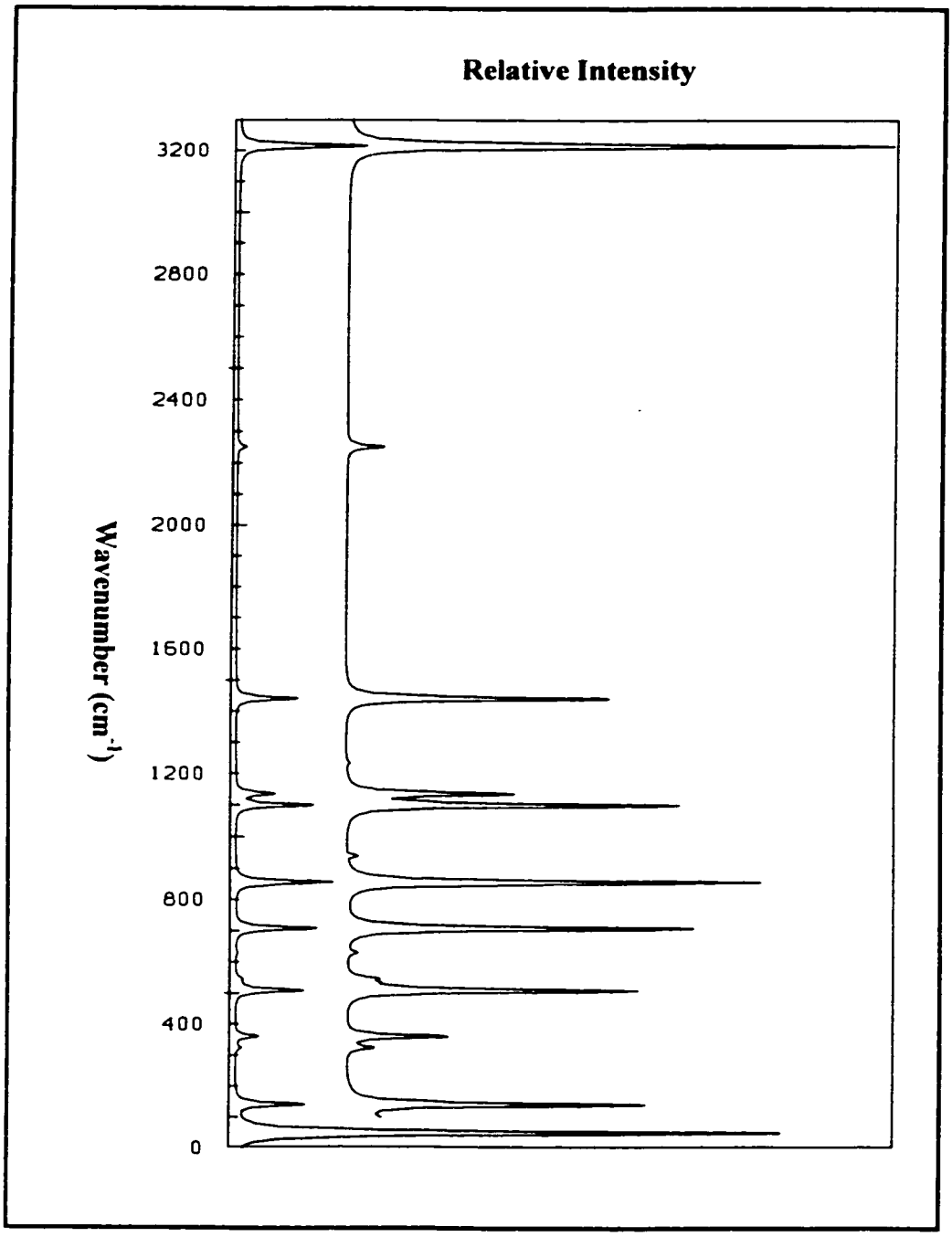

FIGURE VI-4: **Calculated Vibrational Raman Spectrum of Trifluoromethyl Ketene at the DFT-B3LYP/6-311++G** Level.**

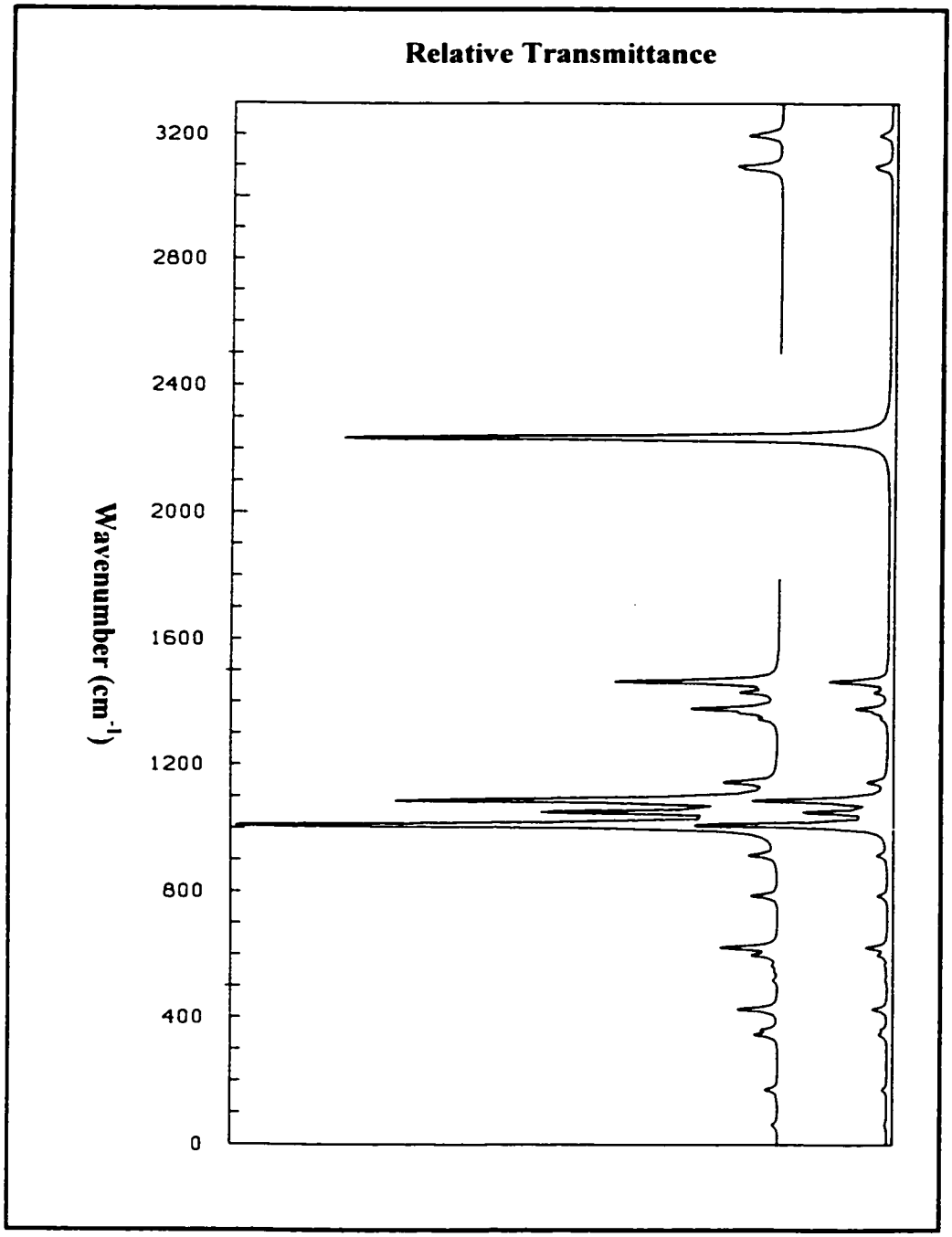

FIGURE VI-5: **Calculated Vibrational Infrared Spectrum of Difluoromethyl Ketene at 300 K at the DFT-B3LYP/6-311++G** Level.**

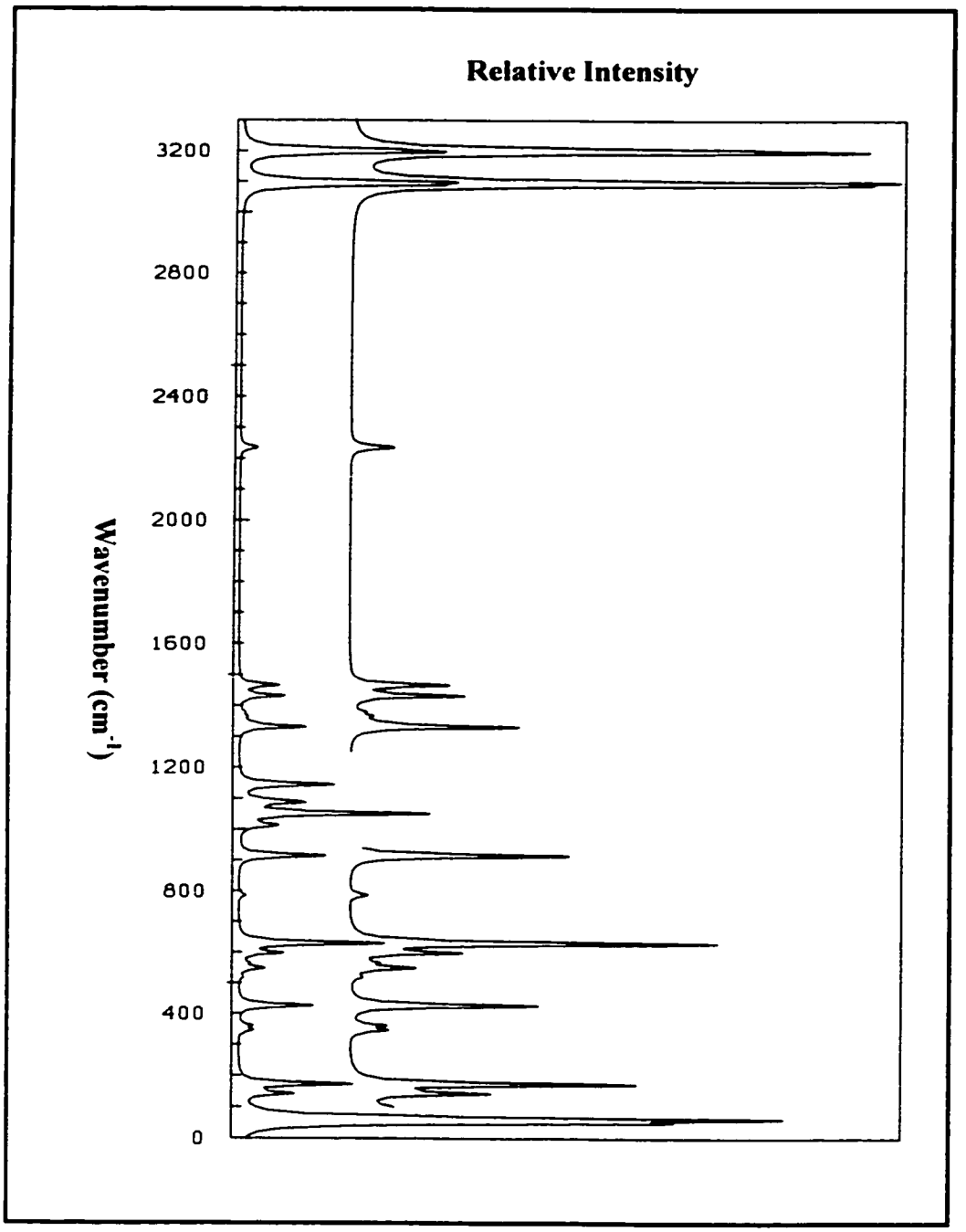

FIGURE VI-6: **Calculated Vibrational Raman Spectrum of Difluoromethyl Ketene at 300 K at the DFT-B3LYP/6-311++G** Level.**

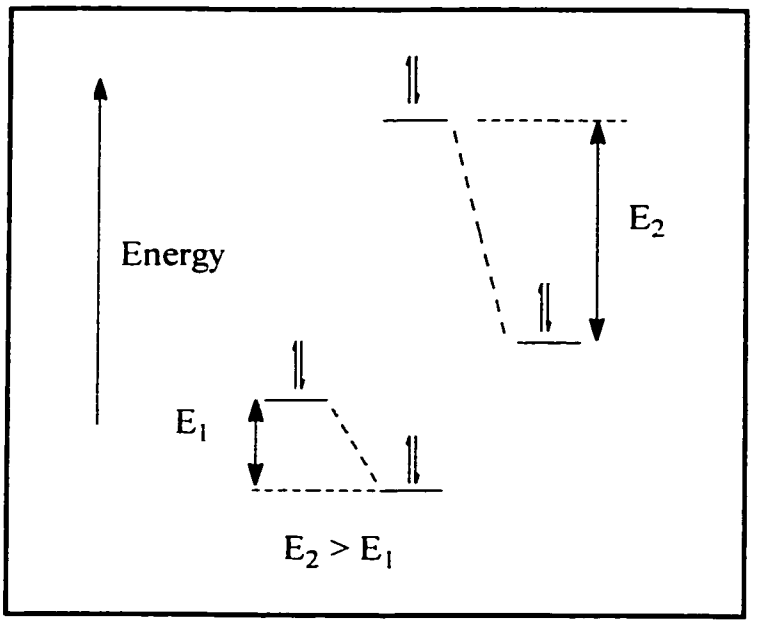

FIGURE VI-7 (a): **Two Filled-Orbitals Destabilization Interaction.**

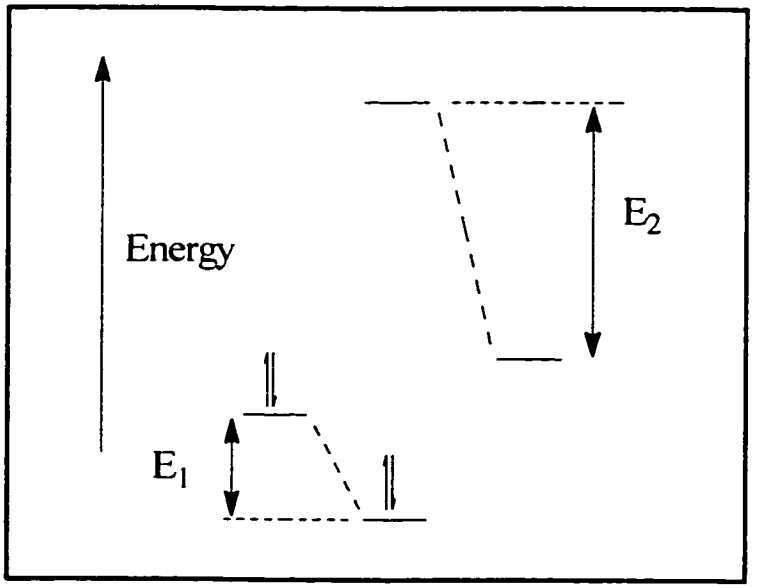

FIGURE VI-7 (b): **A filled and an Unfilled Orbital Stabilization Interaction.**

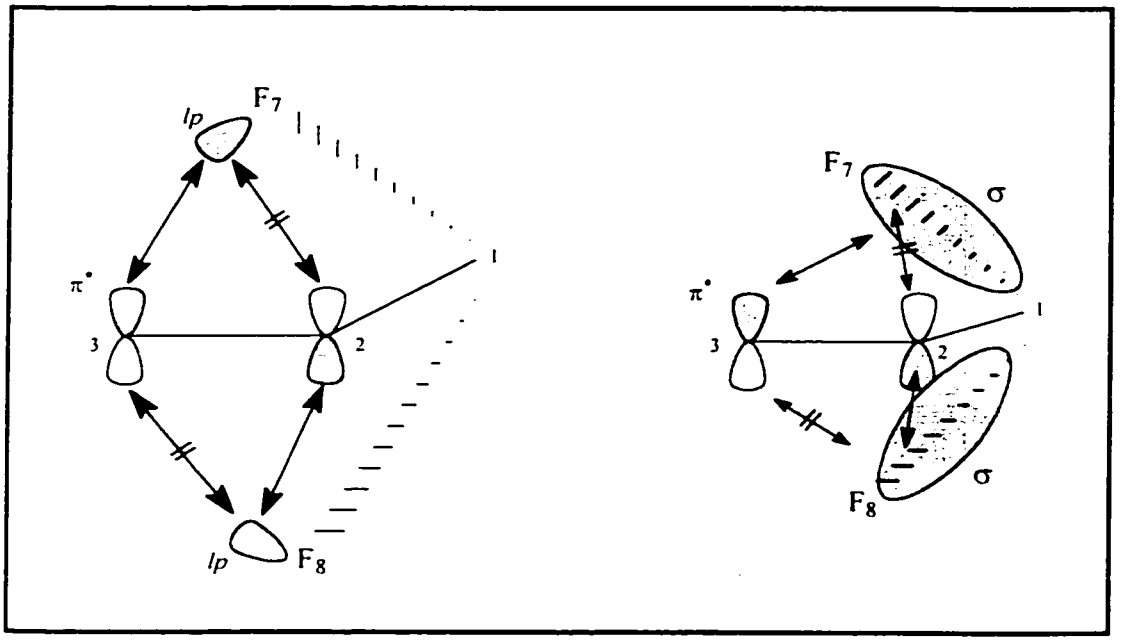

FIGURE VI-7 (c): **MO Interaction of Fluorine Lone Pairs (and C-F σ Orbitals) with the π* Orbital of the C-C π-Bond in the *Trans* Conformation of Trifluoromethyl Ketene.**

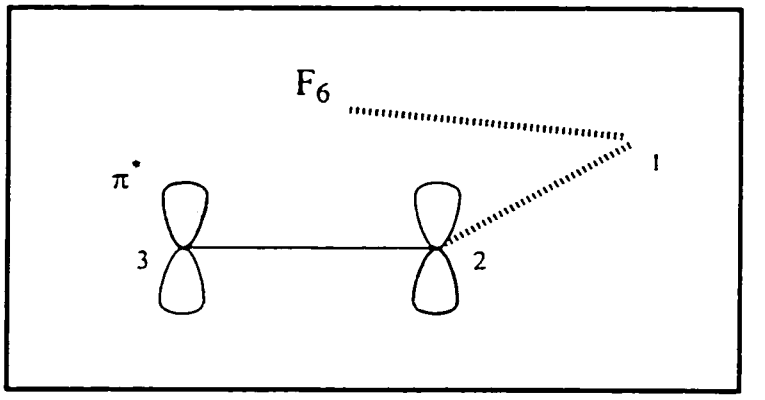

FIGURE VI-7 (d): **MO Interaction of Fluorine Lone Pairs (and C-F σ Orbitals) with the π* Orbital of the C-C π-Bond in the *Cis* Conformation of Trifluoromethyl Ketene.**

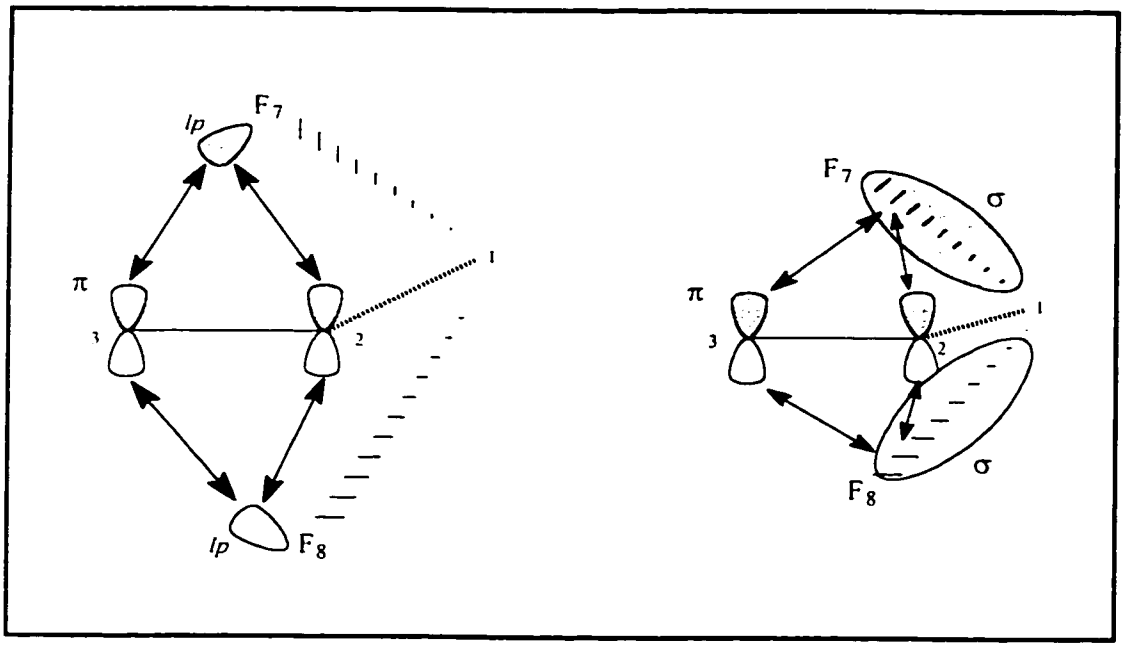

FIGURE VI-7 (e): **MO Interaction of Fluorine Lone Pairs (and C-F σ Orbitals) with the π Orbital of the C-C π-Bond in the *Trans* Conformation of Trifluoromethyl Ketene.**

CHAPTER 7

STRUCTURAL STABILITY AND DERIVED POTENTIAL ENERGY DISTRIBUTIONS FOR FLUORO- AND CHLOROMETHYL KETENE

7.1 INTRODUCTION

In the past few years, the investigations of the conformational stability of some haloacetaldehydes [5,6], haloacetyl halides [12-16] and halomethyl isocyanates [110,145] have been of a great interest. These studies were performed using vibrational and rotational spectroscopic techniques, as well as theoretical ab initio calculations at different levels of sophistication.

Fluoroacetaldehyde [6] and chloroacetaldehyde [5] were found to exist in *cis-trans* equilibrium. In both molecules, the s-*cis* form (the halogen atom eclipses the aldehydic hydrogen) was the more stable conformer, while the s-*trans* form (the halogen atom eclipses the carbonyl group) was predicted to be the high energy form. The energy difference between the two stable conformers was calculated in the case of fluoroacetaldehyde to be 1.70 kcal/mol and in chloroacetaldehyde to be 1.46 kcal/mol.

Indeed, the halogen and the oxygen atoms are away from each other and in the same time the aldehydic and the halomethyl hydrogens are *trans* to each other with a low degree of interaction.

The far-infrared spectra for different conformational haloacetyl halides were reported in the vapor phase and used to study the conformational stability of these molecules [12-16]. They were found to have the *trans* conformation to be the lowest energy form. Only fluoroacetyl chloride [14] and fluoroacetyl fluoride [15] were determined to have the *cis*, while all of the other haloacetyl halides [15,16] have the *gauche* conformer as the high-energy form. The conformational behavior of the molecules was found to be mainly controlled by the interaction between the carbonyl oxygen and the halogen atoms. In all the haloacetyl halides the low energy conformer was again the one in which the halogen atoms are directed away from each other.

In the case of chloromethyl isocyanate [110,145], the *gauche* (or near-*cis*) conformer with minimum interaction between the chlorine atom and the electron lone pair of the nitrogen atom was calculated to be the only thermodynamically stable form.

As a continuation of these studies we investigated the structural stability of fluoromethyl ketene and chloromethyl ketene to understand the nature of the interaction between the halogen atom and the ketenic –CH=C=O group. Full optimization at the DFT-B3LYP/6-311++G** level was performed for various possible conformers of both molecules. Additionally, we calculated the vibrational wavenumbers and carried out normal coordinate calculations. We then derived the potential energy distributions (PED) among symmetry coordinates for the ground state in the two molecules by utilizing ab initio DFT data. The vibrational assignments of the normal modes in the stable conformation of the

fluoro and chloro derivatives were made based on the calculated PED values. The results of the work are presented herein.

7.2 AB INITIO CALCULATIONS

The GAUSSIAN 98 program [65], running on an IBM RS/6000 43P model 260 workstation, was used to carry out the LCAO-MO-SCF DFT-B3LYP calculations. The extended 6-311++G** basis set was employed at the Density Functional B3LYP level to optimize the geometrical parameters and predict the corrected total energies for fluoromethyl ketene and chloromethyl ketene in their stable conformation. The optimized structural parameters, the rotational constants, the total dipole moments and the total energies for the molecules at the ground state are shown in Tables VII-1 and VII-2 and compared to the experimental values for the corresponding fluoroacetyl fluoride [107] and chloroacetaldehyde [5,151].

The potential scan for the internal rotation about the C-C single bond in the two molecules was obtained by allowing the XCCC dihedral angle (ϕ), where X is the fluorine atom in fluoromethyl ketene and the chlorine atom in chloromethyl ketene, to vary from 0° (*cis* position) to 180° (*trans* position). Full geometry optimizations at each of the fixed dihedral angles (ϕ) of 15°, 30°, 45°, 60°, 75°, 90°, 105°, 120°, 135°, 150°, and 165° were carried out at DFT-B3LYP/6-311++G** level of calculation in both systems. From the potential scan, it is clear that the *gauche* conformation is the only energy minimum in both molecules (Figure VII-1). The optimized XCCC dihedral angle in the fluoro system was

calculated to be 102°, while it was calculated for the chloro system to be 103.3°. The two energy maxima on the surface scan, as Figure VII-2 shows, were predicted at the *cis* and the *trans* conformations. This conclusion is exactly opposite to the behavior found in the corresponding haloacetylhalides [5,6].

The vibrational frequencies were calculated at the DFT-B3LYP/6-311++G** level using the optimized structural parameters. Normal coordinate calculations were then carried out to derive the potential energy distributions PEDs for the molecules in the stable *gauche* conformation.

7.2.1 Vibrational Frequencies and Normal Coordinate Analyses

Both fluoro- and chloromethyl ketene in their stable *gauche* conformation have the C_1 symmetry and the vibrational modes span the irreducible representation 18 A. All of the eighteen vibrational modes are polarized in the Raman spectrum of the liquid.

Normal coordinate analyses were carried out for the stable conformers of the molecules to provide a complete assignment of the fundamental vibrational frequencies. A computer program was written for this purpose by following Wilson's method [71]. The cartesian coordinates for the stable conformers together with the normal modes (in cartesian coordinates) and the frequencies from the GAUSSIAN 98 output were used as an input in the program. A complete set of internal coordinates (Table VII-3 and Figure VII-1) was used to form symmetry coordinates (Table VII-4) in the molecular systems. The potential energy distribution (PED) for each normal mode among the symmetry coordinates was calculated and is given in Tables VII-5 and VII-6.

A complete vibrational assignment of the fundamentals was proposed. The assignments were made based on calculated PED, infrared band intensities, Raman line activities and depolarization ratios. The data of the vibrational assignments are listed in Tables VII-5 and VII-6.

7.2.2 Calculation of Vibrational Spectra

To calculate the Raman spectra (Figures VII-4 and VII-6) we used the frequencies ν_j, the scattering activities S_j and the depolarization ratios ρ_j as calculated at the DFT-B3LYP level (6-311++G** basis set for all). The procedure was carried out as before. For the plots we used a grid of a step size of 10 cm^{-1}, but not when a spectral line appears between two consecutive grid points. In this case we inserted 12 points with step size of 0.5 cm^{-1} into this interval which includes the exact location of the center of the line. For the infrared spectra of the two molecules (Figures VII-3 and VII-5), we used the intensities as given by the DFT-B3LYP/6-311++G** calculations and converted them to relative transmittance.

7.3 DISCUSSION

The importance of ketenes in the field of synthetic chemistry and their fascinating electronic structure [37,47,98-107] have recently attracted the attention to investigate the conformational behavior and the structural stability of small ketenic systems, such as the molecules studied in the previous chapters in the thesis.

From the energy optimization of fluoro and chloromethyl ketene as shown in the potential curves (Figure VII-2), the *gauche* conformer with the ketenic hydrogen being in the staggered configuration with respect to the halomethyl moiety was calculated to be the only stable form. However, the *cis* conformer with the halogen atom eclipsing the ketenic –C=C=O group is calculated to be about 4 kcal/mol higher in energy than the *gauche* conformation. On the other hand, the comparison between the *gauche* and the *trans* conformers shows that the ketenic hydrogen is preferably not to be eclipsing the halogen atom as in the *trans* form and, instead, to be staggered in the *gauche* form. These predictions clearly indicate that the steric forces significantly govern the conformational behavior in these molecules.

Another interisting behavior shown on the potential curves (Figure VII-2) is that the cis conformation is about 1.5 kcal/mol lower in energy than the *trans* conformation. One may expect the reversed behavior since the bulky halogen atom eclipses the ketene group in the *cis* form, which would lead to destabilize it more as compared to the *trans* form. However, this could be explained in terms of the electrostatic attraction in the *cis* form between the partially negatively charged fluorine atom and the partially positively charged central carbon atom of the ketene group. This in fact supports our argument of the dipole interaction in the tri- and difluoromethyl ketene stated in the last chapter.

The vibrational wavenumbers of the stable *gauche* conformation of the halomethyl systems were calculated (Tables VII-5 and VII-6) and the IR and Raman spectra were plotted and shown in Figures VII-3 – VII-6. The assignments of most of the fundamental vibrations of the stable conformer in the molecules were made only based on the calculated PED values. Few vibrational modes were predicted to be highly mixed with other modes. A

comparison of the calculated vibrational modes with experimental ones obtained for chlorocarbonyl ketene [105] and chloromethyl isocyanate [145] indicates that a reasonable agreement has been noticed between the calculated modes and the experimental values (Tables VII-5 and VII-6).

Three C-H stretching modes (S_1, S_{10} and S_{15}) were predicted to have the highest vibrational frequencies and Raman activities in the Raman spectra of the two molecules. Among these modes, the ketenic C-H stretch (S_1) was calculated to be of the higher frequency (3191 cm^{-1} for the fluoro- and 3190 cm^{-1} for the chloromethyl ketene) as compared to the other two stretches (S_{10} and S_{15}). Moreover, there are four CH_2 bending modes which were predicted to follow the order: rocking < twisting < wagging < deformation vibrational modes. The order calculated at the DFT-B3LYP level in our systems is in fair agreement with the corresponding experimental values in chloromethyl isocyanate [145].

The highest band in the infrared spectra of the two molecules was assigned based on the PED values to the antisymmetric –C=C=O stretching mode. This prediction is consistent with experimental results observed for chlorocarbonyl ketene [105]. It has a very small degree of mixing with other modes (97% PED for both molecules). The corresponding symmetric stretching mode, however, was calculated to be highly mixed with other modes (Tables VII-5 and VII-6). Since the symmetric –C=C=O stretch was observed in the IR spectrum of chlorocarbonyl ketene [105] at 1376 cm^{-1}, hence this mode could be confidently assigned to ν_6 at 1428 cm^{-1} in the fluoromethyl and at 1425 cm^{-1} in the chloromethyl ketene.

The C-Cl stretch was calculated to be at 677 cm^{-1} in the *gauche*-chloromethyl system. In the gas phase IR spectrum, the C-Cl stretching mode in chloromethyl isocyanate

[145] was observed at 720 cm^{-1}, which supports our assignment of this mode. For the C-F stretching mode, the assignment was made directly from the calculated PED to ν_{11} (94%). Tables VII-5 and VII-6 show that the C-F tretching ode has a higher calculated IR intensity as compared to the corresponding C-Cl mode, whereas the reverse trend was predicted when the Raman activities of the two modes are compared with each other. This prediction is consistent with fact that the IR intensity gets higher with increasing in the induced dipole moment, as in the case of C-F bond, while the greater polarizability change in the C-Cl bond leads to a higher Raman activity.

The in-plane –C=C=O and C=C-H bending vibrational modes were assigned based on the derived PED values to ν_9 and ν_{13}, respectively, in both fluoro- and chloromethyl ketene. The calculated fundamental vibration of the in-plane C=C-H bending, at 1156 cm^{-1} for the fluoromethyl and 1152 cm^{-1} for the chloromethyl derivatives, is comparable with infrared experimental values for chlorocarbonyl ketene [105] (1125 cm^{-1}). The out-of-plane –C=C=O and C=C-H bending vibrational modes of *gauche*-chloromethyl ketene fit excellently with the infrared frequencies of the same modes in the chlorocarbonyl system as shown in Table VII-6. Thus, the highly mixed vibrational frequency at ν_{10} in fluoro- and chloromethyl ketene could then be assigned to the C-C stretching mode (S_2).

The lowest bending modes in the two molecules were the in-plane C-X and C=C-H bending vibrations which were calculated, respectively, at 388 and 208 cm^{-1} for the fluoromethyl system and at 300 and 207 cm^{-1} for the chloromethyl system. The lowest vibrational modes in the spectra of the two ketenic systems were the asymmetric torsion which was predicted at 89 and 76 cm^{-1} for the fluoromethyl and chloromethyl ketene, respectively.

In conclusion, we provided reliable vibrational assignments for all the normal modes in the stable *gauche* conformation in fluoro- and chloromethyl ketene based on normal coordinate analysis. The derived PED values significantly helped in the assignment of most of the stretching and bending modes in the molecules under investigation. The *gauche* conformation in the two molecular systems was predicted from the calculated surface scan to be the only stable conformation with two energy maxima at the *cis* and the *trans* forms. The stability of the halomethyl systems was explained in terms of the steric hinderance.

TABLE VII-1: **Calculated Structural Parameters, Total Dipole Moment, and Rotational Constants for the *Gauche* Conformation of Fluoromethyl Ketene.**

Parameter [a]	B3LYP/6-311++G**	Microwave [b]
	gauche	*trans*
Bond Length (Å)		
$r(C_1\text{-}C_2)$	1.491	1.483 ± 0.007
$r(C_2\text{-}C_3)$	1.316	
$r(C_3\text{-}O_4)$	1.159	
$r(C_2\text{-}H_5)$	1.083	
$r(C_1\text{-}F_6)$	1.414	1.366 ± 0.007
$r(C_1\text{-}H_7)$	1.091	1.096 ± 0.003
$r(C_1\text{-}H_8)$	1.091	1.096 ± 0.003
Bond Angle (deg)		
$(C_1C_2C_3)$	122.0	
$(C_2C_3O_4)$	179.8	
$(C_1C_2H_5)$	120.9	
$(C_2C_1F_6)$	111.4	109.6 ± 1.0
$(C_2C_1H_7)$	110.7	109.2 ± 0.4
$(C_2C_1H_8)$	112.0	109.2 ± 0.4
$(H_7C_1H_8)$	109.6	109.0 ± 1.0
$(C_3C_2C_1F_6)$	102.0	180.0
$(C_3C_2C_1H_7)$	117.8	
$(C_3C_2C_1H_8)$	-119.6	
Dipole Moment μ_t (Debye)	2.1	
Rotational Constants (MHz)		
A	18416	
B	2471	
C	2362	

[a] Calculated total energy, zero-point correction, and the sum of total and zero point energies (in Hartrees) of the *gauche* conformer of fluoromethyl ketene at DFT-B3LYP/6-311++G** level are –291.24227, 0.05415, and –291.18812, respectively.

[b] Data was obtained for fluoroacetyl fluoride, see ref [107].

***TABLE VII-2:* Calculated Structural Parameters, Total Dipole Moment, and Rotational Constants for the *Gauche* Conformation of Chloromethyl Ketene.**

Parameter [a]	B3LYP/6-311++G**	Microwave [b]
	gauche	*cis*
Bond Length (Å)		
$r(C_1\text{-}C_2)$	1.485	1.524 ± 0.015
$r(C_2\text{-}C_3)$	1.317	
$r(C_3\text{-}O_4)$	1.159	
$r(C_2\text{-}H_5)$	1.083	1.093 ± 0.012 [c]
$r(C_1\text{-}Cl_6)$	1.852	1.784 ± 0.015
$r(C_1\text{-}H_7)$	1.087	1.093 ± 0.012
$r(C_1\text{-}H_8)$	1.087	1.093 ± 0.012
Bond Angle (deg)		
$(C_1C_2C_3)$	122.5	123.3 ± 0.6 [c]
$(C_2C_3O_4)$	180.0	
$(C_1C_2H_5)$	120.7	
$(C_2C_1Cl_6)$	113.2	109.2 ± 0.4
$(C_2C_1H_7)$	111.4	110.3 ± 1.5
$(C_2C_1H_8)$	112.7	110.3 ± 1.5
$(H_7C_1H_8)$	109.6	109.5 (fixed)
$(C_3C_2C_1Cl_6)$	103.3	180.0 (fixed)
$(C_3C_2C_1H_7)$	117.1	
$(C_3C_2C_1H_8)$	-119.2	
Dipole Moment μ_t (Debye)	2.2	
Rotational Constants (MHz)		
A	13835	
B	1675	
C	1588	

[a] Calculated total energy, zero-point correction, and the sum of total and zero point energies (in Hartrees) of the *gauche* conformer of fluoromethyl ketene at DFT-B3LYP/6-311++G** level are –651.59876, 0.05273, and –651.54603, respectively.

[b] Data was obtained for chloroacetaldehyde, see ref [5].

[c] Obtained from electron diffraction experiment, see ref [151].

TABLE VII-3: **Internal Coordinate Definitions [a] for Fluoromethyl Ketene (X=F) and Chloromethyl Ketene (X=Cl).**

No.	Coordinate		Definition
1	C_1-C_2	stretch	R
2	C_2-C_3	stretch	P
3	C_3-O_4	stretch	T
4	C_2-H_5	stretch	D
5	C_1-X_6	stretch	Q_1
6	C_1-H_7	stretch	Q_2
7	C_1-H_8	stretch	Q_3
8	$C_1C_2C_3$	bend	γ
9	$C_2C_3O_4$	bend	σ
10	$C_1C_2H_5$	bend	ρ
11	$C_3C_2H_5$	bend	δ
12	$C_2C_1X_6$	bend	α_1
13	$C_2C_1H_7$	bend	α_2
14	$C_2C_1H_8$	bend	α_3
15	$X_6C_1H_7$	bend	β_1
16	$X_6C_1H_8$	bend	β_2
17	$H_7C_1H_8$	bend	β_3
18	C_2=C_3=O_4	wag	χ
19	$H_5C_1C_2C_3$	wag	π
20	$X_6C_1C_2H_5$	(CH_2X) torsion	τ
	$H_7C_1C_2H_5$		
	$H_8C_1C_2H_5$		

[a] See Figure VII-1 for atom denotation.

TABLE VII-4: **Symmetry Coordinates for Fluoromethyl Ketene (X=F) and Chloromethyl Ketene (X=Cl).**

Species	Description		Symmetry Coordinate [a]
A'	C-H	stretch	$S_1 = D$
	C-C	stretch	$S_2 = R$
	C=C=O	symmetric stretch	$S_3 = P + T$
	C=C=O	antisymmetric stretch	$S_4 = P - T$
	C=C=O	in-plane bend	$S_5 = \sigma$
	C=C-H	in-plane bend	$S_6 = \rho - \delta$
	C=C-C	in-plane bend	$S_7 = 2\gamma - \rho - \delta$
	C-X	stretch	$S_8 = Q_1$
	C-X	in-plane bend	$S_9 = [\,(6)^{1/2} + 2\,]\,\alpha_1 - [\,(6)^{1/2} - 2\,]\,\beta_3 - \alpha_2 - \alpha_3 - \beta_1 - \beta_2$
	CH_2	stretch	$S_{10} = Q_2 + Q_3$
	CH_2	wag	$S_{11} = \alpha_2 + \alpha_3 - \beta_1 - \beta_2$
	CH_2	deformation (scissor)	$S_{12} = [\,(6)^{1/2} + 2\,]\,\beta_3 - [\,(6)^{1/2} - 2\,]\,\alpha_1 - \alpha_2 - \alpha_3 - \beta_1 - \beta_2$
A''	C=C=O	out-of-plane bend (wag)	$S_{13} = \chi$
	C=C-H	out-of-plane bend (wag)	$S_{14} = \pi$
	CH_2	antisymmetric stretch	$S_{15} = Q_2 - Q_3$
	CH_2	rock	$S_{16} = \alpha_2 - \alpha_3 + \beta_1 - \beta_2$
	CH_2	twist	$S_{17} = \alpha_2 - \alpha_3 - \beta_1 + \beta_2$
	CH_2X	torsion	$S_{18} = \tau$

[a] Not normalized.

TABLE VII-5: **Calculated Vibrational Frequencies (cm^{-1}) at B3LYP/6-311++G** Level for the *Gauche* Conformer of Fluoromethyl Ketene.**

Symm.	Number	Frequency	IR Intensity [a]	Raman Activity	Depol. Ratio	Obs. [b]	PED [c]
A	ν_1	3191	9.7	82.4	0.2		99% C-H_5 str. (S_1)
	ν_2	3115	19.6	70.8	0.7		99% CH_2 antisymm. str. (S_{15})
	ν_3	3063	29.4	127.3	0.1		100% CH_2 str. (S_{10})
	ν_4	2219	793.7	13.9	0.6	2160	97% C=C=O antisymm. str. (S_4)
	ν_5	1496	4.5	6.8	0.7		100% CH_2 def. (S_{12})
	ν_6	1428	36.2	7.7	0.1	1376	35% C=C=O symm. str. (S_3), 29% C=C-H in-plane bend (S_6), 13% C-C str. (S_2), 10% CH_2 twist (S_{17}), 10% CH_2 wag (S_{11})
	ν_7	1382	22.0	4.6	0.4		96% CH_2 wag (S_{11})
	ν_8	1260	11.7	7.0	0.7		79% CH_2 twist (S_{17})
	ν_9	1156	4.1	12.8	0.4	1125	52% C=C-H in-plane bend (S_6), 23% C=C=O symm. str. (S_3), 16% C-C str. (S_2)
	ν_{10}	1083	33.2	6.0	0.1	1051	23% C-C str. (S_2), 37% CH_2 rock (S_{16}), 12% C=C-C in-plane bend (S_7)
	ν_{11}	953	224.2	11.4	0.4		94% C-F str. (S_8)
	ν_{12}	923	18.2	5.7	0.04		36% CH_2 rock (S_{16}), 29% C-C str. (S_2), 17% C=C=O symm. str. (S_3)
	ν_{13}	656	18.9	1.3	0.3		42% C=C=O in-plane bend (S_5), 19% C=C-C in-plane bend (S_7), 12% C-F in-plane bend (S_9)

TABLE VII-5: **Continue.**

Symm.	Number	Frequency	IR Intensity [a]	Raman Activity	Depol. Ratio	Obs. [b]	PED [c]
A	ν_{14}	605	35.4	3.0	0.3	(531)	38% C=C-H wag (S_{14}), 12% C=C=O in-plane bend (S_5), 11% CH_2F torsion (S_{18}), 11% C=C=O wag (S_{13}), 10% C-F in-plane bend (S_9)
	ν_{15}	555	0.1	0.9	0.6	558	84% C=C=O wag (S_{13}), 10% CH_2F torsion (S_{18})
	ν_{16}	388	23.7	1.9	0.5		65% C-F in-plane bend (S_9), 16% C=C-H wag (S_{14})
	ν_{17}	208	1.3	1.7	0.7		59% C=C-C in-plane bend (S_7), 33% C=C=O in-plane bend (S_5)
	ν_{18}	89	3.5	2.2	0.7		58% CH_2F torsion (S_{18}), 31% C=C-H wag (S_{14})

[a] Infrared intensities and Raman activities are calculated in K m mol^{-1} and $Å^4$ amu^{-1}, respectively.

[b] Observed IR frequencies for *trans*-chlorocarbonyl ketene in argon matrix, the values in brackets are for the *cis*-chlorocarbonyl ketene under the same condition [105].

[c] PED values are obtained by using calculated frequencies at B3LYP level.

TABLE VII-6: **Calculated Vibrational Frequencies (cm^{-1}) at B3LYP/6-311++G** Level for the *Gauche* Conformer of Chloromethyl Ketene.**

Symm.	Number	Frequency	IR Intensity [a]	Raman Activity	Depol. Ratio	Obs. [b]	PED [c]
A	ν_1	3190	10.1	72.0	0.2		94% C-H_5 str. (S_1)
	ν_2	3165	3.6	68.5	0.7	3013	94% CH_2 antisymm. str. (S_{15})
	ν_3	3105	10.5	106.7	0.1	(2989)	100% CH_2 str. (S_{10})
	ν_4	2217	900.0	16.5	0.5	(2160)	97% C=C=O antisymm. str. (S_4)
	ν_5	1483	8.2	6.2	0.7	(1453)	96% CH_2 def. (S_{12})
	ν_6	1425	36.2	27.3	0.2	1376	39% C=C=O symm. str. (S_3), 30% C=C-H in-plane bend (S_6), 13% C-C str. (S_2), 11% CH_2 twist (S_{17})
	ν_7	1291	62.8	7.5	0.7	(1312)	100% CH_2 wag (S_{11})
	ν_8	1203	24.5	21.2	0.5	(1223)	74% CH_2 twist (S_{17}), 13% C-C str. (S_2)
	ν_9	1152	1.0	18.2	0.3	1125	65% C=C-H in-plane bend (S_6), 19% C=C=O symm. str. (S_3)
	ν_{10}	1036	31.8	4.5	0.5	1051	37% C-C str. (S_2), 24% CH_2 rock (S_{16}), 13% C=C=O symm. str. (S_3), 11% C=C-C in-plane bend (S_7)
	ν_{11}	875	13.8	3.8	0.7	(959)	64% CH_2 rock (S_{16}), 21% C-C str. (S_2), 13% C=C=O symm. str. (S_3)
	ν_{12}	677	155.8	35.8	0.3	(720)	41% C-Cl str. (S_8), 25% C=C-H wag (S_{14}), 22% C-Cl in-plane bend (S_9)
	ν_{13}	645	12.4	1.4	0.2		49% C=C=O in-plane bend (S_5), 20% C=C-C in-plane bend (S_7)

TABLE VII-6: **Continue.**

Symm.	Number	Frequency	IR Intensity [a]	Raman Activity	Depol. Ratio	Obs. [b]	PED [c]
A	ν_{14}	561	23.0	13.8	0.1	558	48% C=C=O wag (S_{13}), 32% C-Cl str. (S_8), 13% C=C-H wag (S_{14})
	ν_{15}	538	4.6	11.3	0.2	531*	16% C=C-H wag (S_{14})49% C=C=O wag (S_{13}), 17% CH_2Cl torsion (S_{18}) , 16% C-Cl str. (S_8)
	ν_{16}	300	21.1	6.9	0.3		71% C-Cl in-plane bend (S_9), 15% C-Cl str. (S_8)
	ν_{17}	207	1.0	2.0	0.5		61% C=C-C in-plane bend (S_7), 32% C=C=O in-plane bend (S_5)
	ν_{18}	76	2.3	4.0	0.7		60% CH_2Cl torsion (S_{18}), 35% C=C-H wag (S_{14})

[a] Infrared intensities and Raman activities are calculated in K m mol^{-1} and $Å^4$ amu^{-1} respectively.

[b] Observed IR frequencies for *trans*-chlorocarbonyl ketene in argon matrix [105], the value marked by the star is for *cis*-chlorocarbonyl ketene under the same condition [105], values in brackets are the gas phase IR frequencies for chloromethyl isocyanate [145].

[b] PED values are obtained by using calculated frequencies at B3LYP level.

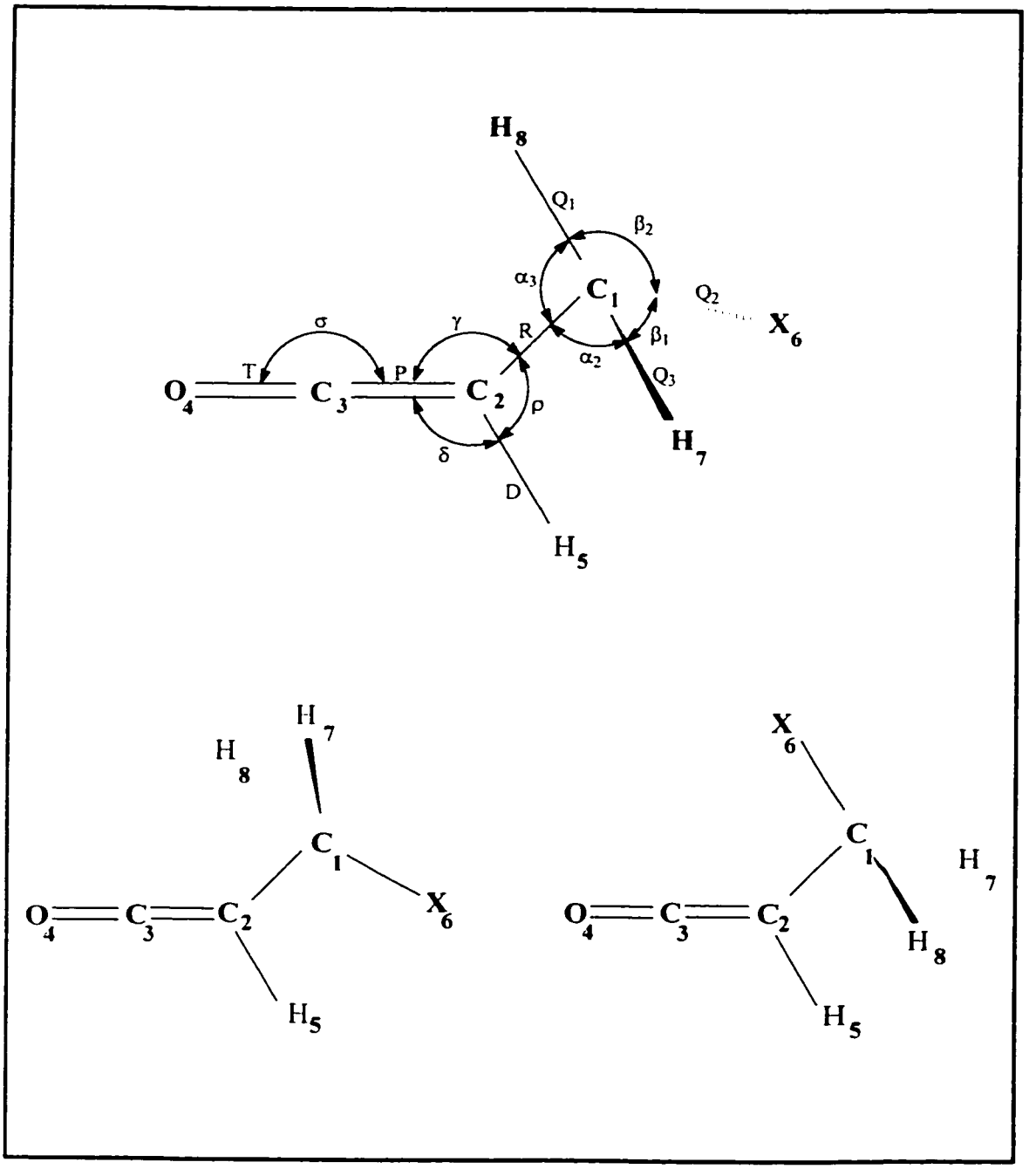

FIGURE VII-1: **Atom Numbering for Fluoromethyl Ketene (X=F) and Chloromethyl Ketene (X=Cl) in the *Gauche* (Upper), the *Cis* (Lower Right) and the *Trans* (Lower Left) Conformations, with the Internal Coordinates Shown on the *Gauche* Form.**

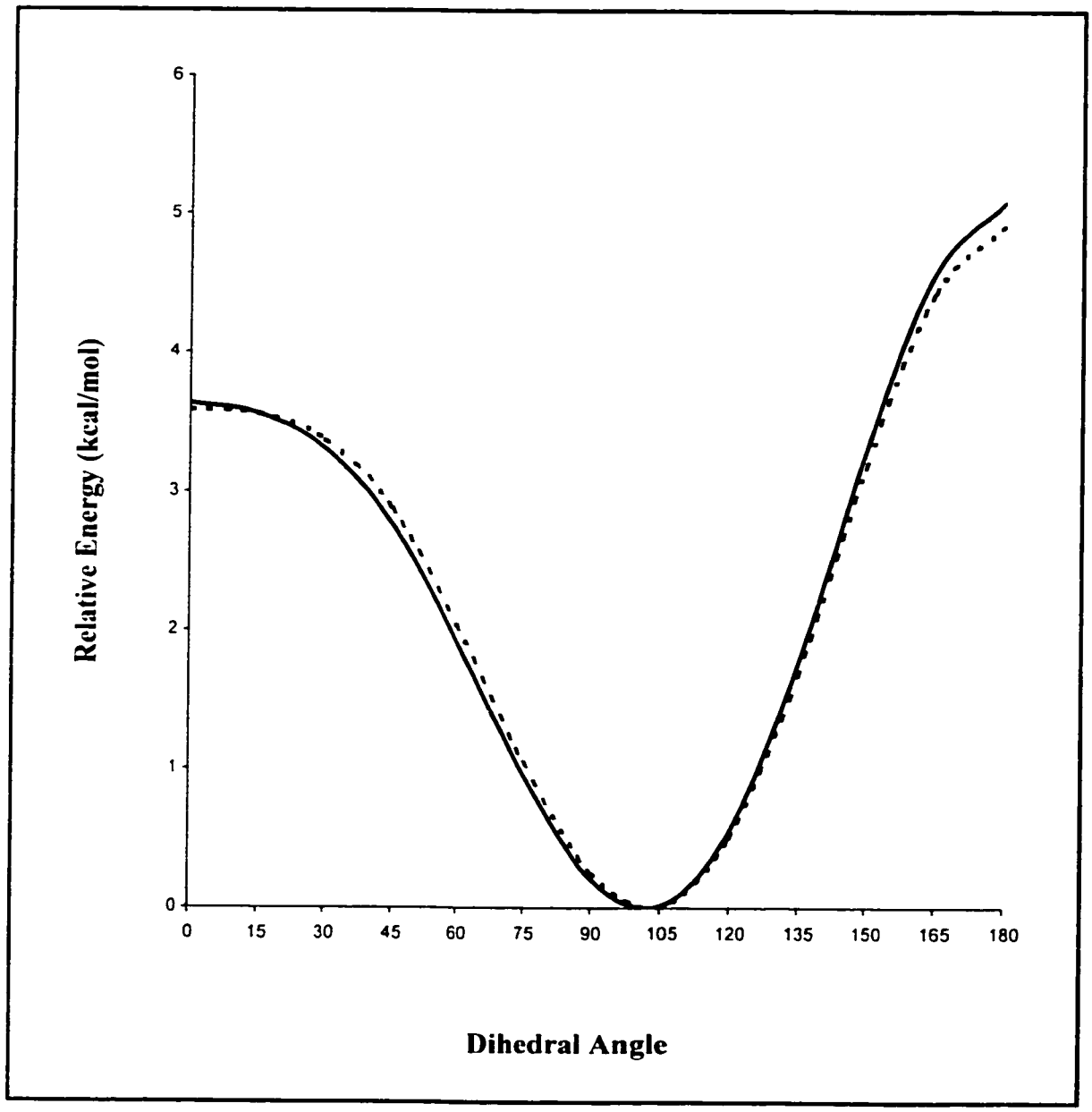

FIGURE VII-2: **Potential Curve for the Internal Rotation in Fluoromethyl Ketene (Solid Line) and Chloromethyl Ketene (Dashed Line) as Determined by Ab Initio Calculations at B3LYP/6-311++G** Level.**

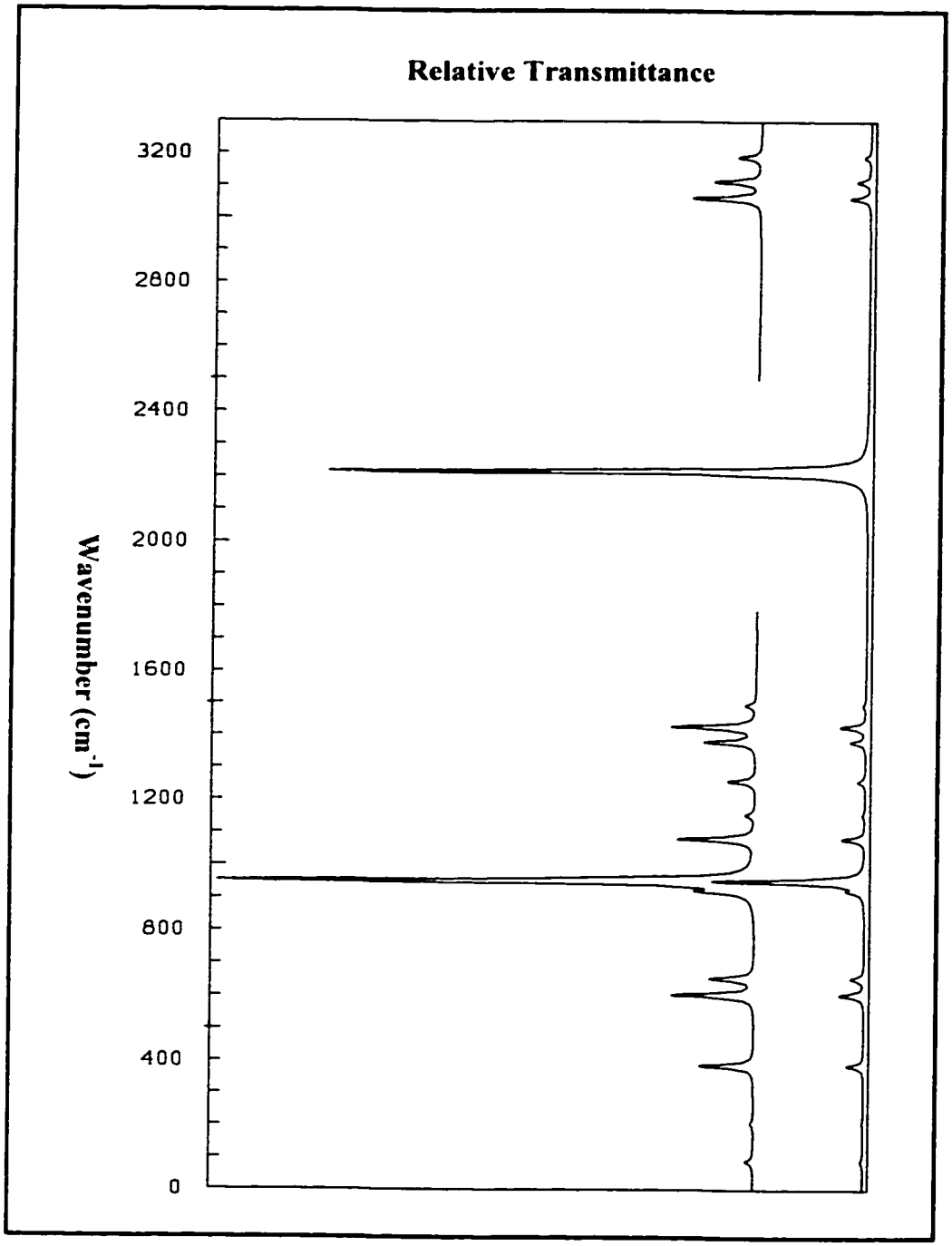

FIGURE VII-3: **Calculated Vibrational Infrared Spectrum of Fluoromethyl Ketene at the DFT-B3LYP/6-311++G** Level.**

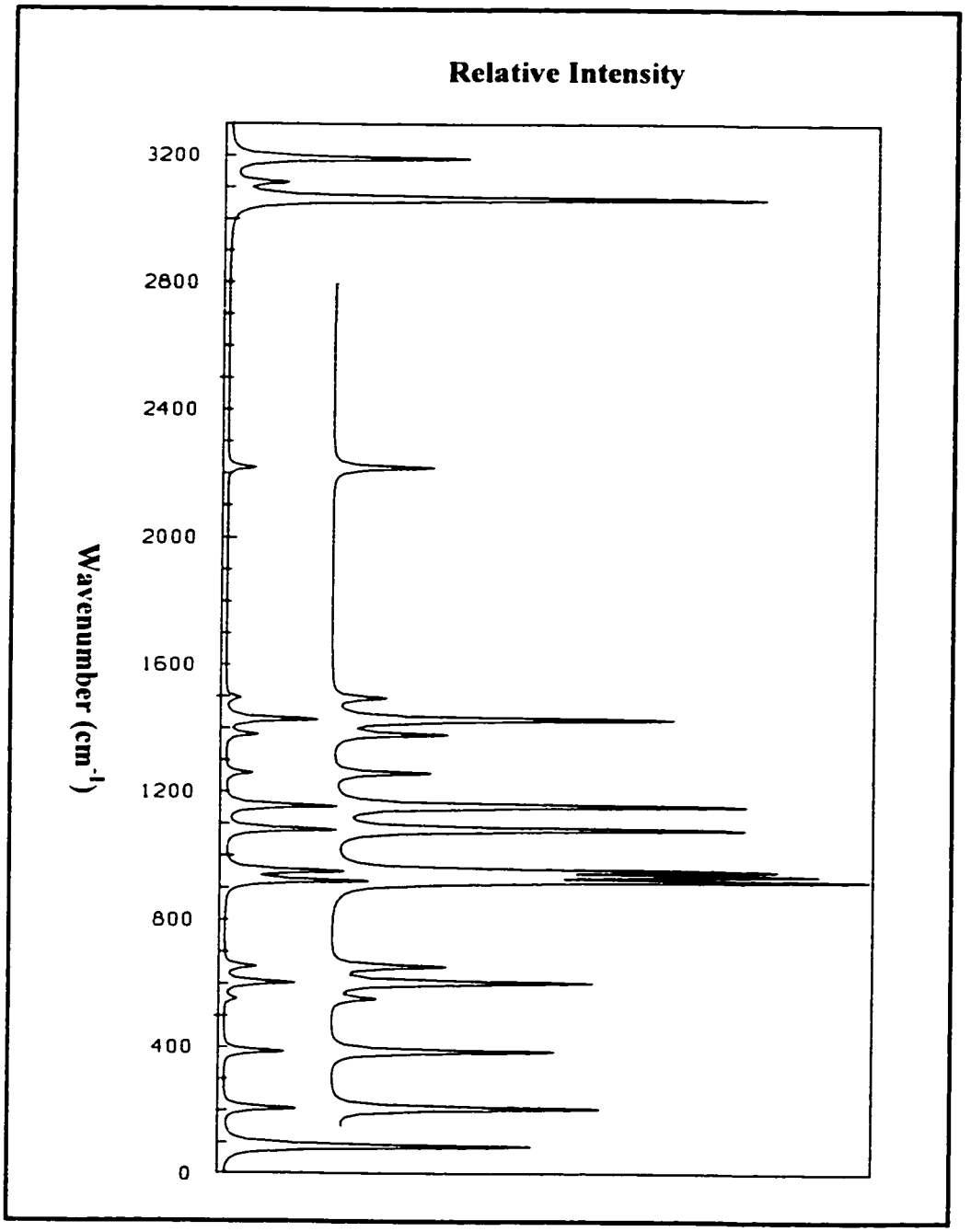

FIGURE VII-4: **Calculated Vibrational Raman Spectrum of Fluoromethyl Ketene at the DFT-B3LYP/6-311++G** Level.**

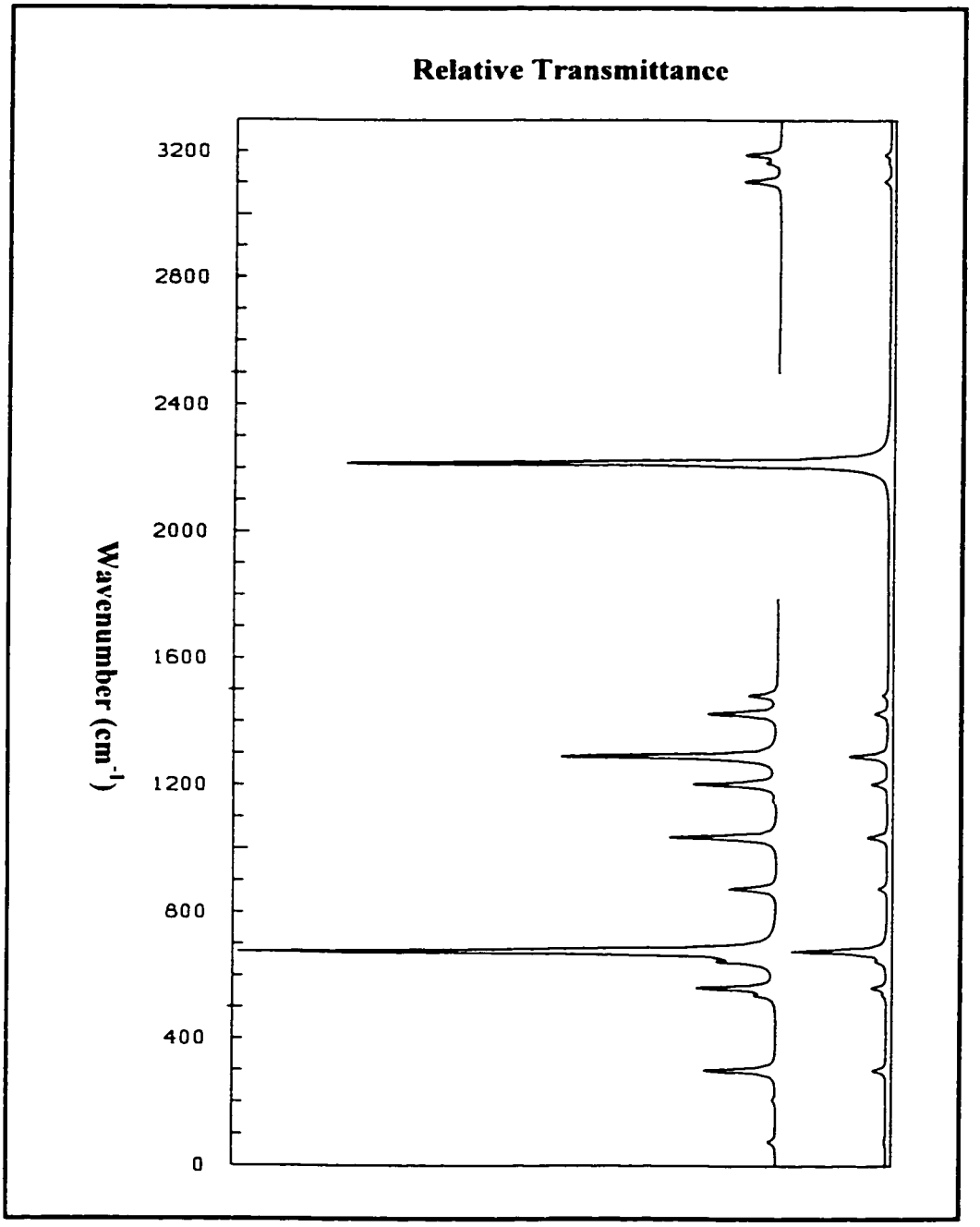

FIGURE VII-5: **Calculated Vibrational Infrared Spectrum of Chloromethyl Ketene at the DFT-B3LYP/6-311++G** Level.**

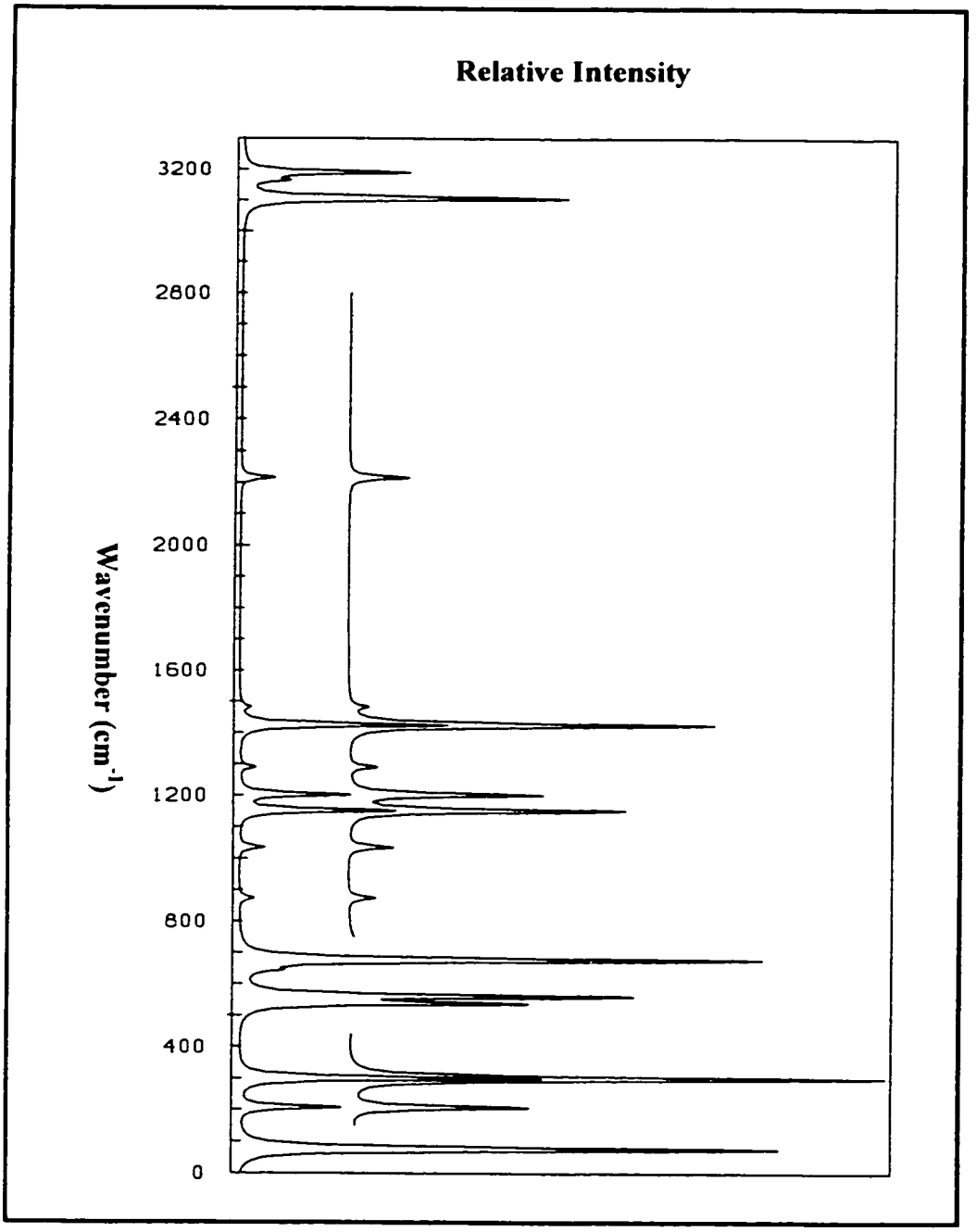

FIGURE VII-6: **Calculated Vibrational Raman Spectrum of Chloromethyl Ketene at the DFT-B3LYP/6-311++G** Level.**

CONCLUSION

We started our work by investigating the conformational equilibrium of formyl ketene which was predicted by all levels to exist only in the planar form. From the energy optimization at HF level and MP2, the *cis* conformer was calculated to be slightly more stable than the *trans* conformer. However, at the DFT-B3LYP level the conformational behavior was reversed, and the *trans* became the thermodynamically more preferred conformation for formyl ketene. This behavior is more consistent with the idea that eclipsing the two hydrogens in the *cis* form should destabilize the molecule in this conformation. For the molecule, the carbonyl oxygen and not the aldehydic hydrogen should eclipse the ketenic hydrogen in the *trans* conformation of the molecule.

Comparative studies on different molecules have been published and showed that the calculations at the DFT level give more reliable results for the dipole moments, harmonic frequencies, atomization energies and potential energy distributions as compared to the HF and MP2 levels. Thus, we decided to use the data given by the higher level of calculations to obtain more well results and more comparable data to experiments. In addition, we utilized the extended basis set in our work.

We found from ab initio calculations at the DFT-B3LYP level that both fluorocarbonyl ketene and chlorocarbonyl ketene exist as a mixture of the *cis* and the

trans planar conformations. The *trans* form in the two ketenic systems (the halogen atom eclipses the ketenic hydrogen) is predicted to be the lowest energy minima. This result is consistent with the experimental data from the IR analysis for chlorocarbonyl ketene. The π-π interaction between the CXO group and the ketenic group –C=C=O in fluoro- and chlorocarbonyl ketene greatly stabilizes the planar forms with a relatively high *trans*-to-*cis* rotational barrier. The comparison shows that there is no difference between the calculated potential scans of the two molecules. This is basically because of the significant domination of the conjugation effect over the steric force.

From the Density Functional Calculations we found that both vinyl ketene and vinyl isocyanate exist as a mixture of the *cis* and the *trans* planar conformations. The *trans* form in vinyl ketene (the vinyl group eclipses the ketenic hydrogen) and in vinyl isocyanate (the vinyl group eclipses the lone pair of the nitrogen atom) are the most stable minima. The two hydrogen atoms in vinyl ketene, and the hydrogen atom and the lone pair in vinyl isocyanate eclipse each other in the *cis* form. This relatively destabilizes the molecule in the *cis* conformation as compared to the *trans* conformation. The situation is clear from the predicted high relative energy between the two conformers in both molecules. In the vinyl systems under investigation, the π-π interaction between the vinyl group CH_2=CH– and the ketenic group –C=C=O in vinyl ketene or the isocyanato group –N=C=O in vinyl isocyanate, greatly stabilizes the planar forms with a relatively high rotational barrier. Moreover, the C-N barrier in vinyl isocyanate was predicted to be much lower in energy than the C–C barrier in vinyl ketene. The significant difference between the two rotational barriers is due to the decrease in the partial π character of the C–N bond in the

isocyanate as compared to that of the C–C bond in the ketene. This difference is the result of the electronegativity change as we go from the C–N bond in vinyl isocyanate to the corresponding C–C one in vinyl ketene. A similar variation was noticed when the energy barrier in formyl ketene was compared to that in formyl isocyanate.

In our study on tri- and difluoromethyl ketenes in which the conjugation force is absent, it turned out that in this series of molecules we faced two effects competing with each other. One of them is due to destabilizing interaction between F-lone pairs and the C=C π-bond (both occupied). This effect is larger, the more the C-F bond is in the staggered positions to the ketenic group, and the lowest when the C-F bond eclipses that group (lone pair MO in the nodal plane of the π-MO). The second effect is the simple steric hinderance.

The electronic structure of trifluoromethyl ketene was very fascinating. On first sight, we expected that the *trans* conformer (a fluorine atom eclipses the ketenic hydrogen) should be more stable than the *cis* form (a fluorine atom eclipses the C=C=O moiety). However, closer inspection shows that actually the reverse was true. The partially negatively charged fluorine atom in the *cis* conformer is calculated to be quite close to the partially positive central carbon atom. Moreover, in both conformers the repulsion between the negative fluorine and the ketenic oxygen atoms is rather small due to the large distances between them. Moreover, the MO effects in trifluoromethyl ketene clearly dominate and outweigh steric effects, whose relative magnitudes are less pronounced, when having only C-F bonds in the rotor. In difluoromethyl ketene the two effects balance each other, since here we have only two fluorine atoms showing MO-

effects. Now with C-H and C-F bonds present, it makes a larger difference whether the C-H or the C-F eclipses the two groups on the other end of the rotor (CH and CCO).

In monohalomethyl ketenes, the tendency proceeds in the same direction. Here with only one C-F or C-Cl bond, the potential curve can be explained solely on grounds of steric hindrance. From the energy optimization of fluoro and chloromethyl ketene, the *gauche* conformer with the ketenic hydrogen being in the staggered configuration with respect to the halomethyl moiety was calculated to be the only stable form. However, the *cis* conformer with the halogen atom eclipsing the ketenic –C=C=O group is calculated to be about 4 kcal/mol higher in energy than the *gauche* conformation. On the other hand, the comparison between the *gauche* and the *trans* conformers shows that the ketenic hydrogen is preferably not to be eclipsing the halogen atom as in the *trans* form and, instead, to be staggered in the *gauche* form. The *cis* conformation is about 1.5 kcal/mol lower in energy than the *trans* conformation. One may expect the reversed behavior since the bulky halogen atom eclipses the ketene group in the *cis* form, which would lead to destabilize it more as compared to the *trans* form. However, this could be explained in terms of the electrostatic attraction in the *cis* form between the partially negatively charged fluorine atom and the partially positively charged central carbon atom of the ketene group. These predictions clearly indicate that the steric forces as well as the intramolecular dipole interactions significantly govern the conformational behavior in these molecules.

Finally, in the present thesis we determined the potential surface scans of some important ketenes and calculated the barriers to internal rotations in these systems. We also provided a complete analysis of vibrational Infrared and Raman spectra of the

molecules based on calculated potential energy distributions of all the normal modes and on comparison with experimental data for similar molecules. The assignments were of very reasonable agreements with the experimental work done for the same or similar molecules.

REFERENCES

1. J. Grundy, "Stereochemistry The Static Principles", pp. 1-2, Butterworths, London, 1964.
2. H. Kagan, "Organic Stereochemistry", pp. 1-78, Butler & Tanner Ltd., Great Britain, 1979.
3. F. A. Carey and R. J. Sundberg, "Advanced Organic Chemistry Part A: Structure and Mechanisms", pp.117-178, Plenum Press, New York, 1990.
4. W. J. Orville and B. H. Thomas, "Internal Rotation in Molecules", pp. 385-424, Wiley, New York, 1974.
5. J. R. Durig, H. V. Phan, T. S. Little and B. J. Van Der Veken, *J. Mol. Struct. (Theochem)*, 202 (1989) 143.
6. H. V. Phan and J. R. Durig, *J. Mol. Struct. (Theochem)*, 209 (1990) 333.
7. S. Bell, A. Bisset and T. J. Dines, *J. Raman Spectrosc.*, 29 (1998) 447.
8. B. S. Hudson and L. M. Markham, *J. Raman Spectrosc.*, 29 (1998) 489.
9. F. Negri and G. Orlandi, *J. Raman Spectrosc.*, 29 (1998) 501.
10. J. Vazquez, J. L. Gozales, F. Marquez and J. E. Boggs, *J. Raman Spectrosc.*, 29 (1998) 547.
11. J. R. Durig, M. J. Lee, H. M. Badawi, J. F. Sullivan and D. T. Durig, *J. Mol. Struct.*, 266 (1992) 59.
12. J. R. Durig, W. Zhao, D. Lewis and T. S. Little, *J. Chem. Phys.*, 89 (1988) 1285.

13. J. R. Durig and H. V. Phan, *Struct. Chem.*, 1 (1989) 61.

14. J. R. Durig, H. V. Phan, J. A. Hardin and T. S. Little, *J. Chem. Phys.*, 90 (1989) 6840.

15. T. S. Little, A. Y. Wang and J. R. Durig, *J. Mol. Struct.*, 217 (1990) 221.

16. J. R. Durig, A. Y. Wang and T. S. Little, *Int. Rev. Phys. Chem.*, 9 (1990) 349.

17. H. M. Badawi, *J. Mol. Struct. (Theochem)*, 336 (1995) 21.

18. J. R. Durig, T. S. Little and H. D. Bist, *J. Mol. Struct.*, 99 (1983) 217.

19. J. R. Durig, T. S. Little and H. D. Bist, *J. Mol. Struct.*, 116 (1984) 345.

20. J. R. Durig, H. V. Phan, T. S. Little and C. L. Tolly, *J. Struct. Chem*, 1 (1989) 459.

21. H. Guo and M. Karplus, *J. Chem. Phys.*, 94 (1991) 3679.

22. J. R. Durig, H. M. Badawi, H. D. Bist and T. S. Little, *J. Chem. Phys.*, 85 (1986) 5446.

23. J. R. Durig, H. M. Badawi, T. S. Little and H. D. Bist, *J. Mol. Struct.*, 190 (1988) 475.

24. J. R. Durig and H. M. Badawi, *J. Chem. Phys.*, 148 (1990) 193.

25. H. M. Badawi, *J. Mol. Struct. (Theochem)*, 205 (1990) 353.

26. H. M. Badawi, *J. Mol. Struct. (Theochem)*, 208 (1990) 7.

27. H. M. Badawi, *J. Mol. Struct. (Theochem)*, 208 (1990) 271.

28. H. M. Badawi, *J. Mol. Struct. (Theochem)*, 228 (1991) 159.

29. H. M. Badawi, *J. Mol. Struct. (Theochem)*, 288 (1993) 93.

30. H. M. Badawi, W. Forner, and A. Al-Rayyes, *J. Mol. Model.*, 4 (1998) 158.

31. H. M. Badawi and A. Al-Rayyes, *Arab. J. Sci. & Eng.*, 24 (1999) 59.

32. H. M. Badawi and W. Forner, *Asian J. Spectrosc.*, 3 (1999) 177.

33. S. Etemad, A. J. Heeger, and A. G. MacDiarmid, *Ann. Rev. Phys. Chem.*, 33 (1982) 443.

34. A. J. Heeger, S. Kivelson, J. R. Schrieffer, and W. P. Su, *Rev. Mod. Phys.*, 60 (1988) 781.

35. C. P. Tsonis and H. M. Badawi, *J. Polym. Sci. ;Polym. Phys. Ed.*, 34 (1996) 853.

36. W. Forner and H. M. Badawi, *Asian J. Spectrosc.*, 2 (1998) 72.

37. G. Davidovics, M. Monnier and A. Allouche, *Chem. Phys.*, 150 (1991) 395.

38. A. C. Scheiner and H. F. Schaefer, *J. Am. Chem. Soc.*, 114 (1992) 4758.

39. M. Monnier, A. Allouche, P. Verlaque and J. Aycard, *J. Phys. Chem.*, 99 (1995) 5977

40. R. Leung-Toung and T. T. Tidwell, *J. Am. Chem. Soc.*, 112 (1990) 1042.

41. Z. Xu, D. Fang, and X. Fu, *J. Mol. Struct. (Theochem)*, 305 (1994) 191.

42. D. M. Birney and P. E. Wagenseller, *J. Am. Chem. Soc.*, 116 (1994) 6262.

43. M. B. Huang and Z. X. Wang, *J. Chem. Phys.*, 109 (1998) 8953.

44. U. Salzner and S. M. Bachrach, *J. Am. Chem. Soc.*, 116 (1994) 6850.

45. P. E. Wagenseller and D. M. Birney, *J. Org Chem.*, 60 (1995) 3853.

46. S. Patia, "The Chemistry of Ketenes, Allenes and Related Compounds Part 1", pp. 279-298, Wiley, New York, 1980.

47. H. R. Seikaly and T. T. Tidwell, *Tetrahedron*, 42 (1986) 2587.

48. A. E. H. El-Rayyes, " Conformational Stability and Barrier to Internal Rotation in Some Unsaturated Hydrocarbons Based on Ab Initio Calculations", pp. 8-9, *M.S. Thesis*, May 1997.

49. R. Hoffmann, *J. Chem. Phys.*, 39 (1963) 1397.

50. I. N. Levine, "Quantum Chemistry", pp. 281-288, 511-515, Prentice-Hall International, Inc., New Jersey, 1991.

51. C. C. J. Roothann, *Rev. Mod. Phys.*, 23 (1951) 69.

52. C. C. J. Roothann, *Rev. Mod. Phys.*, 32 (1960) 179.

53. W. J. Hehre, L. Radom, P. V. R. Schleyer and J. A. Pople, "Ab Initio Molecular Orbital Theory", pp. 11-88, John Wiley & Sons, Inc., USA, 1986.

54. J. A. Pople, J. S. Stephen and R. Seeger, *Int. J. Quant. Chem. Symp.*, 10 (1976) 1.

55. C. Moller and M. S. Plesset, *Phys. Rev.*, 46 (1934) 618.

56. B. B. Laird, R. B. Ross and T. Ziegler, "Chemical Applications of Density-Functional Theory", *ACS Symposium Series*, pp. 1-17, American Chemical Society, Washington, DC, 1996.

57. "The Nobel Prize in Chemistry 1998", The Royal Swedish Academy of Sciences, Information Department, *http://www.nobel.se/announcement-98/chemistry98.html.*

58. P. Hohenberg and W. Kohn, *Phys. Rev.*, 136 (1964) A864.

59. N. D. Mermin, *Phys. Rev.*, 137 (1965) A1441.

60. A. L. L. East and L. Radom, *J. Mol. Struct.*, 376 (1996) 437.

61. P. Carsky and M. Urban, "Ab Initio Calculations Methods and Applications in Chemistry", pp. 17-18, Springer-Verlag, Berlin Heidelberg, Germany, 1980.

62. F. A. Cotton, "Chemical Applications of Group Theory", pp. 295-300, John Wiley & Sons, Inc., USA, 1971.

63. W. A. Guillory, "Introduction to Molecular Structure and Spectroscopy", pp. 238-245, Allyn and Bacon, Inc., 1967.

64. G. Herzberg, "Molecular Spectra and Molecular Structure, II. Infrared and Raman Spectra of Polyatomic Molecules", pp. 131-140, Van Nostrand Reinhold Company, New York, 1968.

65. M. J. Frisch, G. W. Trucks, H. B. Schlegel, G. E. Scuseria, M. A. Robb, J. R. Cheeseman, V. G. Zakrzewski, J. A. Montgomery, Jr. R. E. Stratmann, J. C. Burant, S. Dapprich, J. M. Millam, A. D. Daniels, K. N. Kudin, M. C. Strain, O. Frakas, J. Tomasi, V. Barone, M. Cossi, R. Cammi, B. Mennucci, C. Pomelli, C. Adamo, S. Clifford, J. Ochterski, G. A. Petersson, P. Y. Ayala, Q. Cui, K. Morokuma, D. K. Malick, A. D. Rabuck, K. Raghavachari, J. B. Foresman, J. Cioslowski, J. V. Ortiz, A. G. Baboul, B. B. Stefanov, G. Liu, A. Liashenko, P. Piskorz, I. Komaromi, R. Gomperts, R. L. Martin, D. T. Fox, T. Keith, M. A. Al-Laham, C. Y. Peng, A. Nanayakkara, C. Gonzalez, M. Challacombe, P. M. W. Gill, B. G. Johnson, W. Chen, W. Wong, J. L. Andres, M. Head-Gordon, E. S. Replogle and J. A. Pople, Gaussian 98, Inc., Pittsburgh PA, 1998.

66. A. D. Becke, *J. Chem. Phys.*, 98 (1993) 5648.

67. C. Lee, W. Yang and R. G. Parr, *Phys. Rev.*, B37 (1988) 385.

68. S. H. Vosko, L. Wilk and M. Nusair, *Can. J. Phys.*, 58 (1980) 1200.

69. M. J. Frisch, G. W. Trucks, H. B. Schlegel, P. M. W. Gill, B. G. Johnson, M. A. Robb, J. R. Cheeseman, T. Keith, G. A. Petersson, J. A. Montgomery, K. Raghavachari, M. A. Al-Laham, V. G. Zakrzewski, J. V. Ortiz, J. B. Foresman, J. Cioslowski, B. B. Stefanov, A. Nanyakkara, M. Challacombe, C. Y. Peng, P. Y. Ayala, W. Chen, M. W. Wong, J. L. Andres, E. S. Replogle, R. Gomperts, R. L. Martin, D. T. Fox, J. S. Binkley, D. J. Defrees, J. Baker, J. P. Stewart, M. Head-

Gordon, C.Gonzalez and J.A.Pople, Gaussian 94, Gaussian, Inc., Pittsburg PA, 1995.

70. K. Rasmussen, "Potential Energy Functions in Conformational Analysis", pp. 12-37, Springer-Verlag, Berlin Heidelberg, Germany, 1985.

71. E. B. Wilson, J. C. Decius and P. C. Cross, "Molecular vibrations", McGraw-Hill, New York, 1955.

72. J. R. Durig, G. A. Guirgis, K. A. Krutules, H. Phan and H. D. Stidham, *J. Raman Spectrosc.*, 25 (1994) 221.

73. G. W. Chantry, "The Raman Effect", Vol. 1, Chapter 2, Marcel Dekker, New York, 1971.

74. L. Carreira, *J. Phys. Chem.*, 80 (1976) 1149.

75. C. E. Blom, G. Grassi and A. Bauder, *J. Am. Chem. Soc.*, 106 (1984) 7427.

76. J. R. Durig, J. Qui, B. Dehoff and T. S. Little, *Spectrochim. Acta, Part A*, 42 (1986) 89.

77. H. M. Badawi, *J. Mol. Struct. (Theochem)*, 276 (1992) 251.

78. H. M. Badawi, *J. Mol. Struct. (Theochem)*, 303 (1994) 275.

79. H. M. Badawi, *J. Mol. Struct. (Theochem)*, 343 (1995) 117.

80. H. M. Badawi and A. A. Al-Rayyes, *J. Mol. Struct. (Theochem)*, 397 (1997) 51.

81. H. M. Badawi and W. Forner, *Asian J. Spectrosc.*, 2 (1998) 113.

82. H. M. Badawi and A. Al-Rayyes, *J. Mol. Struct. (Theochem)*, 428 (1998) 247.

83. W. Forner and H. M. Badawi, *J. Mol. Struct. (Theochem)*, 454 (1998) 41.

84. H. M. Badawi and W. Forner, *J. Raman Spectrosc.*, 29 (1998) 1009.

85. H. M. Badawi, A. Al-Rayyes and C. P. Tsonis, *J. Mol. Struct. (Theochem)*, 394 (1997) 49.

86. E. Valenti, M. A. Pericas and A. Moyano, *J. Org. Chem.*, 55 (1990) 3582.

87. J. R. Durig, G. A. Guirgis and H. V. Phan, *J. Raman Spectrosc.*, 21 (1990) 359.

88. J. F. Sullivan, S. K. Nandy, M. J. Lee and J. R. Durig, *J. Raman Spectrosc.*, 23 (1992) 51.

89. N. C. Handy, in "Lecture Notes in Quantum Chemistry II", pp. 91-124, Springer-Verlage, Berlin, Germany,1994.

90. B. Johnson, P. M. W. Gill and J. A. Pople, *J. Chem. Phys.*, 98 (1993) 5612.

91. J. R. Durig, A. Q. McArver, H. V. Phan and G. A. Guirgis, *J. Phys. Chem.*, 59 (1991) 539.

92. J. R. Durig, G. A. Guirgis and H. V. Phan, *J. Mol. Struct.*, 244 (1991) 139.

93. H. M. Badawi and W. Forner, *J. Mol. Struct. (Theochem)*, 452 (1998) 85.

94. J. R. Durig, R. J. Berry and P. Groner, *J. Chem. Phys.*, 87 (1987) 6303.

95. J. R. Durig, A. Y. Wang, T. S. Little, P. A. Brletic and J. R. Bucenell, *J. Chem. Phys.*, 91 (1989) 7361.

96. C. W. Bock, Y. N. Panchenko and S. V. Krasnoshchiokov, *Chem. Phys.*, 147 (1990) 65.

97. J. R. Durig, A. Y. Wang and T. S. Little, *J. Chem. Phys.*, 93 (1990) 905.

98. T. Tidwell, *Acc. Chem. Res.*, 23 (1990) 273.

99. R. Leung-Toung and C. Wentrup, *J. Org Chem.*, 57 (1992) 4850.

100. A. Allen, J. Colomvakos, I. Egle, J. Lusztyk, M. McAllister, T. Tidwell, B. Wagner and D. Zhao, *J. Am. Chem. Soc.*, 117 (1995) 7552.

101. C. O. Kappe, M. W. Wong and C. Wentrup, *J. Org Chem.*, 60 (1995) 1686.

102. G. Bouchoux and J. Slapin, *J. Phys. Chem.*, 100 (1996) 16555.

103. K. Schonwalder, P. Kollat, J. Stezowski and F. Effenberger, *Chem. Ber.*, 117 (1984) 3280.

104. D. M. Birney, *J. Org. Chem.*, 59 (1994) 2557.

105. N. Pietri, T. Chiavassa, A. Allouche, M. Rajzmann and J. Aycard, *J. Phys. Chem.*, 100 (1996) 7034.

106. J. Finnerty, J. Anderson, Y. Yamamoto, M. W. Wong and C. Wentrup, *J. Am. Chem. Soc.*, 120 (1998) 1701.

107. J. J. Keirns and R. F. Curl, Jr., *J. Chem. Phys.*, 48 (1968) 3773.

108. R. Kewley, D. C. Hemphill and R. F. Curl, Jr., *J. Mol. Spectrosc.*, 44 (1972) 443.

109. K. Hagen and K. Hedberg, *J. Am. Chem. Soc.*, 106 (1984) 6150.

110. H. M. Badawi and W. Forner, *Asian J. Spectrosc.*, 3 (1999) 161.

111. H. M. Badawi and W. Forner, *Asian J. Spectrosc.*, 3 (1999) 169.

112. H. W. Moore and O. H. Decker, *Chem. Rev.*, 86 (1986) 821.

113. M. A. McAllister and T. T. Tidwell, *J. Am. Chem. Soc.*, 116 (1994) 7233.

114. W. Huang, D. Fang, K. Temple, T. T. Tidwell, *J. Am. Chem. Soc.*, 119 (1997) 2832.

115. R. F. C. Brown, F. W. Eastwood and K. J. Harrington, *Aust. J. Chem.*, 27 (1974) 2373.

116. R. W. Holder, H. S. Freiman and M. F. Stefanchik, *J. Org. Chem.*, 41 (1976) 3303.

117. J. K. Terlow, P. C. Burgers, J. L. Holmes, *J. Am. Chem. Soc.*, 101 (1979) 225.

118. R. D. Brown, P. D. Godfrey and M. Woodruff, *Aust. J. Chem.*, 32 (1979) 2103.

119. S. Mohamand, T. Hirabayashi and H. Bock, *Chem. Ber.*, 114 (1981) 2609.

120. C. Wentrup and P. Lorencak, *J. Am. Chem. Soc.*, 110 (1988) 1880.

121. A. Maquestiau, P. Pauwels, R. Flammang, P. Lorencak and C. Wentrup, *Org. Mass Spect.*, 21 (1986) 259.

122. M. T. Nguyen, T. Ha, R. A. M. O'Ferrall, *J. Org. Chem.*, 55 (1990) 3251.

123. H. Bibas, M. W. Wong and C. Wentrup, *J. Am. Chem. Soc.*, 117 (1995) 9582.

124. S. Niwayama, E. A. Kallel, C. Sheu and K. N. Houk, *J. Org. Chem.*, 61 (1996) 2517.

125. J. H. Rigby and S. Laurent, *J. Org. Chem.*, 64 (1999) 1766.

126. J. H. Rigby, A. Cavezza and M. J. Heeg, *Tetrahedron Lett.*, 40 (1999) 2473.

127. J. H. Rigbyand D. M. Danca, *Tetrahedron Lett.*, 38 (1997) 4969.

128. W. Mormann and K Schmalz, *Makromol. Chem. Rapid. Commun.*, 13 (1992) 377.

129. Y. Hamada, Y. Nishimura and M. Tsuboi, *Chem. Phys.*, 100 (1985) 365.

130. C. W. Bock, Y. N. Panchenko and S. V. Krasnoshchiokov, *Chem. Phys.*, 125 (1988) 63.

131. J. R. Durig, A. Q. McArver, H. V. Phan and G. A. Guirgis, *J. Phys. Chem.*, 59 (1991) 539.

132. G. A. Guirgis, B. R. Drew, T. K. Gounev and J. R. Durig, *Spectrochim. Acta*, Part A, 54 (1998) 123.

133. J. F. Sullivan, D. T. Durig, J. R. Durig and S. Cradock, *J. Phys. Chem.*, 91 (1987) 1770.

134. H. M. Badawi and W. Forner, Asian J. Spectrosc., *in press.*

135. L. Gong, M. McAllister and T. Tidwell, *J. Am. Chem. Soc.*, 113 (1991) 6021.

136. H. Hagemann, Angew. *Chem., Int. Ed. Engl.*, 16 (1977) 743.

137. J. R. Durig, M. R. Jalilian, J. F. Sullivan and J. B. Turner, *J. Raman Spectrosc.*, 11 (1981) 459.

138. J. R. Durig, K. J. Kanes and J. F. Sullivan, *J. Mol. Struct.*, 99 (1983) 61.

139. S. Cradock, C. M. Huntley and J. R. Durig, *J. Mol. Struct.*, 127 (1985) 319.

140. J. R. Durig, R. J. Berry and C. J. Wurrey, *J. Am. Chem. Soc.*, 110 (1988) 718.

141. A. Kamal, *Heterocycles*, 31 (1990) 1377.

142. J. R. Durig, G. A. Guirgis, K. A. Krutules and J. F. Sullivan, *J. Raman Spectrosc.*, 24 (1993) 259.

143. J. F. Sullivan, H. L. Heusel, W. M. Zunic, J. R. Durig and S. Cradock, *Spectrochim. Acta*, 50A (1994) 435.

144. J. R. Durig, G. A. Guirgis and K. A. Krutules, *J. Mol. Struct.*, 328 (1994) 55.

145. J. R. Durig, T. S. Little, T. K. Gounev, J. K. Gardner, Jr., and J. F. Sullivan, *J. Mol. Struct.*, 375 (1996) 83.

146. F. Brown and W. Musgrane, *J. Chem. Soc.*, (1953) 2087.

147. A. Allen, J. Andraos, A. Kresge, M. McAllister and T. Tidwell, *J. Am. Chem. Soc.*, 114 (1992) 1878.

148. C. Berney, *Spectrochim. Acta*, 25A (1969) 793.

149. R. C. Woods, *J. Chem. Phys.*, 46 (1967) 4789.

150. J. R. Durig and B. van der Vaken, *J. Raman Spectrosc.*, 18 (1987) 549.

151. S. Dyngeseth, H. Schei and K. Hagen, *J. Mol. Struct.*, 102 (1983) 45.

VITA

- Abdulaziz Abdulrahman Al-Saadi.
- Born in Al-Khobar, Saudi Arabia in May 1973.
- Received my B.Sc. in Chemistry from King Fahd University of Petroleum and Minerals (KFUPM) in June 1996.
- Joined KFUPM in Fall 1997 as a graduate assistant and started the M.S. program in chemistry.
- Earned the M.S. degree in physical chemistry from KFUPM in May 2000.
- A co-author of the following puplications:

1. H. M. Badawi, W. Forner, and **A. Al-Saadi**, "An investigation of structural stability and analysis of vibrational spectra of formyl ketene based on ab initio calculations". *J. Mol. Struct. (Theochem)*, ***accepted***.

2. H. M. Badawi, W. Forner, and **A. Al-Saadi**, "Structural stability and derived potential energy distributions of fluoro- and chloromethyl ketene". *Asian J. Spect.*, ***accepted***.

3. H. M. Badawi, W. Forner, **A. Al-Saadi**, and S. A. Ali, "Vibrational assignments and derived potential energy distributions for tri- and difluoromethyl ketene by density functional calculations". *J. Mol. Model.*, ***submitted***.

4. H. M. Badawi, W. Forner, and **A. Al-Saadi**, "C-C and C-N rotational barriers in vinyl ketene and vinyl isocyanate". *J. Mol. Struct. (Theochem)*, ***submitted***.

5. H. M. Badawi, W. Forner, and **A. Al-Saadi**, "Density functional calculations of vibrational wavenumbers and derived potential energy distributions for fluoro- and chlorocarbonyl ketene". ***to be submitted***.

6. H. M. Badawi, W. Forner, and **A. Al-Saadi**, "A theoretical study of the effect of halogen substitution on the structural stability of formyl fluoro- and formyl chloro ketene". ***to be submitted***.